AD A

DEVELOPMENT OF A NATURAL GAS-POWERED APU FOR A HYBRID ELECTRIC S-10 PICKUP TRUCK

FINAL INTERIM REPORT
TFLRF No. 315

By
Daniel J. Podner
William K. Capshaw
U.S. Army TARDEC Fuels and Lubricants Research Facility (SwRI)
Southwest Research Institute
San Antonio, Texas

prepared for

Defense Advanced Research Projects Agency
3701 N. Fairfax Drive
Arlington, Virginia 22203-1714

Under Contract to
U.S. Army TARDEC
Petroleum and Water Business Area
Warren, Michigan 58397

Contract No. DAAK70-92-C-0059

Approved for public release; distribution unlimited

December 1997

REPORT DOCUMENTATION PAGE

Form Approved
OMB No. 0704-0188

1. AGENCY USE ONLY (Leave blank)	2. REPORT DATE	3. REPORT TYPE AND DATES COVERED
	December 1997	Interim May 1994-April 1995

4. TITLE AND SUBTITLE

Development of a Natural Gas-Powered APU for a Hybrid Electric S-10 Pickup Truck

5. FUNDING NUMBERS

DAAK70-92-C-0059; WD 22

6. AUTHOR(S)

Podner, Daniel J. And Capshaw, William K.

7. PERFORMING ORGANIZATION NAME(S) AND ADDRESS(ES)

U.S. Army TARDEC Fuels and Lubricants Research Facility (SwRI)
Southwest Research Institute
P.O. Drawer 28510
San Antonio, Texas 78228-0510

8. PERFORMING ORGANIZATION REPORT NUMBER

TFLRF No. 315

9. SPONSORING/MONITORING AGENCY NAME(S) AND ADDRESS(ES)

U. S. Army TARDEC
Petroleum and Water Business Area
Warren, Michigan 58397-5000

10. SPONSORING/MONITORING AGENCY REPORT NUMBER

11. SUPPLEMENTARY NOTES

12a. DISTRIBUTION/AVAILABILITY STATEMENT

Approved for public release; distribution unlimited

12b. DISTRIBUTION CODE

13. ABSTRACT (Maximum 200 words)

A natural gas-fueled Auxiliary Power Unit (APU) was developed for use in a hybrid electric vehicle. The project involved conversion and development of the powerplant from gasoline to natural gas operation, application of an engine control system, application of a three-way catalyst system, development of an APU controller, and integration and testing of the APU in the laboratory and vehicle environment. The project was divided into three phases: (1) engine development, (2) APU control system development, and (3) APU integration/testing. The resultant APU was integrated into a hybrid electric utility truck for use as a range extender in a series hybrid configuration. The project resulted in an APU configuration producing ultra-low emissions levels while achieving high efficiency due to implementation of a unique APU operating strategy.

14. SUBJECT TERMS

hybrid electric vehicle, auxiliary power unit, compressed natural gas, natural gas engine, electronic engine control, electronic APU control

15. NUMBER OF PAGES

38

16. PRICE CODE

17. SECURITY CLASSIFICATION OF REPORT	18. SECURITY CLASSIFICATION OF THIS PAGE	19. SECURITY CLASSIFICATION OF ABSTRACT	20. LIMITATION OF ABSTRACT
Unclassified	Unclassified	Unclassified	

TABLE OF CONTENTS

Section **Page**

LIST OF ILLUSTRATIONS

LIST OF ILLUSTRATIONS (Cont'd)

1.0 BACKGROUND

1.1 Objective

The technical objective of this work was to develop, integrate, and test a natural gas-powered auxiliary power unit (APU) for a hybrid electric vehicle application. The specific technical objectives for the APU were to achieve very low emissions levels, high efficiency, and allow extended vehicle range over an electric vehicle. Vehicle emissions below CARB ULEV (0.04 g/mile NMOG, 1.7 g/mile CO, 0.2 g/mile NO_x) levels were desired, while engine efficiency and vehicle range were to be maximized. This report describes the engine selection, and development process, as well as the APU and APU controller development, integration, and testing performed.

1.2 Technical Background

Southwest Research Institute (SwRI) has converted many diesel engine models to operate with natural gas in a lean-burn combustion mode. Exhaust emissions have been far lower than their diesel counterparts[1,2]*. SwRI has typically developed these engines to produce oxides of nitrogen (NO_x) emissions of less than 2.5 g/hp-hr. While achieving these NO_x levels, non-methane hydrocarbons (NMHC) emissions have been near or less than 1 g/hp-hr while total hydrocarbons (THC) have been in the 4 to 6 g/hp-hr range. These emissions are "engine-out," that is, they do not rely on a catalyst. These lean-burn combustion engines are more efficient than stoichiometric combustion engines but do not lend themselves to the extremely low emissions possible with effective three-way catalyst-equipped engines.

The use of an automotive three-way catalyst can provide exhaust emissions levels far below those of lean-burn combustion engines. However, for a three-way catalyst to operate at peak efficiency, the engine must operate very near stoichiometric equivalence ratios. The methodology of three-way catalyst operation is well documented in the literature for gasoline engines.[3] There is also literature documenting the use of three-way catalysts with natural gas fuel.[4,5] Natural gas engines with three-way catalysts operate very much like their gasoline counterparts with one notable exception. While gasoline engines must operate about stoichiometric conditions, natural gas engines, (equipped with three-way catalysts), operate at an equivalence ratio slightly rich of stoichiometry in order to generate sufficient carbon monoxide (CO) to allow complete NO_x reduction in the catalyst.[6] The window of peak conversion for both NO_x and HC emissions is narrower for natural gas than for gasoline. This requires even greater control of equivalence ratio when using natural gas fuel.

1.3 APU Duty-Cycle

APUs in series hybrid electric vehicles typically operate in a limited and well defined speed and load range. This application required the engine to run between 1500 and 3600 rpm and essentially only at wide open throttle (WOT). This allowed the engine to be finely tuned for peak efficiency and power while maintaining minimum exhaust emissions at these operating points. Furthermore, the APU control strategy chosen was such that the APU would operate in "quasi

* Superscript numbers refer to references listed at the end of this report.

steady-state," i.e., relatively slow changes to engine operating conditions were made, and therefore rapid transients would not be encountered. This would result in even lower emissions levels and potentially increased efficiency.

1.4 Target Hybrid Vehicle

The vehicle for which the APU was developed was a Chevrolet S-10 pickup truck. The conventional drive train was removed from the vehicle and replaced with an electric drive system by Solar Car Corp. (a vehicle converter). The vehicle was equipped with 20 - 12 Volt lead acid batteries for which the APU provided the charging power.

Solar Car Corp. ceased operation in 1996. The vehicle integration, at the time of this report, is being completed by the Florida Solar Energy Center.

2.0 TECHNICAL DISCUSSION

2.1 Engine Development

Development of the engine for the APU included an engine selection process, engine baselining on gasoline, conversion to operation on compressed natural gas (CNG), and performance and emissions testing. As part of the engine development process, engine modeling and simulation was conducted in order to aid in the performance development of the engine. The details of the engine development process are described in this section.

2.1.1 Engine Selection

A set of engine selection criteria were agreed upon by SwRI, DARPA, and the vehicle integrator, Solar Car Corp. It was concluded that the engine must be produced within the United States, produce about 20 kW, and fit within the S-10 pickup electric vehicle space requirements. Due to the limited space requirements and consideration for keeping the engine weight to a minimum, only air-cooled utility engines met the requirements. All of the US manufactured water-cooled engines were too large and heavy for this application. The largest air-cooled utility engine made in the US is the new Kohler Command Series product line. This engine is shown in Figure 1.

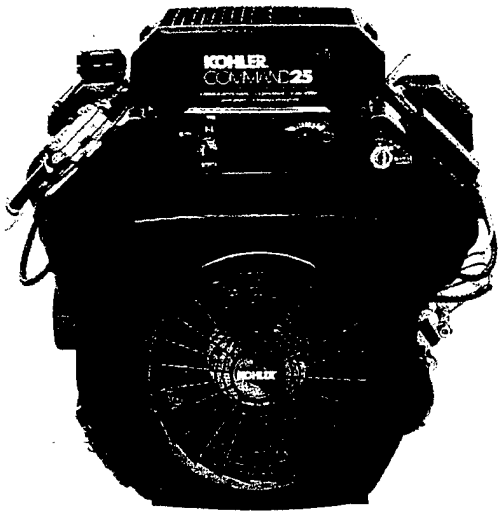

FIGURE 1. STOCK KOHLER CH-25 ENGINE

The largest of the Kohler Command series engines is the CH25 which displaces 44 cubic inches (.725 liters). The engine is rated at 25 hp (18.6 kW) at 3600 rpm. The Kohler CH22 is slightly smaller at 38 CID (.625 liters) and rated 22 hp (16.4 kW) at 3600 rpm. The CH22 utilizes a cast iron cylinder liner whereas the CH25, with a larger bore size, does not. In the CH25 engine, the piston operates on the parent aluminum of the block. Both of these engines were performance tested at SwRI on gasoline fuel. The maximum dyno power produced by the engines were very similar. Due to the small differences in power output, it was determined that the CH22 engine with the smaller bore and iron liner would be used in order to maximize engine durability.

2.1.2 Engine Baseline Tests

During the engine baseline tests, two Kohler engines, CH25 and CH22, were operated in their stock configuration at SwRI. The baseline tests resulted in a set of performance data for which the natural gas engine could be compared. The Kohler CH25 and CH22 engines were instrumented to measure relevant parameters such as temperatures, pressures, and fuel flow and were coupled to an eddy current dynamometer, as shown in Figure 2. The engine was operated on gasoline to determine baseline performance, efficiency, cylinder pressure, and emissions data. This mapping provided a basic understanding of power, fuel consumption, volumetric efficiency, emissions, and acoustic noise.

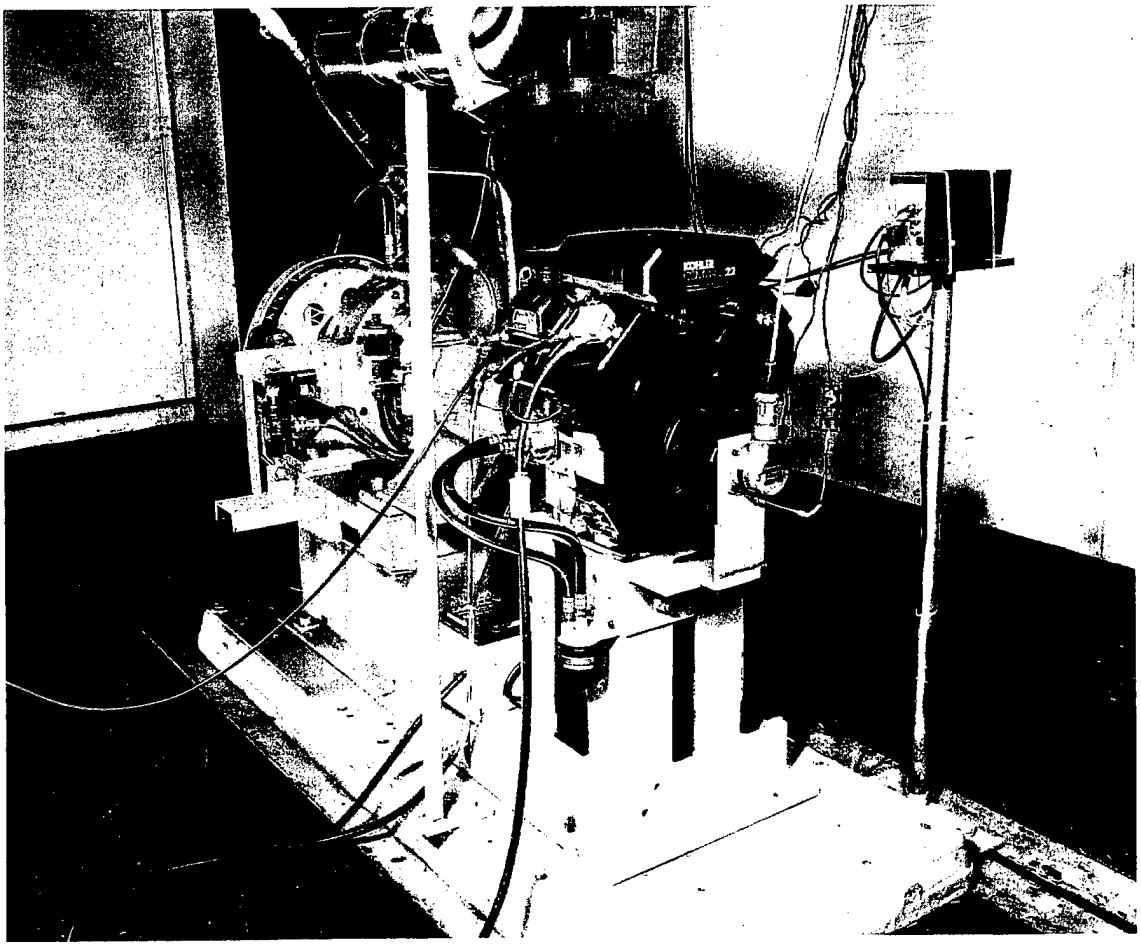

FIGURE 2. CH-22 ENGINE INSTALLED ON TEST STAND

Baseline data for the CH25 and CH22 engines at WOT conditions are shown in Figures 3 and 4, respectively. It should be noted that the WOT torque curves measured at SwRI for each of the baseline engines was less (up to 18 percent less for the CH25, and up to 11 percent less for the CH22) than that advertised by Kohler. This is possibly due to differences in parasitic loads, such as the cooling fan, between the SwRI data and the manufacturer's data.

2.1.3 CNG Conversion

A stock Kohler CH22 engine was converted to operate on compressed natural gas (CNG). The conversion process included numerous engine modifications as well as engine control system modifications. The details of the conversion process are described in the following paragraphs.

2.1.3.1 Engine Control System Application

As part of the CNG conversion process, the stock gasoline carburetor and ignition system were replaced with an electronic control system obtained from Mesa Environmental. This system, referred to as GEM (Gas Engine Management), allowed the engine to be operated near stoichiometric air-fuel ratios with complete control of ignition timing. A speed/density calculation was utilized for open-loop fueling calculations, with a closed-loop adaptive learn algorithm based on information from an exhaust gas oxygen (EGO) sensor to allow very accurate control of equivalence ratio around the stoichiometric point. The GEM system utilized a single gasoline-type fuel injector for metering of the CNG to a centralized fuel injection ring located immediately above the throttle body. The fuel injector operated as a critical flow orifice utilizing the opening time, (or injector pulse width), as the means of modulating the metered fuel flow rate. In order to compensate for fuel density changes upstream of the injector, natural gas pressure and temperature measurements were also incorporated into the fuel metering block of the GEM system.

In addition to fuel control, the GEM system also provided control of the spark ignition timing and ignition coil dwell functions. This was provided through a distributorless ignition system which utilized ignition coil driver circuits integrated into the GEM unit, along with production Ford ignition coils. Thus, the spark timing and coil dwell time could be accurately controlled to any value desired.

2.1.3.2 Intake Modifications

The stock intake system for the Kohler CH22 and CH25 engines is a compact design incorporating minimal length from the air cleaner, through the carburetor, throttle body, and intake manifold. Since increasing the maximum power output of the engine was of primary concern, engine simulation and experimental evaluations were conducted to investigate the sensitivity of engine power output to the intake system length. As part of this investigation, SwRI's engine cycle simulation, called Virtual Indicated Performance of Reciprocating Engines (VIPRE), was used. Details of the overall simulation study are contained in the Engine Modeling section of this report. The simulation predicted significant power increases could be realized through modification or "tuning" of the intake system length. The results from the simulation are shown in Figure 5. As can be seen from the data, the simulation predicted a large increase in power output when the intake runner length was set at roughly 0.5m. Based on the simulation results, a "snorkel"- type intake

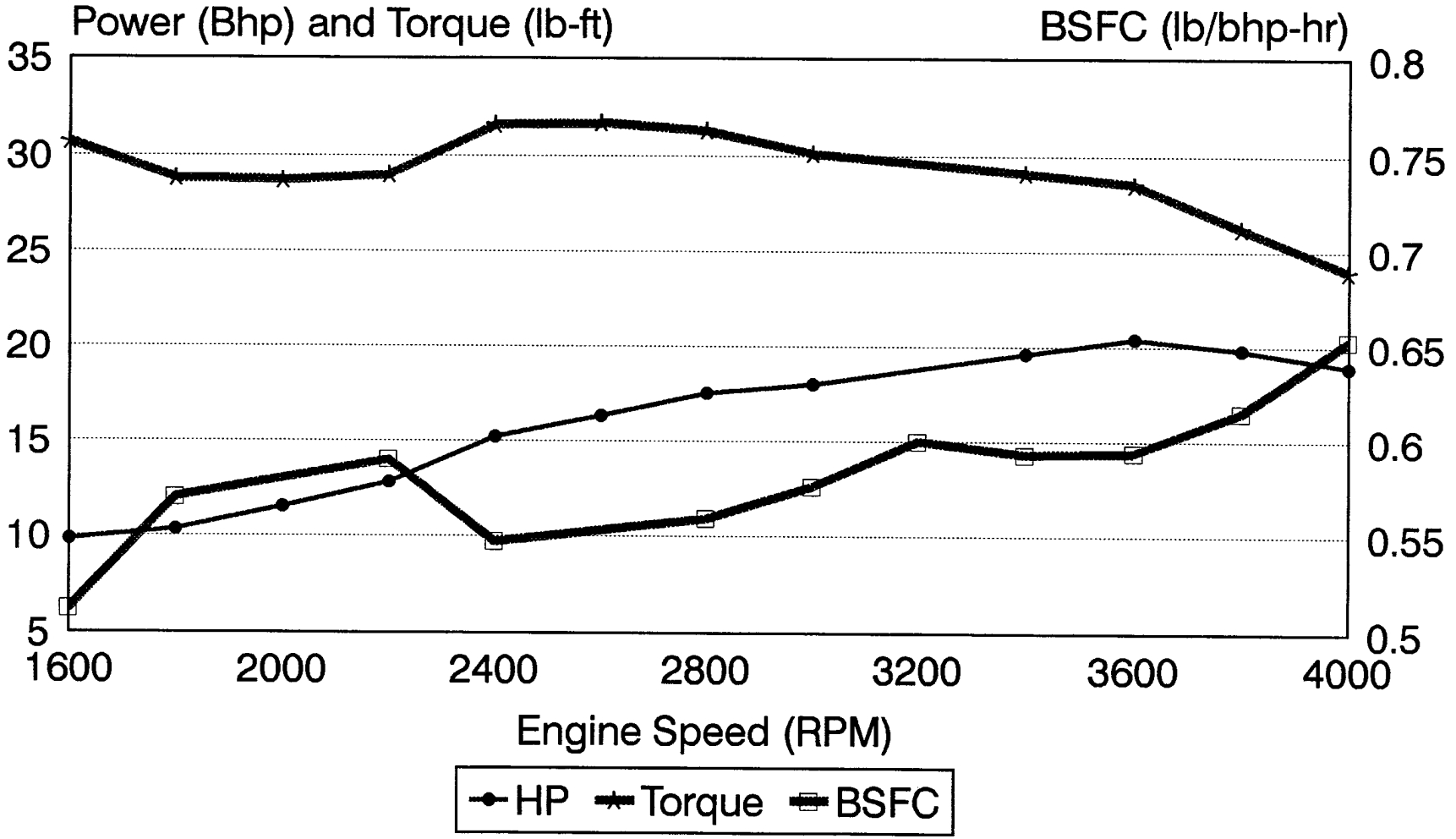

FIGURE 3. BASELINE CH-25 PERFORMANCE

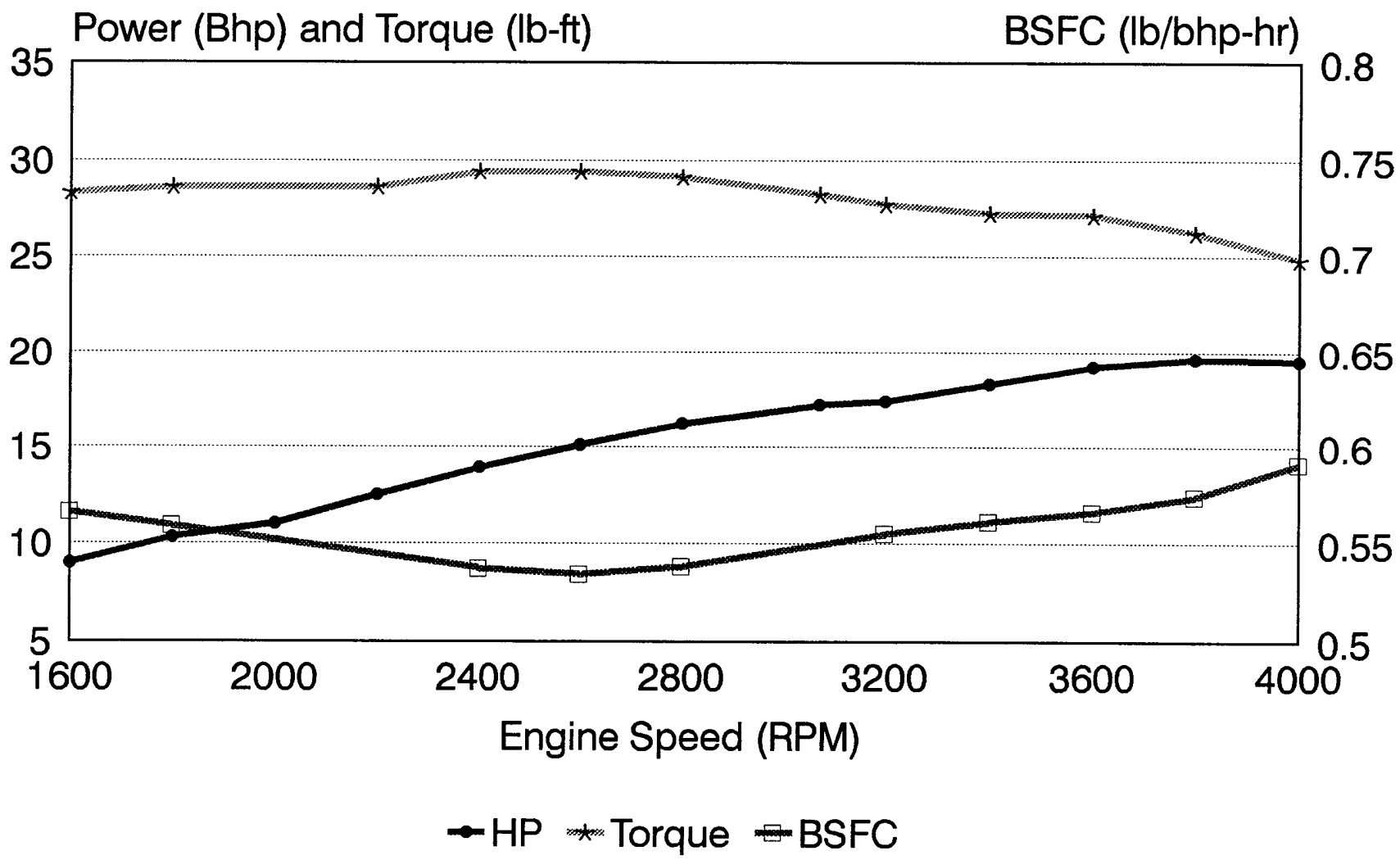

FIGURE 4. BASELINE CH-22 PERFORMANCE

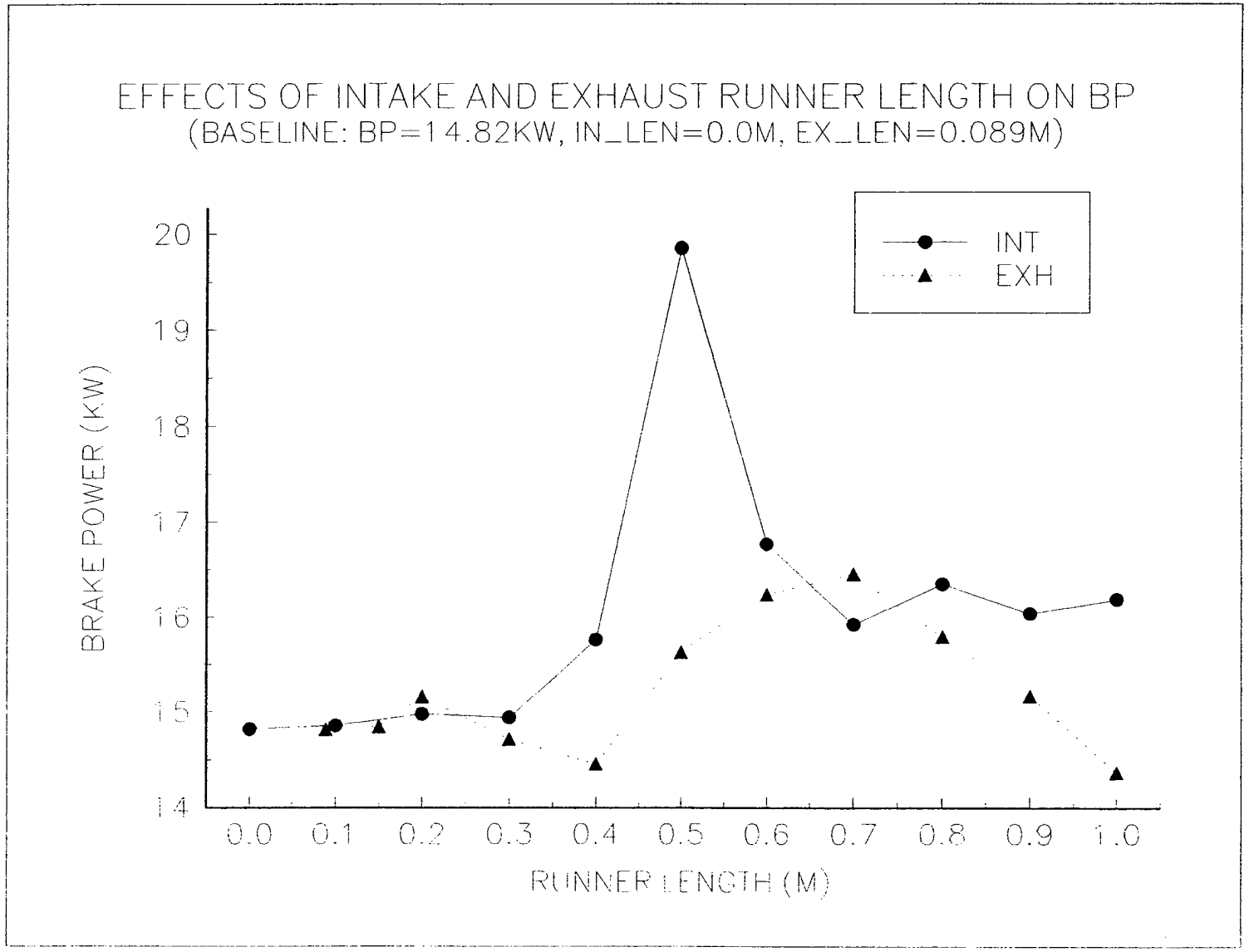

FIGURE 5. SIMULATED EFFECTS OF RUNNER LENGTH ON ENGINE POWER

system was fabricated for the engine. The snorkel attached to the engine throttle body and was made up of a long length of piping, of which the length was adjusted. Experimental data was gathered to quantify the maximum power output from the engine as a function of the intake snorkel length. This data is shown in Figure 6. As can be seen from the data, the significant power increase predicted by the simulation was not achieved in the engine tests. Problems with the simulation were later found and corrected by SwRI as a result of this effort.

2.1.3.3 Fuel Introduction

The key to providing low emissions from a catalyst-equipped natural gas engine is good equivalence ratio control to each cylinder. It is important to operate as close to the optimum equivalence ratio as possible to maintain catalyst efficiency. In order to accomplish this, a homogeneous fuel-air charge must be maintained in each cylinder. In addition, each cylinder should operate at the same fuel-air equivalence ratio. Two basic fuel introduction schemes were tried, central point fuel injection and port fuel injection, with multiple variations on both.

2.1.3.3.1 Central Point Fuel Injection

The first fuel delivery method tried was to admit the fuel from a tubular ring inside of the air filter above the throttle. The ring was made from 1/4 inch copper tubing and contained a series of spray holes around the inside diameter and top of the ring. This is shown in Figure 7. The holes on top of the ring are .042 inches (1.07 mm) in diameter spaced about 1 (25 mm) inch apart. The holes on the inside of the ring are .111 inches (2.82 mm) in diameter.

A second ring was made from 1/4 inch stainless steel tubing and contained 15 holes, each with a diameter of .052 inch (1.32 mm), spaced about 1 inch apart around the top of the ring. This is shown in Figure 8.

Both ring configurations were tested on the engine. The second ring, with larger diameter holes was found to give better performance in terms of the quality of the EGO sensor signal in the exhaust. Improved homogeneity of the charge mixture was found to produce an improved EGO sensor signal (i.e., free of noise or high frequency switching content) during closed-loop engine operation. During the development process, it was later found that the best configuration for the fuel metering ring was to reduce the number of holes by as much as 50 percent. The improvement can likely be attributed to an increase in natural gas flow velocity at the ring holes and thus increased penetration into the intake air stream.

In addition to the fuel admission rings previously described, several other mixing device designs were investigated on the engine. Among the designs tested was a "spray bar," which was simply an open ended piece of 1/4 inch tubing angled into the intake air stream. Also, a "shower head"-type device was fabricated and tested. The shower head fuel mixer consisted of a fitting placed onto the end of the tubing with small holes drilled into the fitting to allow the natural gas to escape into the air stream. Both of these mixer designs proved to be inferior to the spray ring approach, which was finally chosen as the preferred method of fuel-air mixing.

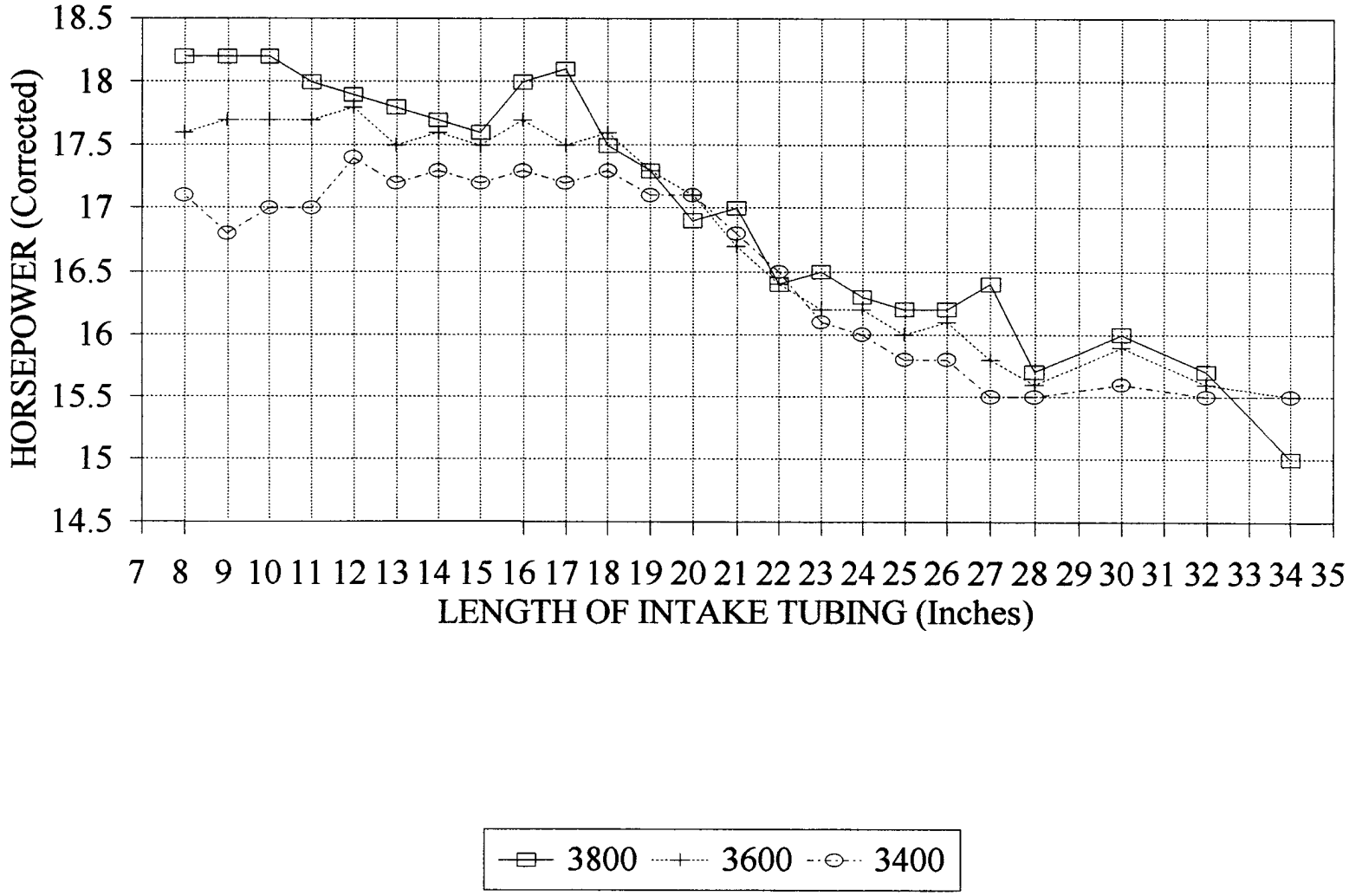

FIGURE 6. HORSEPOWER COMPARISON TREND DUE TO INTAKE LENGTH ADJUSTMENT

FIGURE 7. COPPER TUBING FUEL SPRAY RING

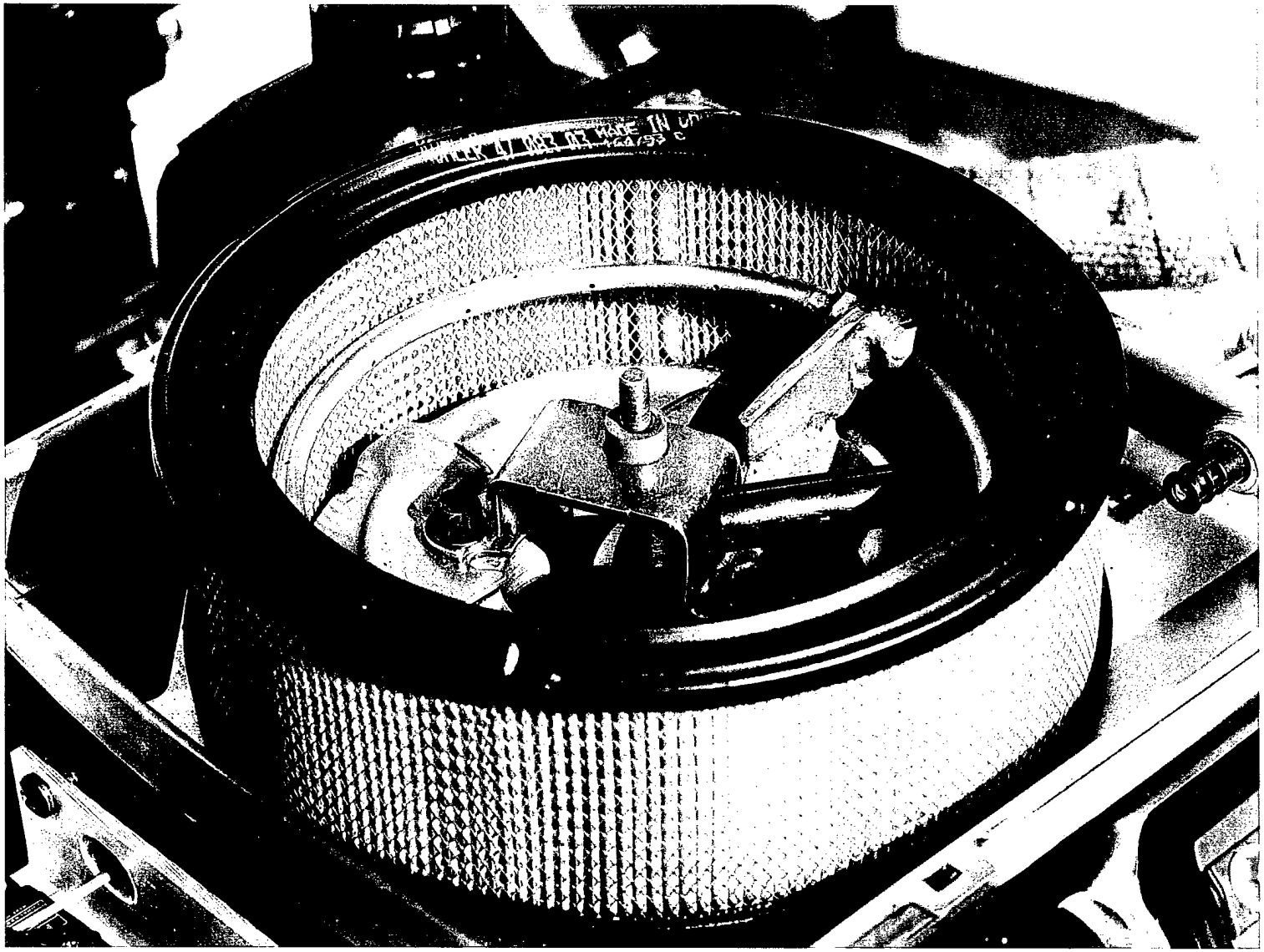

FIGURE 8. UPGRADED STAINLESS STEEL FUEL SPRAY RING

combined with a properly tuned intake system, would allow higher power levels to be achieved. The port injection system utilized separate injectors located in the intake manifold (roughly 2 inches away from the respective intake port). Natural gas at roughly 120 psig, from the fuel regulator, was supplied to each injector via individual fuel lines. An illustration of the port injection system installation on the engine is shown in Figure 9.

Results from port fuel injection engine testing are shown in Figure 10. As was previously stated, the objective of the testing was to achieve increased engine power output. As can be seen from the data, this objective was not met. The likely reason for the reduced performance is that there was inadequate mixing of the fuel-air charge in the cylinder. This is a common problem among port-injected natural gas engines. Thus, since the fuel-air charge in the cylinder was non-homogeneous, or stratified, incomplete and inefficient combustion was taking place within the cylinder. Given the objective of the test and the results of the engine testing performed, port injection was not considered to be an adequate approach for the engine. Therefore, central fuel injection, using the fuel mixing ring previously described, was the strategy which was finalized upon.

2.1.3.4 Cylinder Head/Intake Manifold/Throttle Body Modifications

Since maximum power output from the engine was limited only by the amount of airflow which the engine could pump through it, modifications were made in order to reduce flow restrictions on the intake side of the engine. Namely, three major modifications were made to the engine: (1) cylinder head machining or "porting," (2) intake manifold smoothing, and (3) throttle body diameter increases.

The cylinder heads on the Kohler Command 22 engine feature typical die-cast intake and exhaust ports. These ports have runners which intersect at a 90 degree angle (which is preferred for simplicity in the die-casting setup), and the resulting transition area is very abrupt. The zero short side radius of these ports results in a very large recirculation zone which inhibits air flow, particularly at high lifts. Since this engine would be operated with a gaseous fuel which displaces much more volume than the equivalent mass of liquid fuel, port restriction was a major concern. SwRI has vast experience with intake and exhaust port testing, design, and evaluation, and was positioned well to improve on flow performance of the Kohler heads. The intake and exhaust ports were flow tested on the SwRI flow bench to determine baseline performance.

The intake port was modified by adding a small radius to the short side of the port runner. A larger radius would have been even more beneficial, but there was limited room available for modification. It would have also been desirable to fill the transition area on the long side of the port to create a large radius, but this option was not exercised due to time constraints. The simple modification to the short side of the port resulted in approximately 10 percent improvement in flow at medium to high valve lifts as shown in Figure 11. This is a significant flow improvement, particularly if a revised camshaft profile is considered. Figure 11 shows volumetric flowrate in SCFM vs. non-dimensional valve lift.

The exhaust port was modified by increasing the available flow area in the transition between the horizontal and vertical runners. Material was removed, and the transition was made as smooth as possible. The port surfaces were lightly polished to improve flow and reduce heat transfer within the exhaust port. The exhaust port was re-tested, as shown in Figure 12, resulting in significant flow

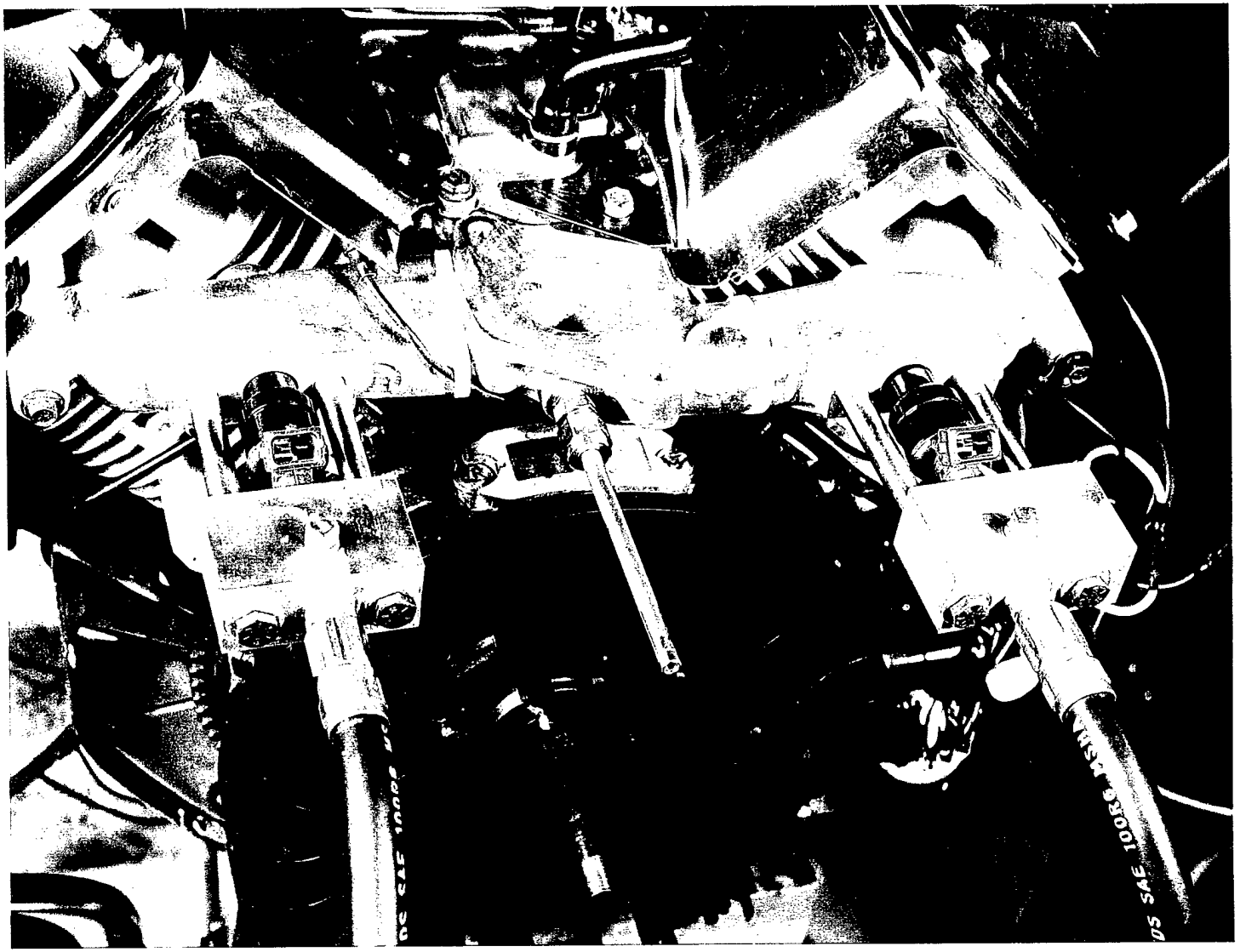

FIGURE 9. PORT INJECTION HARDWARE

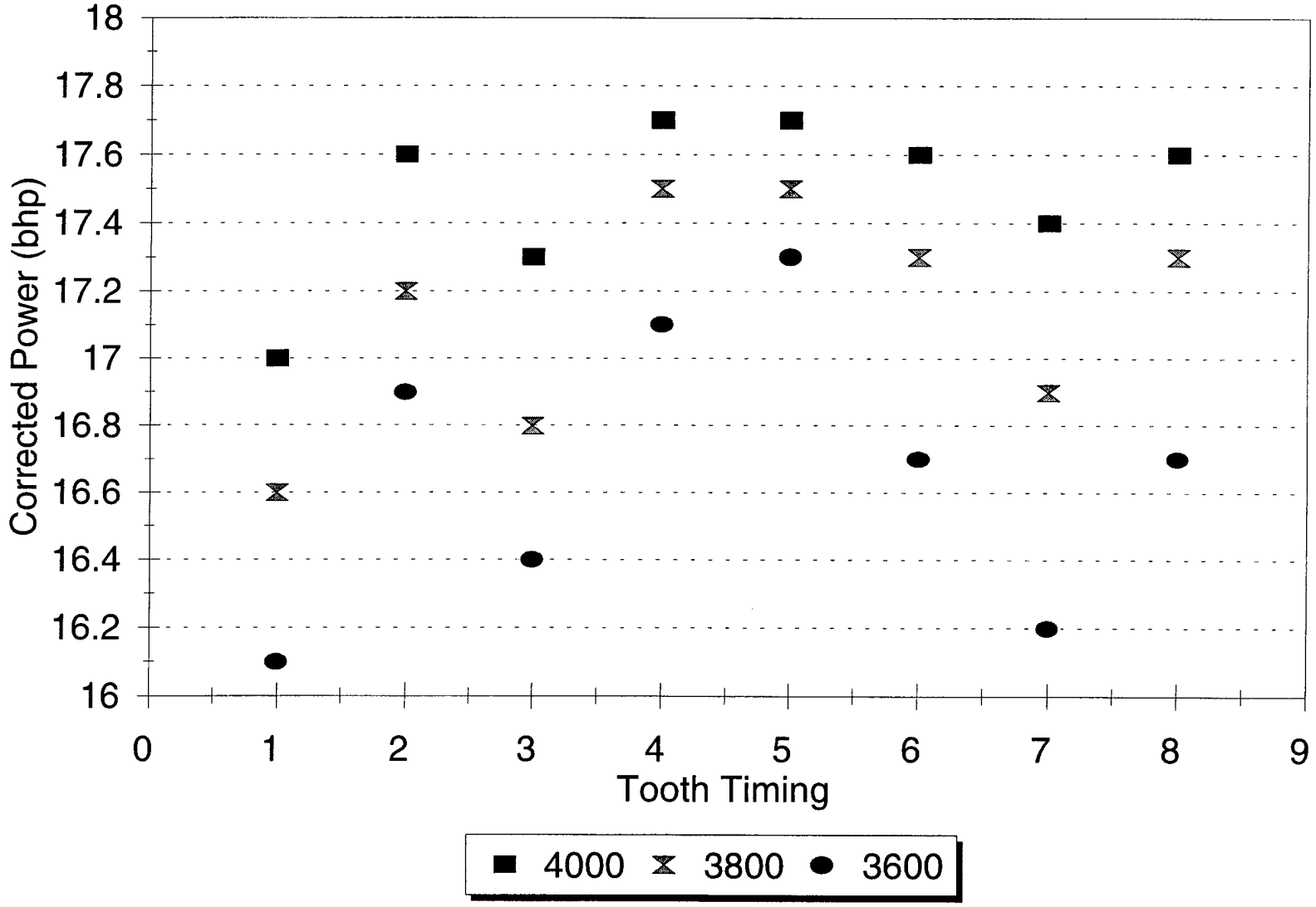

FIGURE 10. PORT INJECTION, MAXIMUM POWER VS. INJECTION TIMING

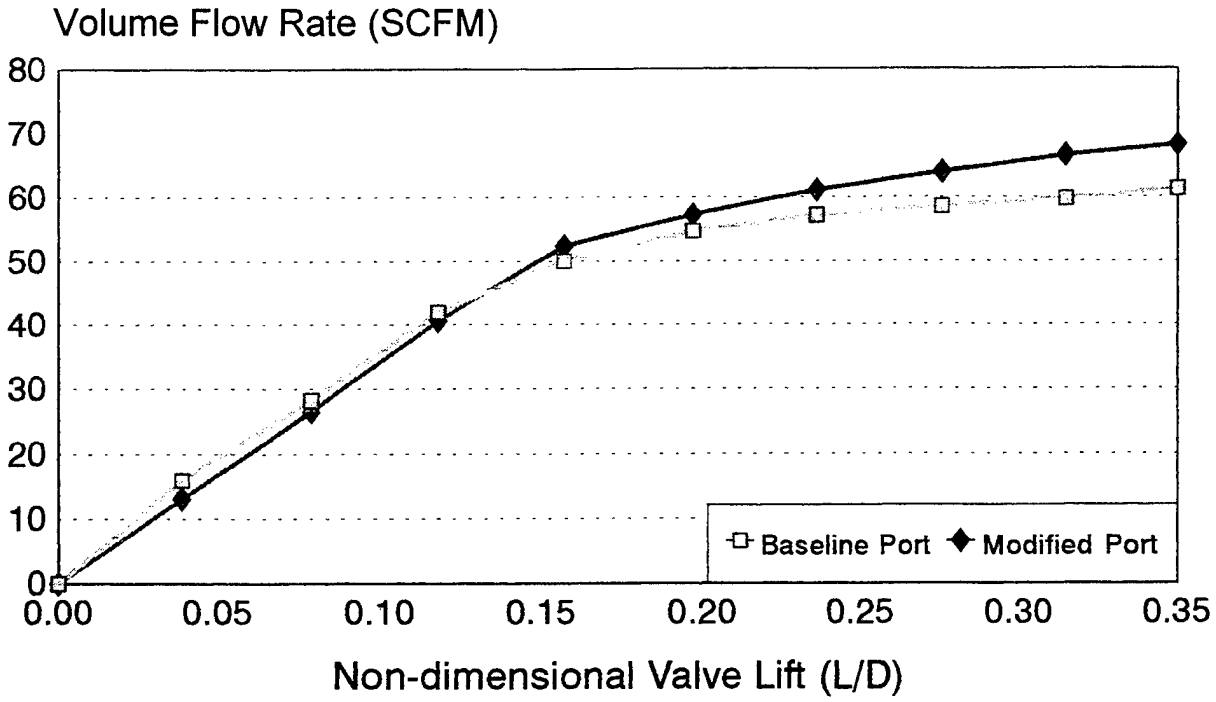

FIGURE 11. CH-22 INTAKE PORT FLOW COMPARISON

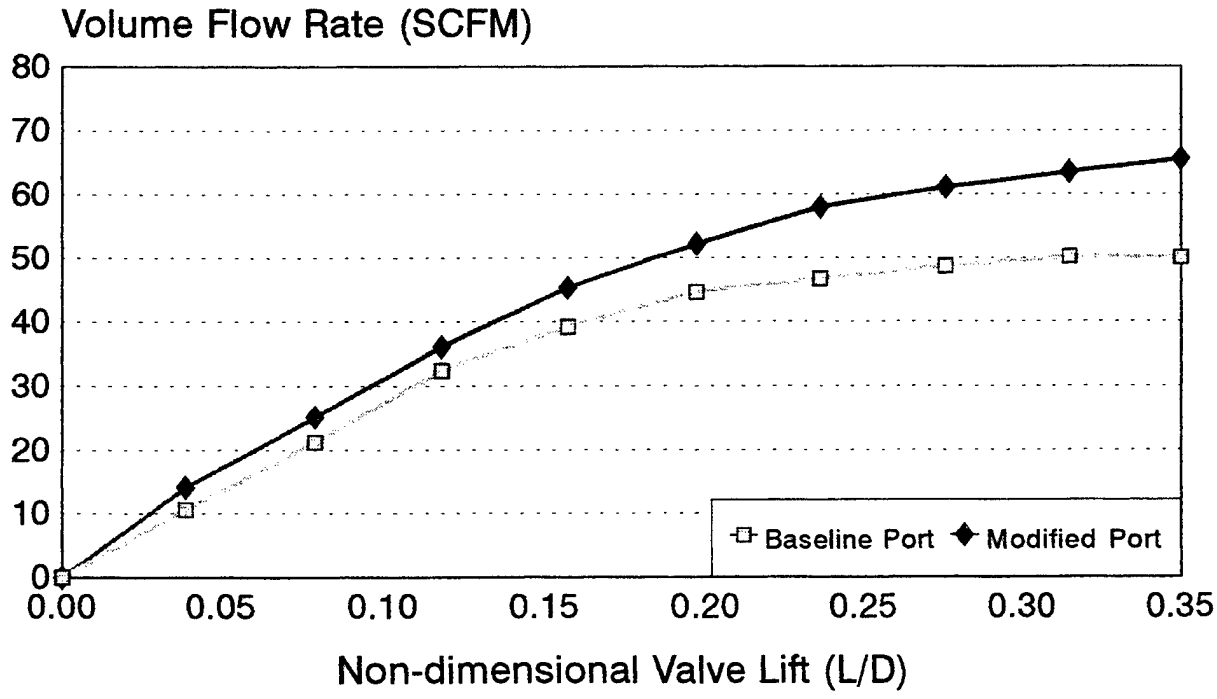

FIGURE 12. CH-22 EXHAUST PORT FLOW COMPARISON

The exhaust port was modified by increasing the available flow area in the transition between the horizontal and vertical runners. Material was removed, and the transition was made as smooth as possible. The port surfaces were lightly polished to improve flow and reduce heat transfer within the exhaust port. The exhaust port was re-tested, as shown in Figure 12, resulting in significant flow improvements at all valve lifts. At high lifts, flow increased by approximately 25 percent. These relatively simple modifications resulted in measurable improvements in volumetric efficiency and power density.

2.1.3.5 Piston Modifications

Methane has a much higher octane rating, or knock resistance, than gasoline. Common natural gas blends contain about 90-95 percent methane and have octane numbers over 130. This compared to typical gasoline blends with octane numbers under 90. This means that higher compression ratios can be tolerated when operating on natural gas. It is advantageous to raise the compression ratio since the result is increased power and efficiency. The Kohler CH22 has a compression ratio of 8:1 in stock form. Natural aspirated spark ignition engines have been run at compression ratios in excess of 15:1.

It was determined that overall engine efficiency could be improved through the use of a higher compression ratio, which was allowed due to the higher octane rating of compressed natural gas. The production Kohler Command 22 piston has a relatively deep dish and slightly negative deck height. SwRI estimated that an increase in compression ratio in the area of 10:1 up to 14:1 would provide significant improvements in efficiency and power density.

To keep prototype design and fabrication time to a minimum, it was determined that a suitable existing piston design be modified for use with the Kohler engine. Such a piston was found available in blank form from Arias Pistons for the Yamaha FJ1200 motorcycle engine. This was a forged piston design, which provided superior strength compared to the cast Kohler production piston, with a small increase in mass. The pistons were ordered from Arias through consultant Glenn O'Neal, who machined the ring grooves to match the production Kohler piston rings. Arias provided the pistons with ½" additional crown height to facilitate machining of any required piston dome at a later date. The piston ring depth was raised slightly compared to the production piston in order to reduce the dead volume above the top ring. This was intended to help reduce trapped hydrocarbon emissions. The wrist pin bores in the piston were sized to match the Kohler connecting rods, and a high strength, lightweight wrist pin was obtained to work with the pistons. The wrist pins were retained by circlips in this design.

For a 10:1 compression ratio, SwRI milled the pistons flat with a zero deck height. Since a higher 14:1 compression ratio was also desired for testing, a domed piston was also designed. The dome outlined the shape of the combustion chamber, with a radiused transition to the piston deck surface. The final 14:1 dome design was made in 3-D CAD, and transferred to Mastercam for CNC toolpath generation. A three axis CNC controlled milling machine in the SwRI machine shop was used to cut the domes first into wax for verification, and then into the prototype pistons. The underside of the pistons were machined in the wrist pin boss areas to match the weight between the 10:1 and 14:1 piston sets.

Both the flat-top and domed pistons were tested in the engine, without any problems. The increased loading on the pistons due to the higher compression ratios did result in failure of a stock Kohler connecting rod, but this was later rectified through an SwRI redesign of the rod. The high compression ratio pistons made a significant contribution towards power and efficiency goals for the project.

Figure 13 shows the performance of the engine operating with increased compression ratio. This is the final power data (i.e., maximum power output on CNG). An illustration of the thermal efficiency levels achieved with the final engine concept is shown in Figure 14. The figure shows thermal efficiency using lower heating value over the engine's entire operating range. Note the data in the figure also represents the flow improvements from the cylinder head modifications.

2.1.3.6 Connecting Rod Modifications

During the course of engine testing, a catastrophic engine failure was experienced. Upon investigation, it was found that a connecting rod failure was experienced near the wrist pin. Based on force calculations performed by SwRI, it was determined that the increased forces on the connecting rod, associated with the increased compression ratio, were the likely cause of the failure. This conclusion was supported by a second failure of a similar engine. Given this, it was decided that a new connecting rod be designed to withstand the increased compression forces of the modified CNG engine. The upgraded connecting rods were designed, fabricated, and tested at SwRI and found to solve the problem. The upgraded connecting rod is shown in Figures 15 and 16. Details of the upgraded connecting rod design are contained in the following paragraphs.

As previously noted, shortly after installation of the high compression ratio pistons, the Kohler engine experienced failure of a stock connecting rod. Analysis of the failure showed that the upper end of the rod beam split vertically, starting from the base of the wrist pin bore in the small end of the rod. It was determined that a combination of increased loading from the high compression ratio pistons and inadequate lubrication of the wrist pin bore with the stock connecting rod design were responsible for failure. The other connecting rod in the same engine was also analyzed and found to have galling of the wrist pin bore, indicating that failure of the second rod would have happened shortly thereafter.

Based on this analysis, SwRI decided to redesign the connecting rods in the engine for improved strength and durability under higher load conditions. Since the production connecting rod was made of cast aluminum and was relatively light, the new design needed to increase strength with minimal increase in mass. It was determined that 6061-T6 aluminum had the best combination of strength to weight ratio, cost, and machinability for the new rod design. 7075 aluminum alloy was originally considered until it was realized that the high oil sump temperatures in this air-cooled engine resulted in lower strength properties of the 7075 alloy at elevated temperatures compared to the 6061 alloy. Titanium was also considered, but was regarded as too expensive and difficult to machine for this application.

The bottom end (or main journal end) of the new connecting rod design was basically left the same as the original design, with some material removed in less critical areas for weight savings. The beam of the rod was redesigned to take advantage of the superior strength of the 6061-T6 alloy (as compared to the stock cast material), particularly in the direction where bending stresses were

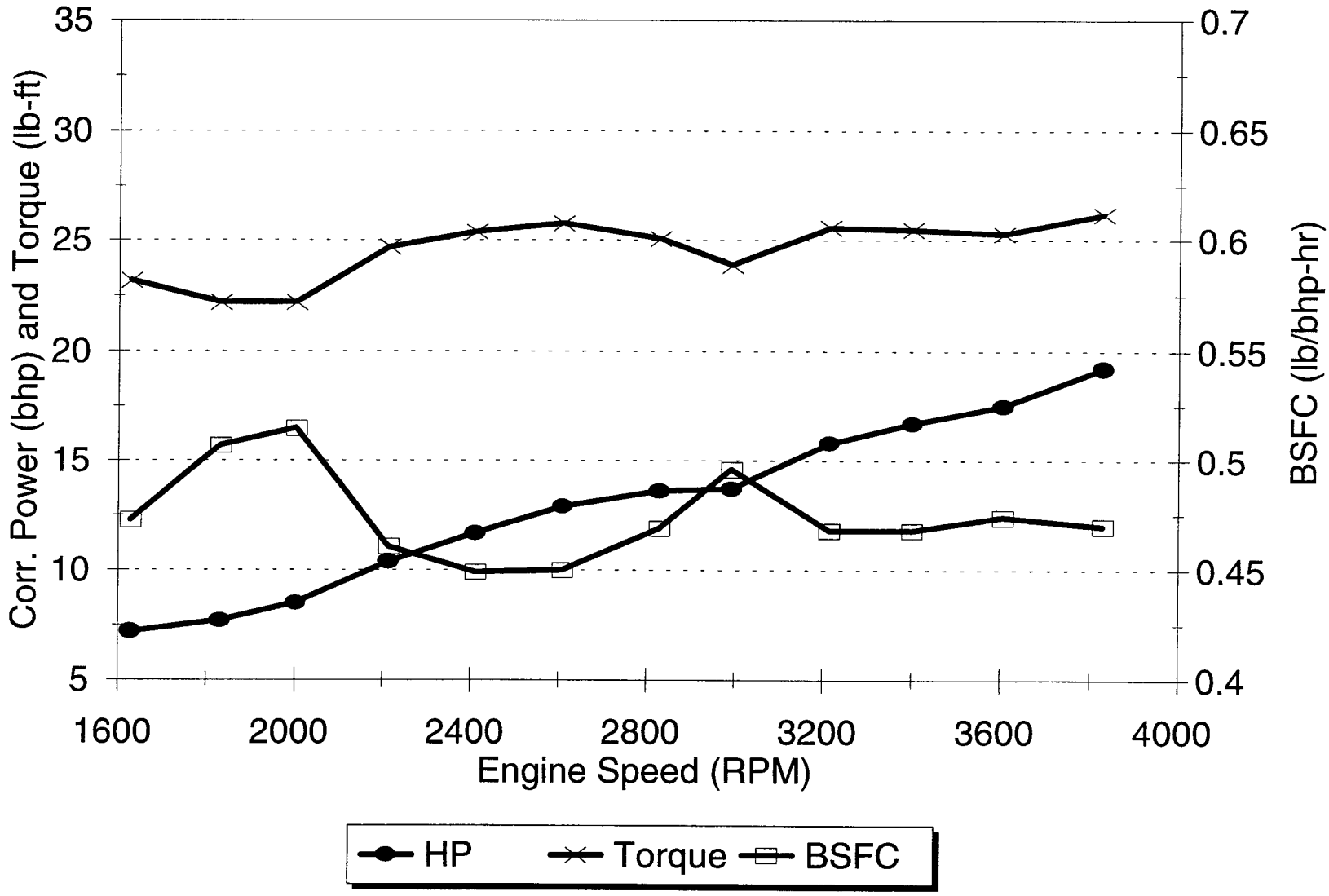

FIGURE 13. CH-22 NG ENGINE PERFORMANCE, 12:1 CR/PORTED HEADS

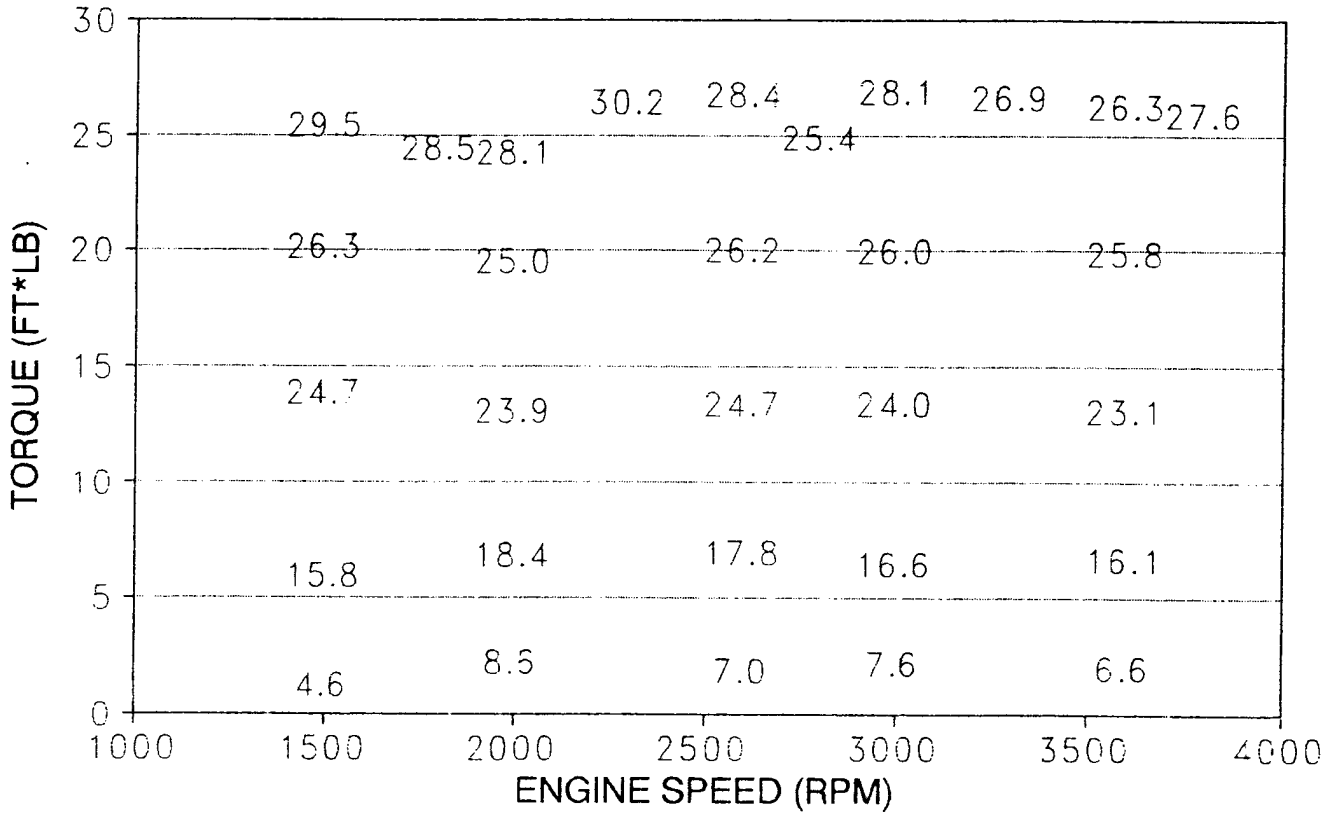

FIGURE 14. FINAL ENGINE THERMAL EFFICIENCY MAP WITH MIRATECH CATALYST

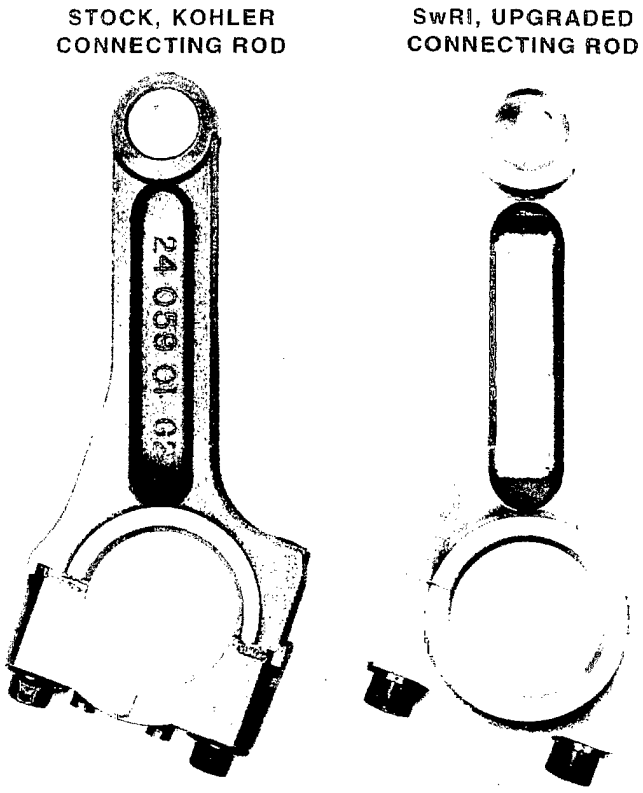

FIGURE 15. KOHLER ENGINE CONNECTING RODS, STOCK VS. SwRI DESIGN

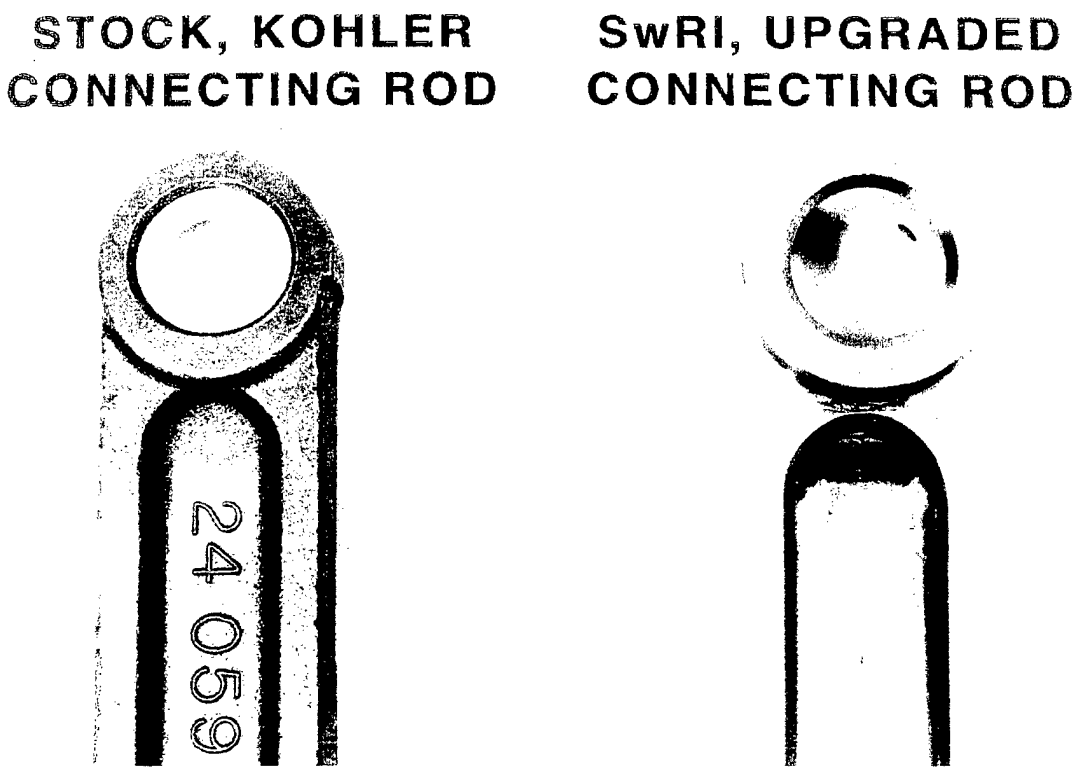

FIGURE 16. CLOSE-UP VIEW OF CONNECTING ROD COMPARISON

After the design was completed, the connecting rods were machined from a billet of 6061-T6 aluminum. Steel dowel pins were added for alignment of the connecting rod cap, along with grade 8 fasteners. The cap was installed on the rod for final boring of the main journal. Both ends of the rods were finish honed to the appropriate size. The upper end oil holes were chamfered to enhance oil retention in the wrist pin area.

The resulting connecting rod weighed within 5% of the stock cast rod, with much improved strength and upper end lubrication characteristics. The prototype pistons were machined in the wrist pin area to allow for extra clearance of the wider wrist pin boss of the new connecting rods. After an initial run-in period with the new connecting rods, the rods were removed and examined, and no galling or preliminary indications of failure were found. The connecting rods were re-installed, and testing resumed without any additional connecting rod failures.

2.1.4 CNG Engine Performance/Emissions Testing

SwRI contacted catalyst suppliers to select an appropriate three-way catalyst for the test engine. A sample catalyst was obtained from Johnson Matthey. This catalyst was equipped with a heating coil for electrical pre-heating of the catalyst for rapid light-off during cold starting conditions. The catalyst was installed on the test engine and mapped for emissions. Catalyst conversion efficiency for NO_x, CO, and THC emissions was measured over a range of operating conditions and fuel-air equivalence ratios near stoichiometry. The pre- and post-catalyst emissions, at full-load conditions, are shown in Figures 17 through 19. Note that post-catalyst emissions are shown with and without the electrically-heated catalyst (EHC).

Close attention was paid to catalyst light-off temperature. In order to minimize vehicle emissions, it is important to insure proper catalyst performance at any engine operating condition used during vehicle operation. Furthermore, it is also important that the catalyst become effective (i.e., catalyst light-off) quickly upon engine startup. For this reason, the Johnson Matthey catalyst was equipped with an electrically-heated element. The intent was to use the heater element only during and shortly after engine start up. For emissions testing, catalyst conversion efficiency was measured both with and without the heating element active. Small improvements in catalyst efficiency were measured with electrical power applied to the heater.

As can be seen from the data, the conversion efficiencies measured from the Johnson Matthey catalyst were less than desirable. Expected conversion efficiencies from a "good" catalyst were hoped to be in upwards of 95 percent conversion of CO and NO_x, and 90 percent conversion of THC. Since the conversion efficiencies of the Johnson Matthey catalyst were found to be well below these levels, a catalyst from a second supplier was sought.

A sample catalyst from Miratech was secured for testing on the engine. Miratech had supplied catalysts for another natural gas engine project at SwRI. Very high conversion efficiencies were measured for the Miratech catalyst used on that project. The Miratech catalyst was not equipped with an electrical heating element. This was not considered to be major obstacle considering that the initial focus would be on achieving increased catalyst conversion efficiencies under hot conditions.

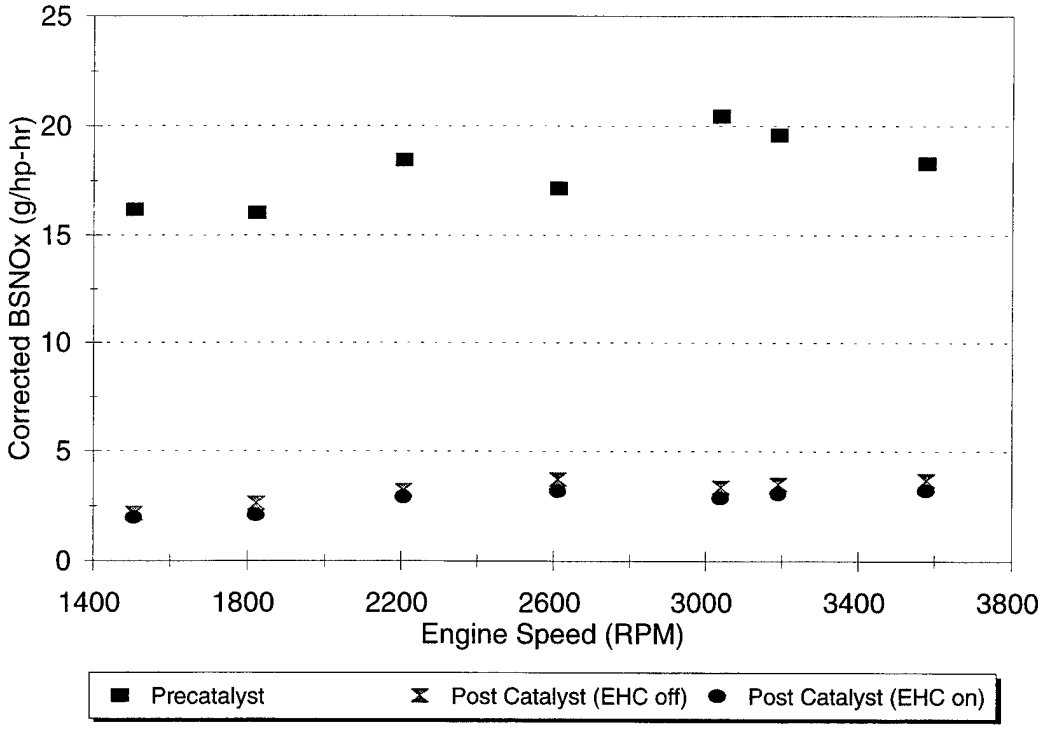

FIGURE 17. WOT NO_x EMISSIONS, JOHNSON MATTHEY CATALYST

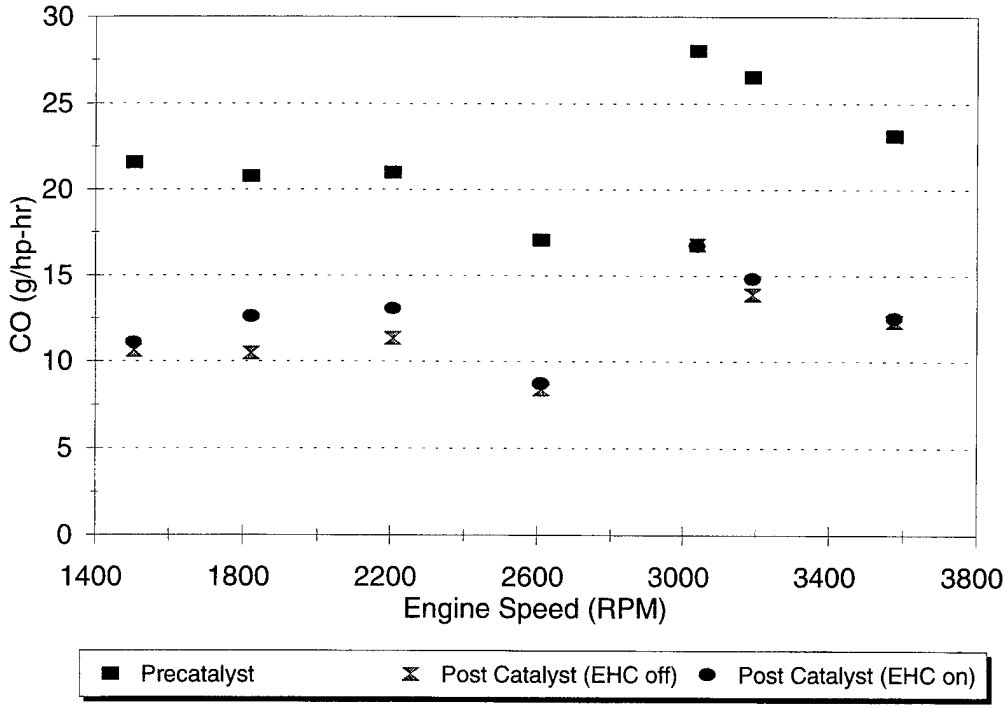

FIGURE 18. WOT CO EMISSIONS, JOHNSON MATTHEY CATALYST

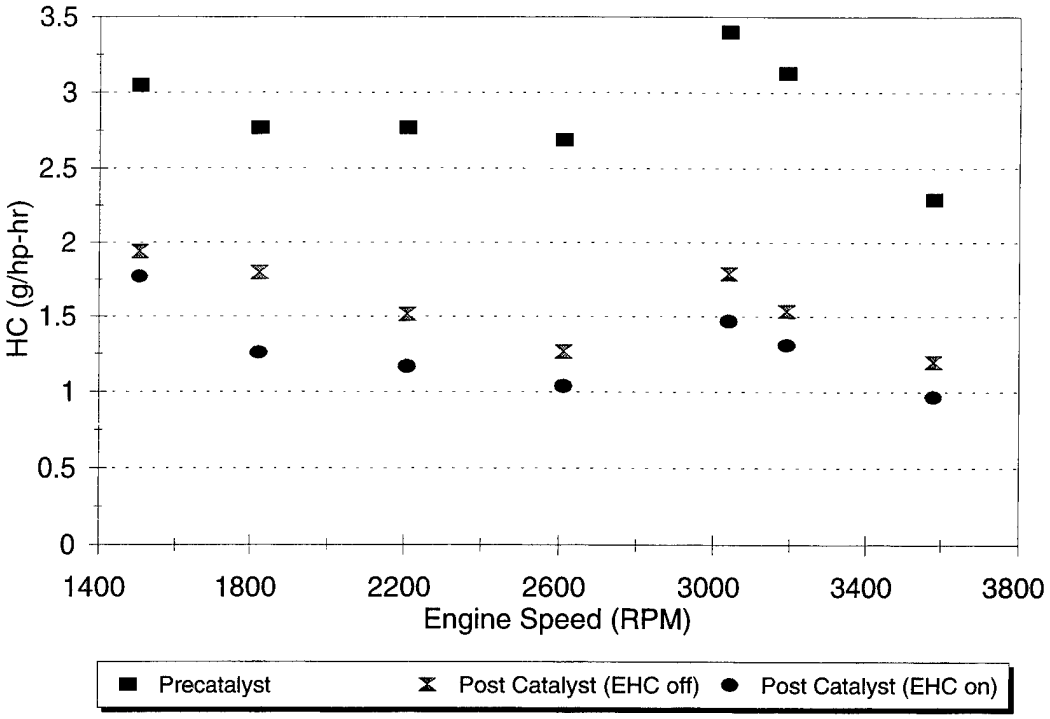

FIGURE 19. WOT HC EMISSIONS, JOHNSON MATTHEY CATALYST

A sample catalyst from Miratech was secured for testing on the engine. Miratech had supplied catalysts for another natural gas engine project at SwRI. Very high conversion efficiencies were measured for the Miratech catalyst used on that project. The Miratech catalyst was not equipped with an electrical heating element. This was not considered to be major obstacle considering that the initial focus would be on achieving increased catalyst conversion efficiencies under hot conditions.

The Miratech catalyst was emissions tested on the engine at SwRI under the same operating conditions and equivalence ratios evaluated during the previous catalyst testing. The conversion efficiencies, engine-out, and catalyst-out NO_x, CO, and THC emissions are shown in Figures 20 through 28. As can be seen from the data, extremely high conversion efficiencies were achieved using the Miratech catalyst at virtually every engine condition tested. Conversion efficiency of THC was found to be the lowest at low speed, light-load operation. This is due to the reduced exhaust temperatures at those low power conditions. NO_x conversion was also found to be above 99 percent at all conditions except those near idle. CO conversion was found to be above 97 percent at all conditions tested, and roughly 99 percent at most operating conditions. Catalyst-out emissions were found to be at or below equivalent zero emissions or Best Available Control Technology (BACT) levels as specified by the South Coast Air Quality Management District (SCAQMD). Catalyst degradation as a function of time was not measured, although the catalyst accumulated over 20 hours of operation prior to final emissions testing.

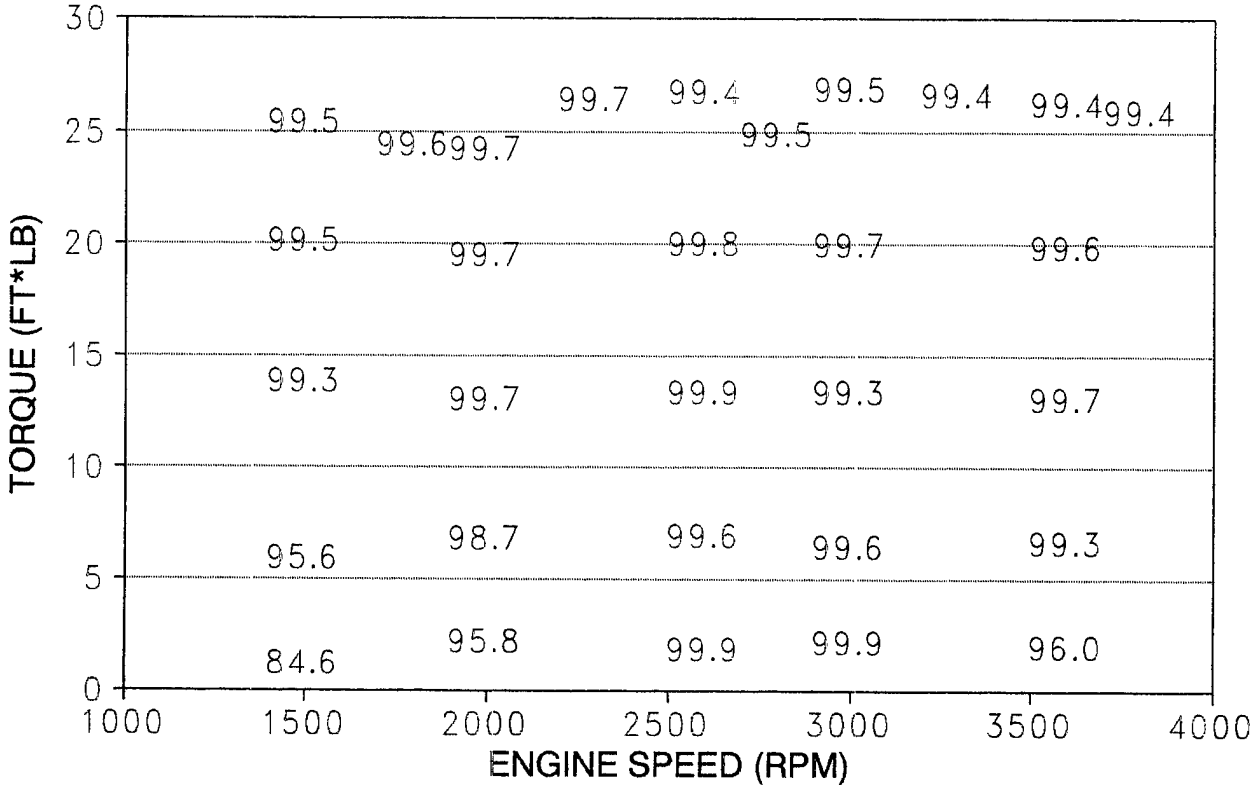

FIGURE 20. NO_x CONVERSION EFFICIENCY (%), MIRATECH CATALYST

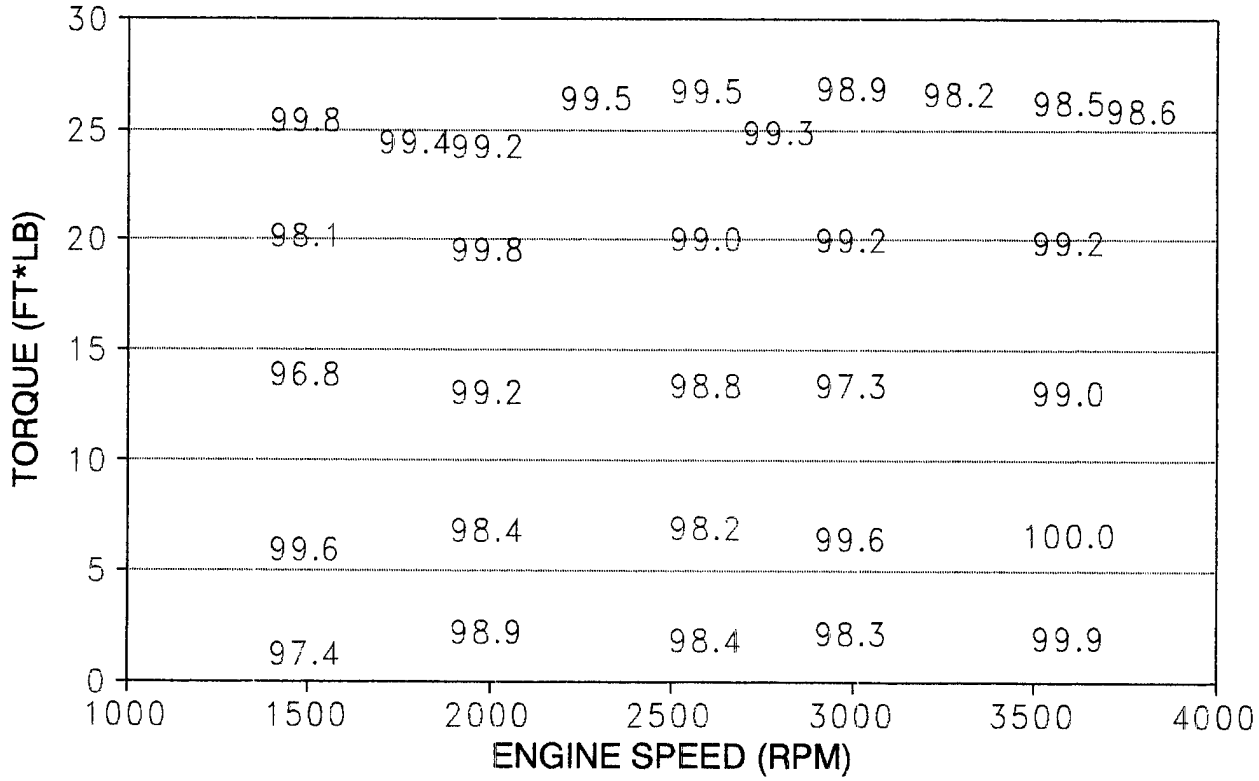

FIGURE 21. CO CONVERSION EFFICIENCY (%), MIRATECH CATALYST

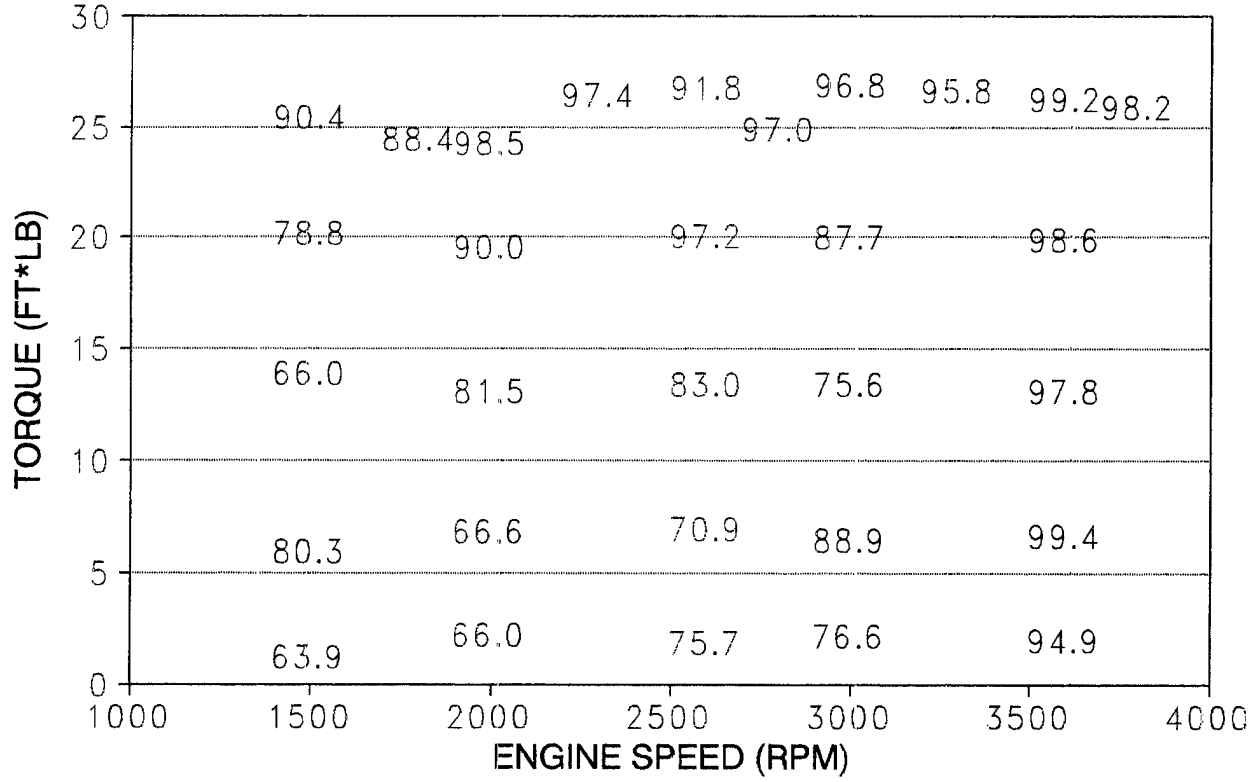

FIGURE 22. HC CONVERSION EFFICIENCY (%), MIRATECH CATALYST

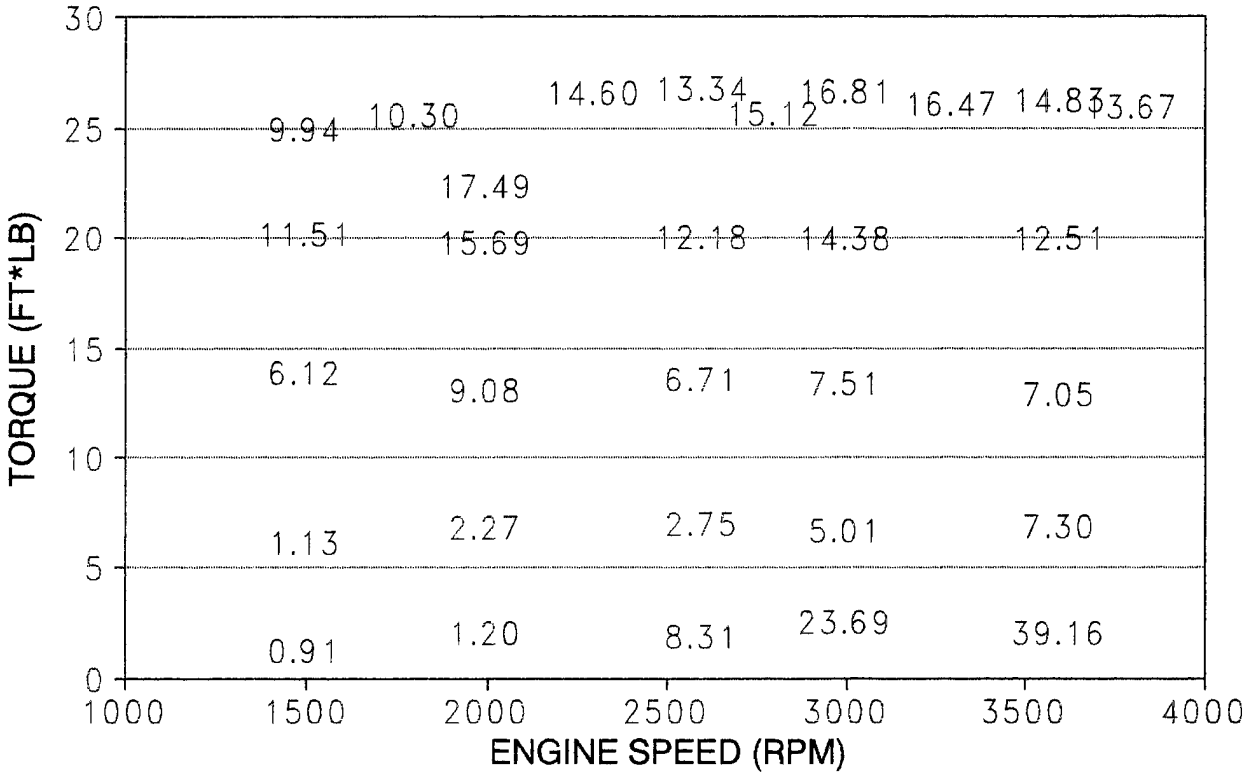

FIGURE 23. PRE-CATALYST BSNO$_x$ (G/BHP-HR), MIRATECH CATALYST

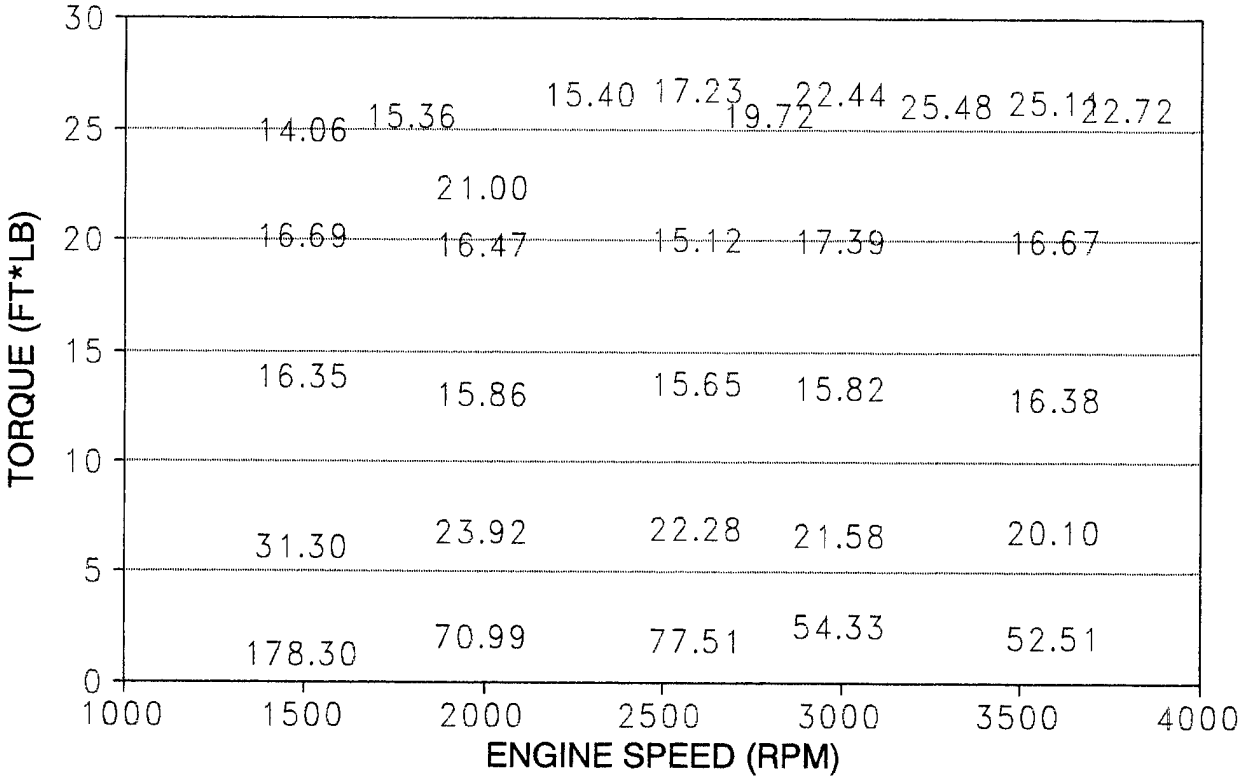

FIGURE 24. PRE-CATALYST BSCO (G/BHP-HR), MIRATECH CATALYST

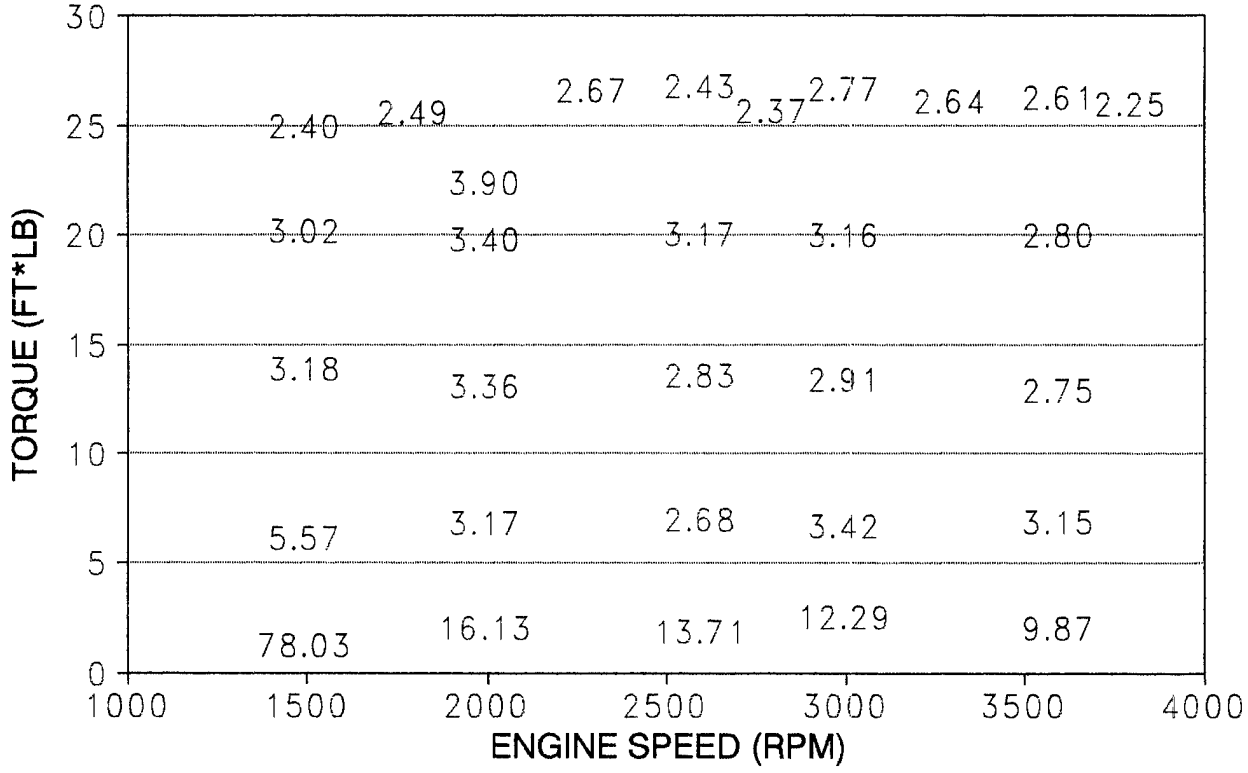

FIGURE 25. PRE-CATALYST BSHC (G/BHP-HR), MIRATECH CATALYST

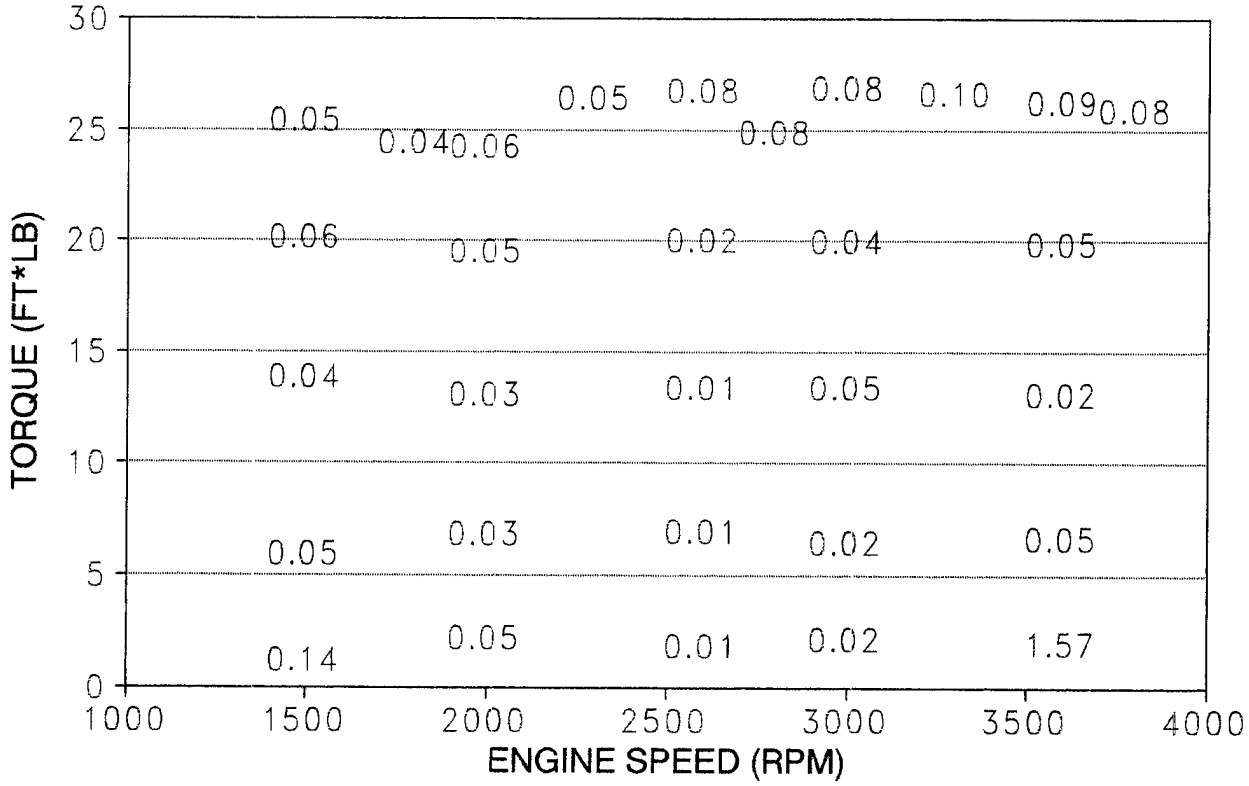

FIGURE 26. POST-CATALYST BSNO$_x$ (G/BHP-HR), MIRATECH CATALYST

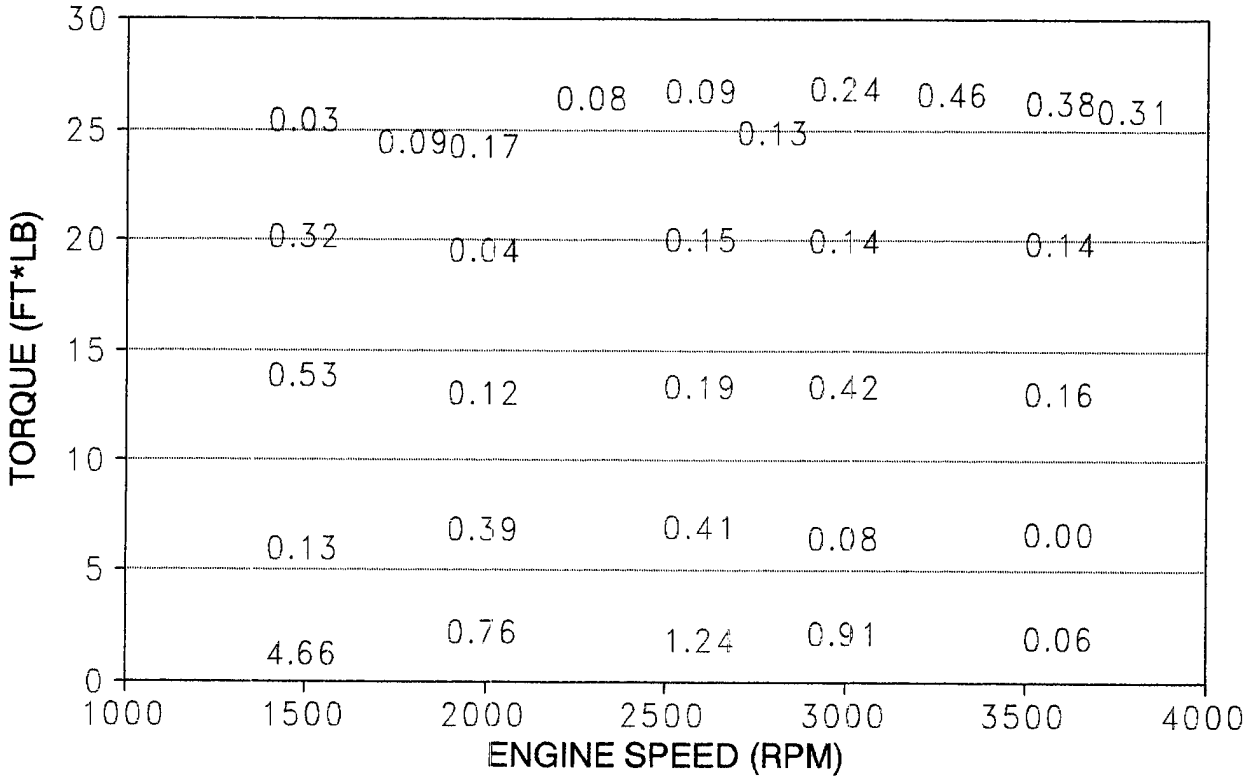

FIGURE 27. POST-CATALYST BSCO (G/BHP-HR), MIRATECH CATALYST

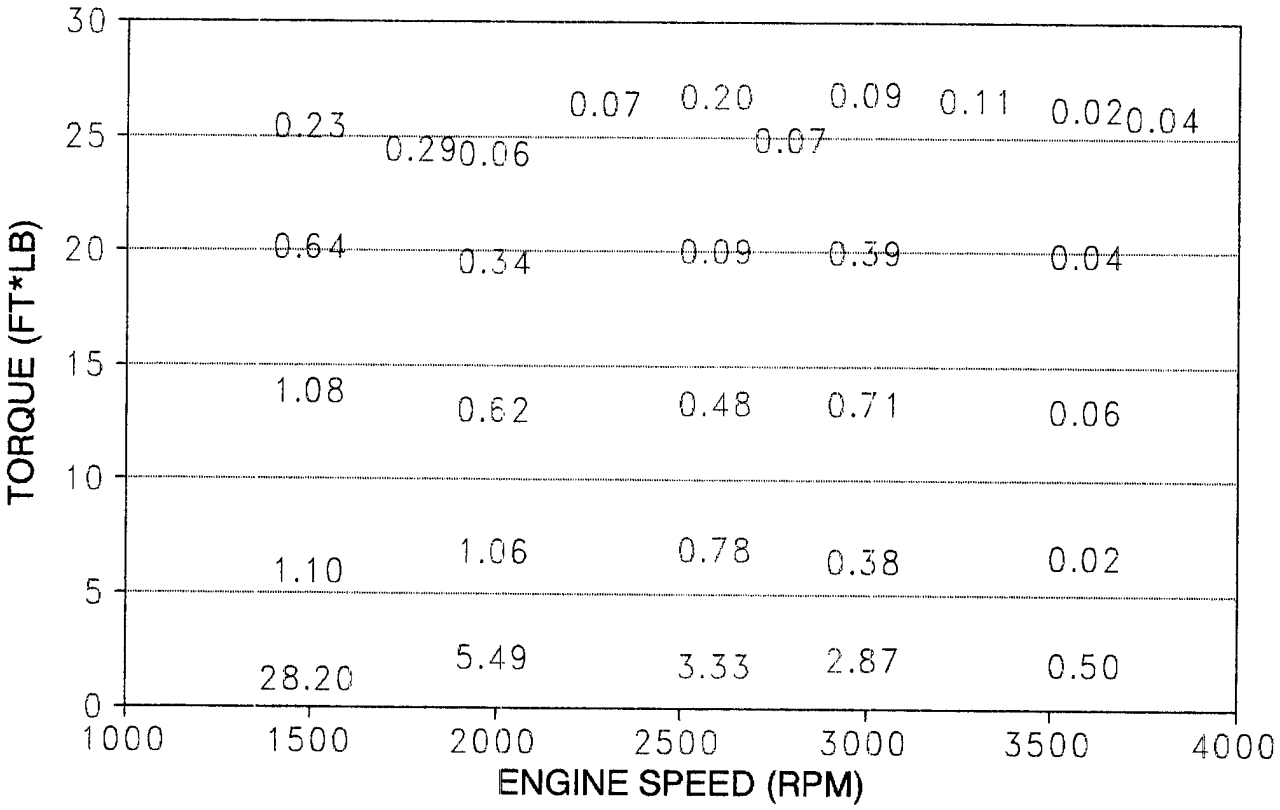

FIGURE 28. POST-CATALYST BSHC (G/BHP-HR), MIRATECH CATALYST

2.1.5 Engine Modeling

An engine modeling effort was undertaken to aid in the task of increasing engine power output. SwRI's VIPRE cycle simulation software was used in the modeling effort. Details of the engine modeling effort are described in Appendix A of this report.

2.1.6 Engine Acoustic Testing

Engine acoustic noise was believed to be an important issue in the vehicle application of the APU. During the engine development process, engine acoustic testing was performed to quantify the acoustic signature of the engine at various operating conditions and physical locations. The results of the acoustic testing were used to help select a suitable muffler for the engine to reduce engine exhaust noise. The details of the engine acoustic testing are contained in Appendix B.

2.2 APU Control System Development

As part of the APU system which SwRI was tasked to deliver on the project, an APU control system was necessary to provide control of the engine operating point and control the battery charging profile. SwRI designed and constructed a PC-based APU/Energy Management control system to accomplish these functions. The SwRI-developed controller was a design based on its Rapid Prototyping Electronic Control System (RPECS) platform. The RPECS is a highly flexible PC-based prototyping tool used for real-time control in a variety of applications from engine and powertrain control to test cell control and many others.

The APU control system was developed and tested with all other APU components at SwRI. The APU control system was shipped to Solar Car Corporation, along with the remainder of the APU hardware. It was installed in the vehicle and successfully stand alone tested on the S-10 pickup at Solar Car in April 1995.

2.2.1 Control Functions

The SwRI APU controller was designed to provide numerous control functions as related to the APU components and battery pack. Fundamentally, the APU controller provided control of the APU operating point through manipulation of the engine throttle and control of the generator output via the voltage boost unit. The APU controller also computed the state of charge of the battery pack and adjusted the charging current accordingly to maintain adequate charging of the batteries on the vehicle. In addition, the APU controller was responsible for the engine start and stop functions, as well as control of the electrically-heated catalyst (EHC) heater function. The EHC function was not ultimately used since the final catalyst configuration was not electrically heated.

2.2.2 Controller Hardware Platform

As previously noted, the APU controller platform was based on an industrial PC. The controller utilized a commercially available 486 66MHz CPU card, with a 1.44 MB solid state RAM disk emulator as the primary memory device. The controller utilized commercially available data acquisition and control cards, as well as a commercial watchdog timer board for protection. The controller enclosure for the APU controller is shown in Figure 29. In order to provide the necessary signal conditioning and driver circuitry for interfacing with the APU hardware, a custom interface enclosure was designed and constructed by SwRI. Electrical power for the control system, on the vehicle, was provided via a 500 Watt inverter through a single 12 VDC connection.

2.2.3 Control Software/Algorithm Descriptions

The APU control software was written in C language and executed in the MS DOS environment. The control software was written to utilize floating point arithmetic in order to allow modifications to be made to the algorithms with minimum development time. The 486 processor capably executed all control equations in a time-based interrupt driven routine operating at 100 Hz. Because the system was built around the existing SwRI RPECS platform, built-in functions such as real-time plotting and datalogging were easily integrated into the control system. A detailed description of the APU control algorithms is contained in the following paragraphs.

The APU controller's most fundamental function was to control the power output of the APU. APU power output was modulated in accordance with the average power needed at the traction motor in conjunction with the desired charging current (which was dependent on the state of charge of the batteries). The battery state of charge calculation was based on an integration of power into and out of the battery pack. The state of charge calculation also had a reset function at no-load conditions based on the no-load battery voltage level. This function would reset the power integration periodically to eliminate the accumulation of error from inaccurately modeled or neglected effects.

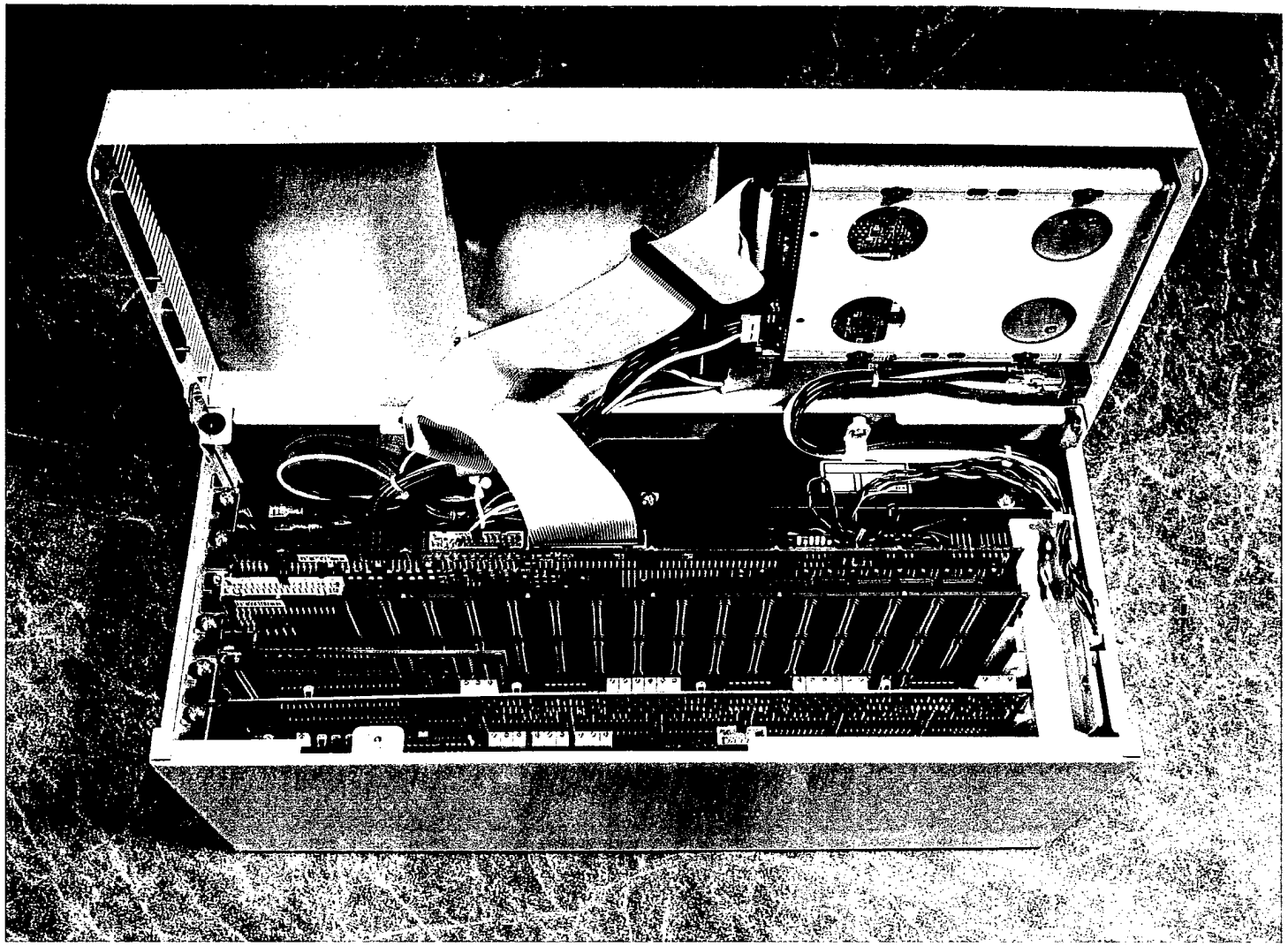

FIGURE 29. PROTOTYPE APU CONTROLLER

curve of the engine. Therefore, the engine operation trajectory programmed into the APU controller entailed transitioning the engine to the wide open throttle point at the lowest engine speed (i.e., 1500 RPM), and running the engine at WOT up to the maximum power point of the engine (i.e., 3800 RPM). In turn, if the desired power output from the APU was set above roughly 4 kW, the engine was always operated at WOT. Only when the desired APU power output was less than 4 kW was the engine operated at a less efficient, part-throttle condition. This approach was anticipated to provide the benefits of both maximum vehicle fuel economy and minimum vehicle emissions.

Having computed the desired engine speed and throttle position, the APU controller first provided the necessary signal to the throttle actuator in order to achieve the desired action. The engine throttle actuator was driven with a standard pulse width modulated (PWM) signal of a variable duty cycle. In order to achieve the desired engine speed, the APU controller utilized information from an engine speed sensor for feedback control. In order to control engine speed, the APU controller modulated the load applied to the engine via the generator. The generator control was provided through a voltage boost controller provided by SuperPower Inc. Through manipulation of the voltage boost controller, the output voltage of the generator and thus the load could be controlled. The APU power control functions, including the state of charge calculation function, are shown in block diagram form in Figure 30.

In addition to the APU power output control function and energy management functions, the APU controller also provided control of the engine start and stop functions. The engine start control was accomplished by controlling the stock starter motor on the Kohler engine. The APU did not have the ability to start the engine via motoring from the generator. Engine stop was accomplished through control of the 12 VDC power available to the engine control system. Also, in order to accommodate the EHC, the APU controller was also capable of controlling a relay to energize the heater on the EHC for pre-heating prior to engine start. This function was ultimately not necessary since the final catalyst was not electrically heated.

In conjunction with the control functions and algorithms previously described, the APU controller also had a limited set of diagnostics designed into it. Out of range diagnostics for each of the sensors used by the APU controller were implemented to detect and react to sensor failures. Furthermore, system level diagnostics and protections were built into the APU controller to detect and prevent APU operation that could damage the unit, (i.e., engine protection diagnostics). The diagnostic functions of the APU were designed to be sufficient to prevent operation that could cause permanent damage to the unit and also could provide valuable information for diagnosing problems should they occur.

2.3 APU Integration/Testing

The components which made up the APU system for the S-10 vehicle, i.e., the engine, generator, engine controller, APU controller, and voltage boost controller were integrated and stand alone tested both at SwRI before shipment and at Solar Car after initial installation on the vehicle. The performance of the system was found to be satisfactory in each environment. Since the drive motor system for the S-10 vehicle was not delivered before the end of this project, the APU has not been tested in a completely integrated vehicle environment.

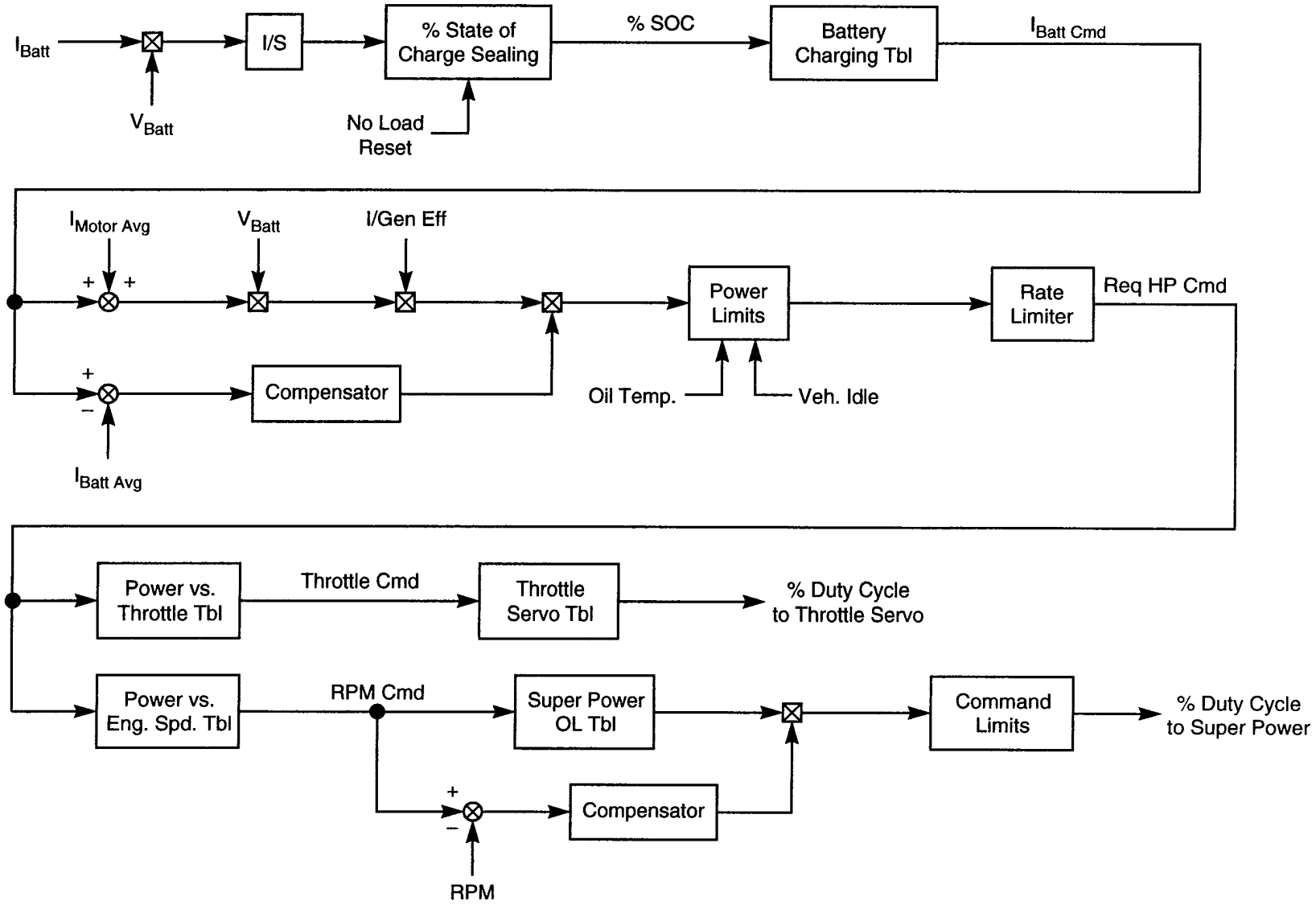

FIGURE 30. APU CONTROL STRATEGY BLOCK DIAGRAM

alone tested both at SwRI before shipment and at Solar Car after initial installation on the vehicle. The performance of the system was found to be satisfactory in each environment. Since the drive motor system for the S-10 vehicle was not delivered before the end of this project, the APU has not been tested in a completely integrated vehicle environment.

2.3.1 Laboratory Environment

Prior to shipment of the APU to Solar Car, the components were integrated together and tested in the laboratory environment at SwRI. For purposes of this testing, a battery pack consisting of 20-12V lead acid batteries, and a resistive load bank were used to simulate the vehicle battery pack and drive system load, respectively. Various load step transients were used to simulate the changing load of the drive system in order to test the response and stability of the APU controller and all APU subsystems. Performance of the APU system was found to be quite favorable in all aspects including APU efficiency, response, and stability. Upon completion of the APU testing at SwRI, the APU system was shipped to Solar Car for vehicle installation.

2.3.2 Vehicle Environment

The APU system was initially installed in the S-10 vehicle by Solar Car personnel. Initially, the engine/generator, along with the engine control system, was installed at the rear of the vehicle underneath the bed of the truck. This was done since it was believed that inadequate space was available in the engine compartment due to the location of other vehicle components. The APU controller was installed in the cab behind the passenger's seat. The voltage boost controller was installed in the engine compartment. Photographs of the initial vehicle installation of the APU hardware at Solar Car are included in Figures 31 and 32.

In order to verify the performance of the APU system, once integrated into the vehicle, SwRI personnel went to Solar Car to debug the vehicle installation and test the APU under similar conditions to those at SwRI. Testing of the APU system at Solar Car involved charging into a charge depleted battery pack, as no resistive load bank was available at their facility. The final APU stand alone testing was completed at Solar Car and the APU performance was found acceptable.

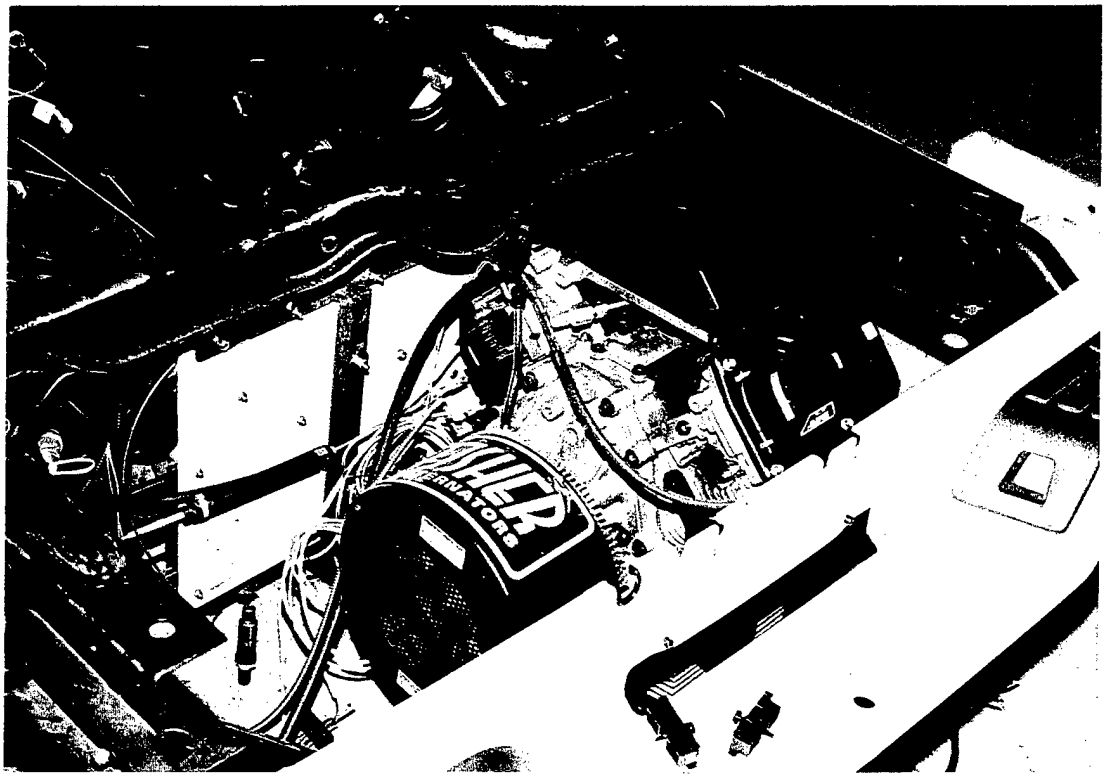

FIGURE 31. SwRI APU INSTALLED IN S-10 VEHICLE (REAR MOUNT)

FIGURE 32. PROTOTYPE APU CONTROLLER HARDWARE IN S-10 VEHICLE

3.0 SUMMARY

A natural gas-powered APU was developed and integrated into an S-10 hybrid electric vehicle. The APU utilized a modified Kohler CH-22 engine, a Fisher permanent magnet generator, and appropriate control and power electronics to produce a regulated DC output suitable for charging a battery pack from a range of roughly 100 VDC to 300 VDC. Maximum electrical power output from the APU was approximately 13 kW.

The engine for the APU was developed and optimized for operation on natural gas and utilized an electronic engine control system for enhancement of the performance and emissions characteristics of the engine. Engine thermal efficiency levels, as high as 30 percent (using lower heating value), were measured from the final engine configuration. Extremely low emissions levels, (i.e., at or below those levels deemed by CARB as Equivalent Zero Emissions Vehicle), were achieved from the engine using a three-way catalyst system from Miratech, paired with a precisely calibrated fuel control system. In addition, maximum engine power output essentially equal to the original gasoline engine configuration was achieved using natural gas fuel.

A prototype APU control system was developed by SwRI for energy management, battery charging profile management, and control of APU power output. The prototype controller was designed around a personal computer platform for maximum flexibility in control algorithm development, control system calibration, and sensor and actuator flexibility. The resultant APU controller, along with its signal conditioning electronics, was integrated into the vehicle cab area unobtrusively, behind the passenger's seat.

4.0 RECOMMENDATIONS

The APU was successfully developed for the project. The APU delivered adequate power output, with high efficiency, and ultra-low emissions. However, in order to improve and bring the concept into commercial viability, SwRI has the following recommendations.

First, an alternative engine should be considered. The primary consideration for the APU development was to achieve higher power output. Originally, a 16 kW APU was thought necessary for the vehicle in order to achieve a target vehicle cruise speed of 65 mph. Given this and assuming a 90 percent efficiency level for the generator and boost regulator electronics, the necessary power output from the engine was about 24 hp. None of the Kohler engines tested at SwRI, (including the CH25 gasoline engine), produced above 21 hp. By starting out with an under-powered engine, it was necessary to push the base engine to its limits, (and occasionally beyond its limits), in terms of compression ratio and flow increases. Furthermore, the Kohler CH22 and CH25 engines are not designed for the high-duty cycle operation needed for this APU application. As a result of these factors, the durability of the engine in this application is less than desirable. Also, in order to minimize the acoustic noise from the engine and to simplify the vehicle installation requirements, a water-cooled engine would be better suited for the APU application.

Secondly, in order to vastly improve the installation of all the electronic subsystems on the vehicle, the electronics subsystems should be integrated into a single package. On the S-10, the engine control system, APU control system, and boost regulator are all separate electronic subsystems. Each of these systems has its own space and electrical power requirements. These subsystems should be integrated together into a single hardened electronic subsystem. This same concept could be carried through to include the drive motor control system. This approach would likely result in the most cost effective approach as well. A closely related topic to integrating the electronic subsystems is to utilize a field controllable generator. Utilizing a generator of this type would eliminate the need for the large and costly boost regulator controller. The boost regulator controller could be substituted for a simple rectifier/regulator circuit.

Lastly, in order to achieve extremely low (EZEV) driving cycle emissions, it would be necessary to incorporate some type of cold start emissions reduction technology, such as an EHC or thermal reactor type system. A rapid catalyst light-off will be necessary since engine emissions during and immediately after startup will comprise a significant portion of the cycle emissions. Either of the above mentioned technologies could be readily tailored for the APU application.

REFERENCES

1. *The 3rd Biennial International Conference & Exhibition on Natural Gas Vehicles*, Proceedings, Part II, Göteborg, Sweden, September 24, 1992, pp. 322.

2. Meyer, R. C., D. P. Meyers, S. M. Shahed, and V. K. Duggal, "Development of a Heavy-Duty On-Highway Natural Gas-Fueled Engine," SAE Paper No.922362.

3. Heywood, J. B., *Internal Combustion Engine Fundamentals,* McGraw Hill, 1988, pp. 655.

4. Weaver, Christopher, S., "Natural Gas Vehicles - A Review of the State of the Art," SAE Paper No. 892133, September 1989.

5. Klimstra, Jacob, "Catalytic Converters for Natural Gas Fueled Engines -- A Measurement and Control Problem," SAE Paper No. 872165, November 1987.

6. White, Jeff, "Low Emission Catalysts for Natural Gas Engines," GRI Topical Report GETA 91-09, SwRI Project No. 03-3178, August 1991.

APPENDIX A

REPORT ON VIPRE SIMULATIONS FOR KOHLER V2 ENGINE

VIPRE SIMULATIONS FOR KOHLER V2 ENGINE

In this report, parametric studies on the intake runner and exhaust runner lengths, the air cleaner volume and valve timing were carried out using VIPRE (Virtual Indicated Performance of Reciprocating Engines) code. VIPRE is a full-cycle simulation designed for engine performance prediction/analysis. VIPRE's calculations showed that the increase of the intake runner length to 0.5m could increase power by 34 percent, while experiments indicated that there was no improvement on power. A study was carried out to understand this contradictory result. It was found that the reason for the erroneous results could be traced to the simplified model used in VIPRE where a characteristic method was employed to solve gas dynamics in the piping system. This method is not capable of directly predicting the pressure loss due to a bend or an elbow, and junction, which is critical to affect tuning. In order to model the pressure loss due to elbows, special provisions are required. In this study, a restriction with a diameter of 0.014m and length of 0.02m was imposed between the intake manifold and the intake port to model the pressure loss due to the elbow in the intake manifold. As a result, it was found that "tuning" was not seen at the intake runner length of 0.5m. This suggests that the strong tuning effect originally found by VIPRE is not correct due to its limitation to model the elbow pressure loss. On the other hand, this suggests that improving the elbow shape could reduce the pressure loss, yielding some power improvement.

1.0 Technical Approach

VIPRE is a suite of engine cycle simulation code that was developed for prediction of engine performance and fuel economy. The techniques are based on the first principles of thermodynamics and gas dynamics. The characteristics method is used for the piping system, while relatively simple submodels are employed for combustion, heat transfer, charge motion and mixing for the engine. Due to its simplicity of characteristics, this method is not able to predict pressure losses due to a bend, or T-junction, nor does it model heat transfer in the piping system. However, previous experience shows that, if it is used judiciously, it can help to reduce the scope of testing and development required to achieve design goals.

The approach taken to perform the parametric study was first to construct a baseline engine model at 3600 rpm. The intake, exhaust, and engine geometry were provided by SwRI personnel while the cam profile and valve timing were provided by Kohler. Valve flow coefficients were not identified. Therefore, the flow coefficients of a similar engine were used. The air cleaner was modeled as a volume, and an orifice was used to model the pressure loss across the air cleaner. Due to a lack of pressure measurements at the air cleaner, this orifice diameter was varied in order to match experimental data. However, once the simulated result was correlated to actual engine data, the parametric studies were then carried out.

2.0 Simulated Results

In this section, no restriction was imposed at the connection between the intake manifold and the intake port. Actual engine data was matched as closely as possible.

2.1 Baseline Model Simulation

Table 1 lists performance comparison data between the baseline simulation and actual measurements. Note that the results predicted by VIPRE agree well with the actual engine data.

TABLE 1. COMPARISON BETWEEN DATA AND VIPRE SIMULATION

Source	Brake Power (kW)	Air Flow (kg/s)
Engine Data	13.80	0.0164
Simulation Result	13.57	0.0168

In view of the above comparison, parametric studies were performed. Parametric studies of valve timing, air cleaner volume, and exhaust and intake runner length were then performed, respectively. It should be pointed out that a compression ratio of 8:1 was used for the above baseline model and the valve timing simulations, while a compression ratio of 12:1 was used for the remaining parametric studies.

2.2 Parametric Studies

2.2.1 Valve Timing Optimization

Valve timing optimization consisted of varying the intake and exhaust opening and closing timings. Whenever one timing event was varied, all other timings remained fixed. Table 2 through 5 list the results of the simulation.

TABLE 2. INTAKE VALVE CLOSING (IVC)*

IVC	Brake Power (kW)	Air Flow (kg/s)
Baseline (270 ATDC)	13.57	0.0168
220	12.98	0.0161
230	13.43	0.0165
240	13.68	0.0168
250	13.80	0.0169
260	13.76	0.0169
280	13.55	0.0164
285	12.98	0.0161
*Values are CAD with respect to TDC at the beginning of the intake stroke.		

TABLE 3. INTAKE VALVE OPENING (IVO)

IVO	Brake Power (kW)	Air Flow (kg/s)
Baseline (-41 BTDC)	13.57	0.0168
-11	13.28	0.0167
-21	13.47	0.0169
-31	13.56	0.0169
-51	13.55	0.0170
-61	12.81	0.0161
-71	12.75	0.0161

TABLE 4. EXHAUST VALVE OPENING (EVO)*

EVO	Brake Power (kW)	Air Flow (kg/s)
Baseline (-249)	13.57	0.0168
-219	12.89	0.0163
-229	13.20	0.0165
-239	13.43	0.0166
-259	13.61	0.0164
-269	13.50	0.0167
-279	13.43	0.0168

* Angles are CAD with respect to TDC at the beginning of the intake stroke (TDC).

TABLE 5. EXHAUST VALVE CLOSING (ECV)

EVC	Brake Power (kW)	Air Flow (kg/s)
Baseline (72)	13.57	0.0168
42	13.43	0.0166
52	13.51	0.0167
62	13.59	0.0168
82	13.46	0.0166
92	13.30	0.0164
102	12.90	0.0160

From the preceding tables, it is shown that power increases were predicted with IVC at 250 CAD ATDC. The baseline values for all other events were found to be nearly optimal.

2.2.2 *Air Cleaner Volume*

Table 6 shows the results of the parametric study on the air cleaner volume. The volume was varied from 0.0008 m^3 to 0.004 m^3 (piston displacement is 0.000312 m^3). The basic trend is that the increase of the volume is accompanied with an increase of power.

TABLE 6. OPTIMIZATION OF AIR CLEANER VOLUME

Air Cleaner Volume (m^3)	Brake Power (kW)	Air Flow (kg/s)
Baseline (0.001 m^3)	14.82	0.01670
0.0008	14.94	0.01675
0.0015	15.27	0.01702
0.0025	15.78	0.01736
0.0035	16.15	0.01754
0.0040	16.23	0.01755

2.2.3 *Exhaust Runner Length*

The exhaust runner length was varied from 0.15m to 0.60m. It was found that with an exhaust runner length of 0.7m, power was increased from 14.82 kW to 16.45 kW. The results are shown in Table 7.

TABLE 7. PARAMETRIC STUDY ON EXHAUST RUNNER LENGTH

Exhaust Runner Length (m)	Brake Power (kW)	Air Flow (kg/s)
Baseline (0.089m)	14.82	0.01670
0.15	14.85	0.01670
0.20	15.16	0.01696
0.30	14.72	0.01659
0.40	14.46	0.01636
0.50	15.63	0.01745
0.60	16.24	0.01800
0.70	16.45	0.01814
0.80	15.79	0.01753
0.90	15.17	0.01689
1.00	14.37	0.01609

2.2.4 Intake Runner Length

The simulations show that power can be increased to 19.85 kW if the intake runner length was set at 0.5m. This represents a 34 percent improvement compared to the baseline model (14.82 kW). Table 8 lists the predicted results.

TABLE 8. PARAMETRIC STUDY FOR INTAKE RUNNER LENGTH

Intake Runner Length (m)	Brake Power (kW)	Air Flow (kg/s)
Baseline (0.00m)	14.82	0.01670
0.10	14.86	0.01668
0.20	14.98	0.01682
0.30	14.94	0.01684
0.40	15.76	0.01769
0.50	19.85	0.02195
0.60	16.77	0.01856
0.70	15.92	0.01790
0.80	16.35	0.01710
0.90	16.04	0.01684
1.00	16.19	0.01701

An engine experiment immediately followed based on the runner length VIPRE suggested. However, the experiment did not show any significant power improvement. In order to understand the source of error in the simulation, another study was conducted. Details of this study are provided in the next section.

3.0 Discussion and Comments on VIPRE

Three possible sources of error were identified in setting up the VIPRE model for the Kohler engine. The first was that the orifice of the air cleaner was incorrectly modeled. The second may have been the incorrect use of the valve flow coefficients. The third could be linked to the sharp elbow in the intake manifold going to the intake ports. This was not directly modeled by VIPRE.

Due to the nature of the one-dimensional model, the only way to model the pressure loss across the air cleaner is to use an orifice. A parametric study was carried out by varying the orifice diameter. The results show that varying the orifice diameter changes the magnitude of tuning, but peak power was still seen in the intake runner length around 0.5m, suggesting that this orifice was not the reason for the tuning.

The intake port contains a very sharp corner, which should cause a noticeable pressure loss. The valve flow coefficient used for the Kohler engine was from another engine. However, the flow behavior of the Kohler engine could be quite different due to the sharp corner. To understand this effect, the flow coefficients were varied from -100 percent to +100 percent. Interestingly, the strong tuning at the length of 0.5m was still found, although power was changed noticeably.

It was noticed that the orifice, representing the air cleaner, and the sharp corner of the intake port were located at the ends of the intake system. The above results indicate that the variation of the end conditions only change wave magnitude. This resulted in a change of power magnitude, but did not change the wave pattern in the intake system. This means that the compression or expansion wave still remains the same type during valve opening or closing, regardless of the variation of the end conditions. Therefore, the only components that would cause the wave pattern to change must be located in the middle of the intake system.

By carefully checking the intake manifold, a sharp elbow in the outlet of the manifold was discovered. Due to model limitations, VIPRE can not directly model the pressure loss across the bend or elbow without special treatment. In order to model this pressure loss, a restriction with a diameter varying from 0.010m to 0.014m and a length of 0.02m was imposed at the location between the intake manifold and the intake port. Figure 1 shows the VIPRE simulation results. It is clear that this restriction changes the wave pattern significantly, resulting in tuning disappearance around the intake runner length of 0.5m. This finding was consistent with that found in the engine experiments.

Two conclusions can be drawn from this study. First, VIPRE does require special provisions in order to handle the pressure loss across sharp elbows. This can be accomplished by imposing a restriction around this location. Secondly, the elbow on the actual engine should be redesigned to reduce the pressure loss.

Report prepared by:

Houshun Zhang
Senior Research Engineer
Department of Engine Design
Tel: (210) 522-5290
Fax: (210) 522-4673

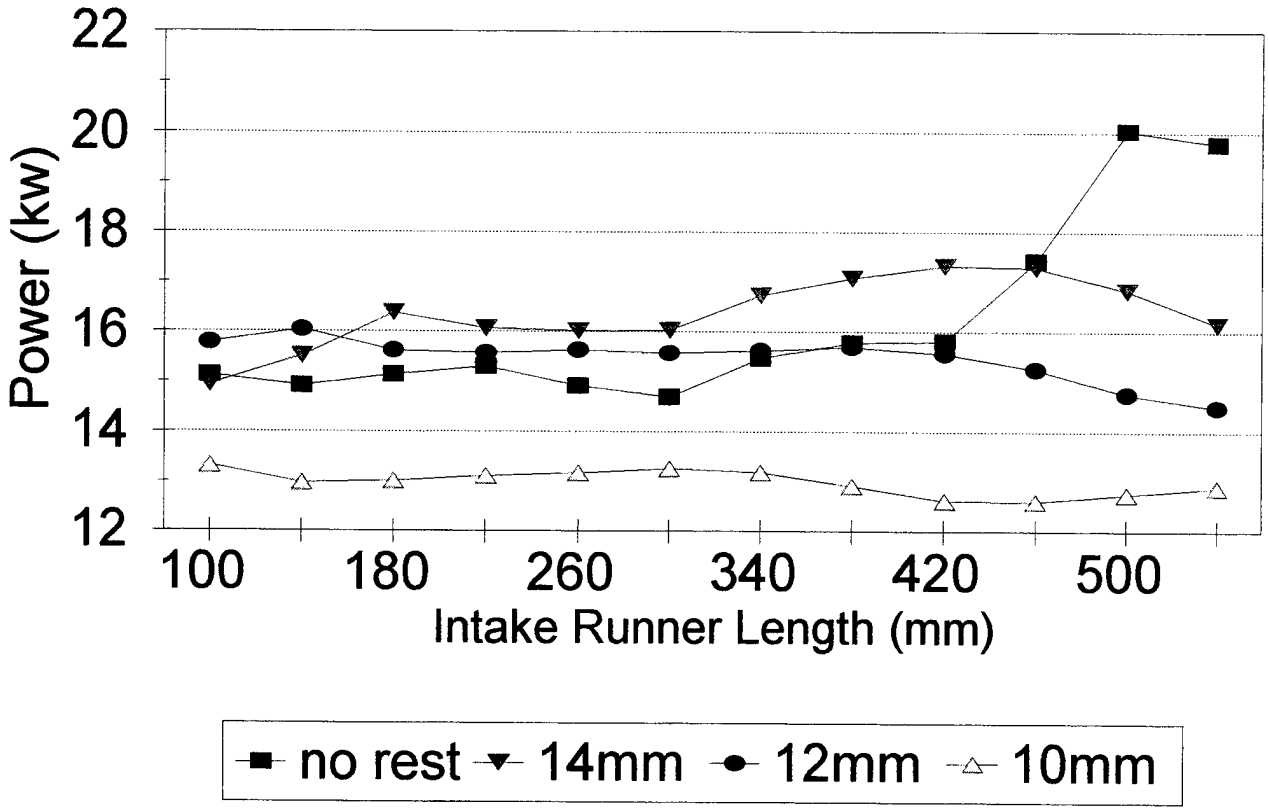

FIGURE 1. EFFECT OF ELBOW RESTRICTION ON TUNING

APPENDIX B

REPORT ON ACOUSTIC SURVEY OF THE SwRI/KOHLER COMMAND 22 NATURAL GAS ENGINE

ACOUSTIC SURVEY OF THE SwRI/KOHLER COMMAND 22 NATURAL GAS ENGINE

Acoustic Test Setup

An acoustic survey was performed on a Kohler Command 22 natural gas engine while it was operating in an engine test cell. Figure 1 shows the test setup. The engine test cell is not an ideal location for acoustic measurements due to the highly reflective walls and confined spaces. Acoustic intensity measurements were taken so as to reduce the problems associated with the poor environment. Acoustic intensity is a vector quantity and thus indicates direction of acoustic energy flow as well as amplitude. However, acoustic intensity measurements can be severely compromised in a reflective environment due to standing wave interference.

The equipment used (as shown in Figure 2) included a Rockland System/90 spectral analyzer with built-in A-weighting acoustic filters, an intensity probe with two opposing ½-inch pressure microphones separated by a 16 mm spacer, and a battery power supply for the microphones. The choice of the microphone size and spacer dimension provided accurate measurements in the frequency range of 100 Hz to 3,150 Hz with reduced accuracy beyond this range. The analyzer was triggered off the engine rpm so that sound levels not synchronous with the engine operation would be reduced.

The Kohler Engine was operated at three constant speeds: 3600 rpm, 2600 rpm, and 1600 rpm. The acoustic survey was performed on November 15, 1994. The condition of the engine on this date was recorded by the engine operator. The engine was operated continuously while all of the measurements were completed at each speed. Each side of the engine was identified as follows: front towards the blower (Figure 3), right side towards the solenoid (Figure 4), left side towards the cooling fins (Figure 5), back towards the drive shaft (Figure 6), and top towards the top cover. The plastic cover was removed from the blower throughout the testing.

Acoustic Measurements: Sound Pressure Levels

A-Weighted sound pressure level (SPL) measurements were taken at each engine operating speed to determine general acoustic trends. Four measurements were made at each speed: (1) one meter in front, (2) one meter from the right side, (3) one meter from the left side, and (4) ½ meter from the top. The back and bottom of the engine were inaccessible for acoustic measurements.

Figures 7 through 9 show the SPL results over the frequency range of 0 to 10,000 Hz for each of the 1600 rpm, 2600 rpm and 3600 rpm operating speeds, respectively. The general trends of the data are similar for each operating speed:

- High amplitudes at lower frequencies associated with engine firing orders,
- Large increase in SPL near 2,600 Hz, possibly due to a structural resonance,
- Overall decrease in SPL with increasing frequency above 3,000 Hz.

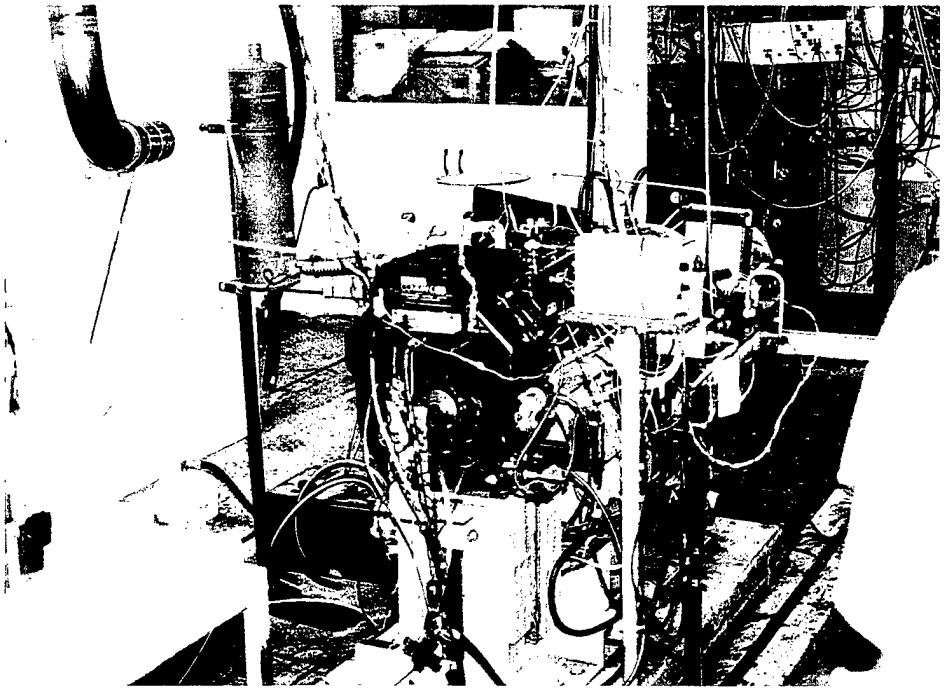

FIGURE 1. ACOUSTIC TEST SETUP

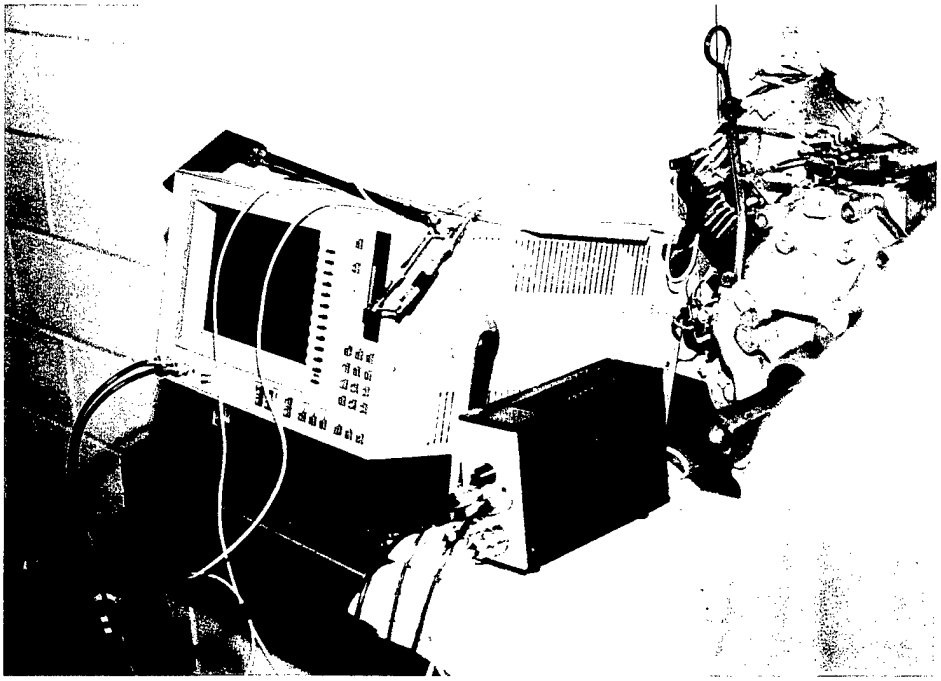

FIGURE 2. ACOUSTIC INTENSITY EQUIPMENT

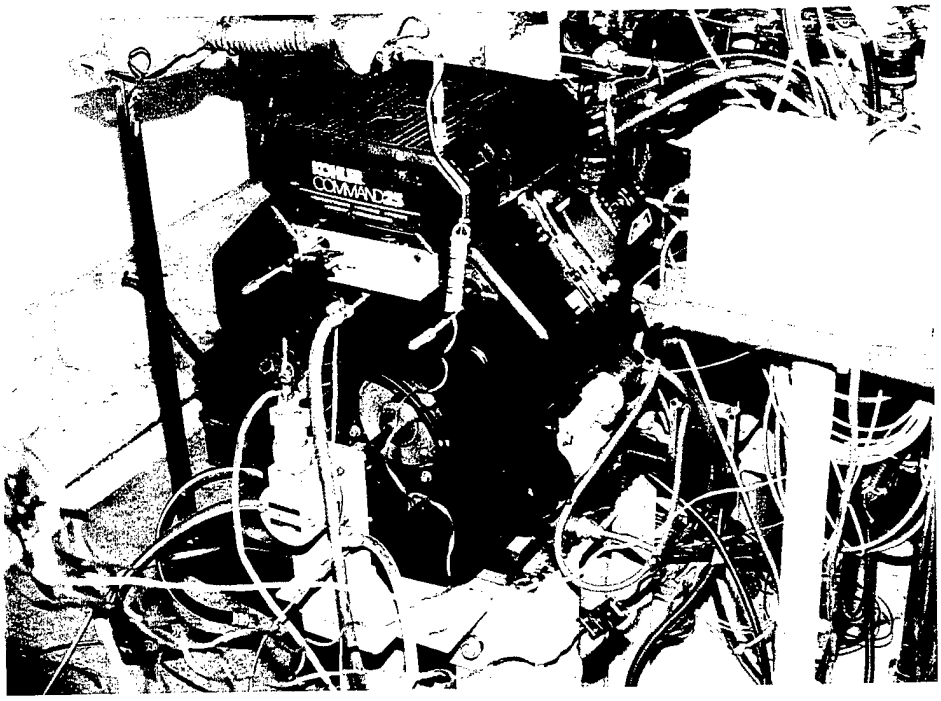

FIGURE 3. FRONT OF ENGINE

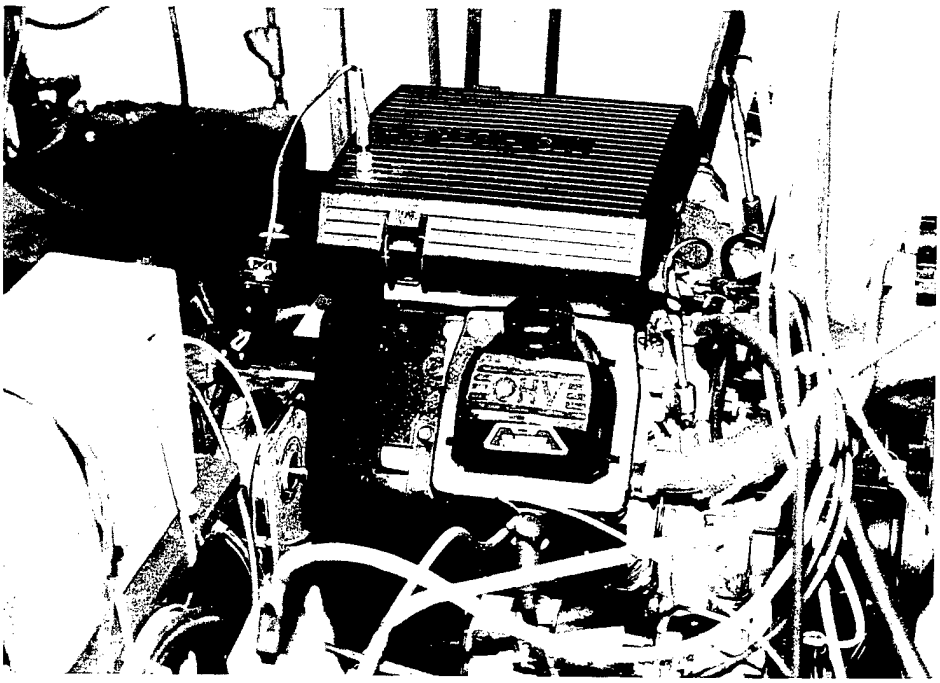

FIGURE 4. RIGHT SIDE OF ENGINE

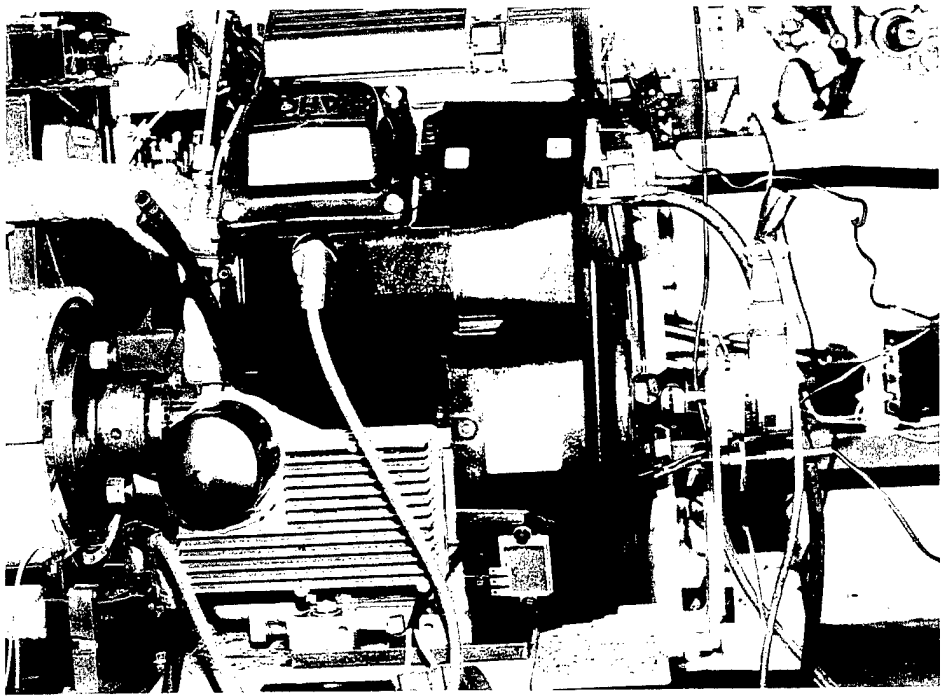

FIGURE 5. LEFT SIDE OF ENGINE

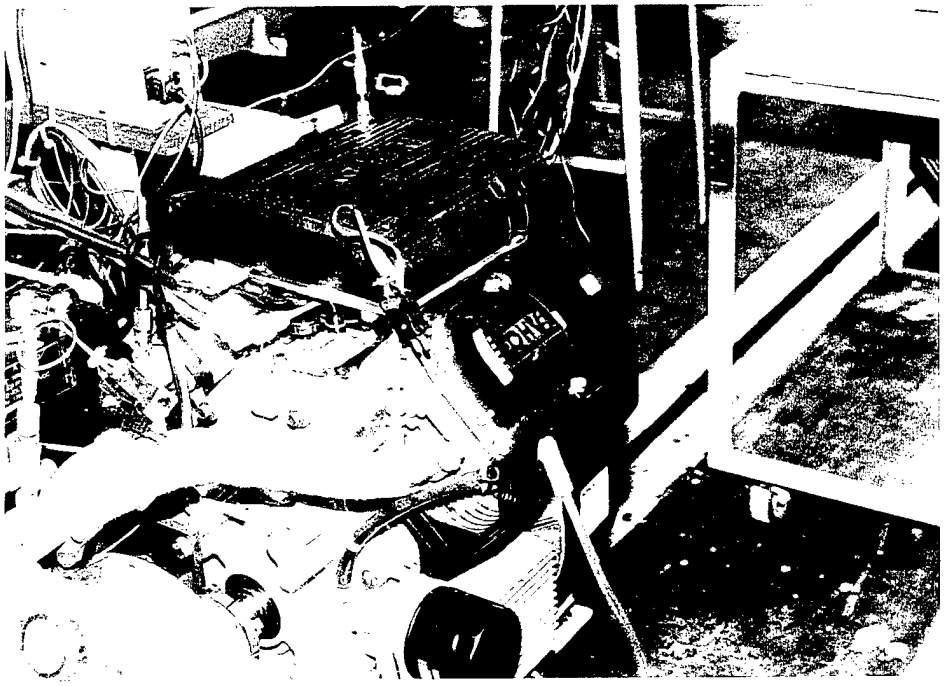

FIGURE 6. BACK OF ENGINE

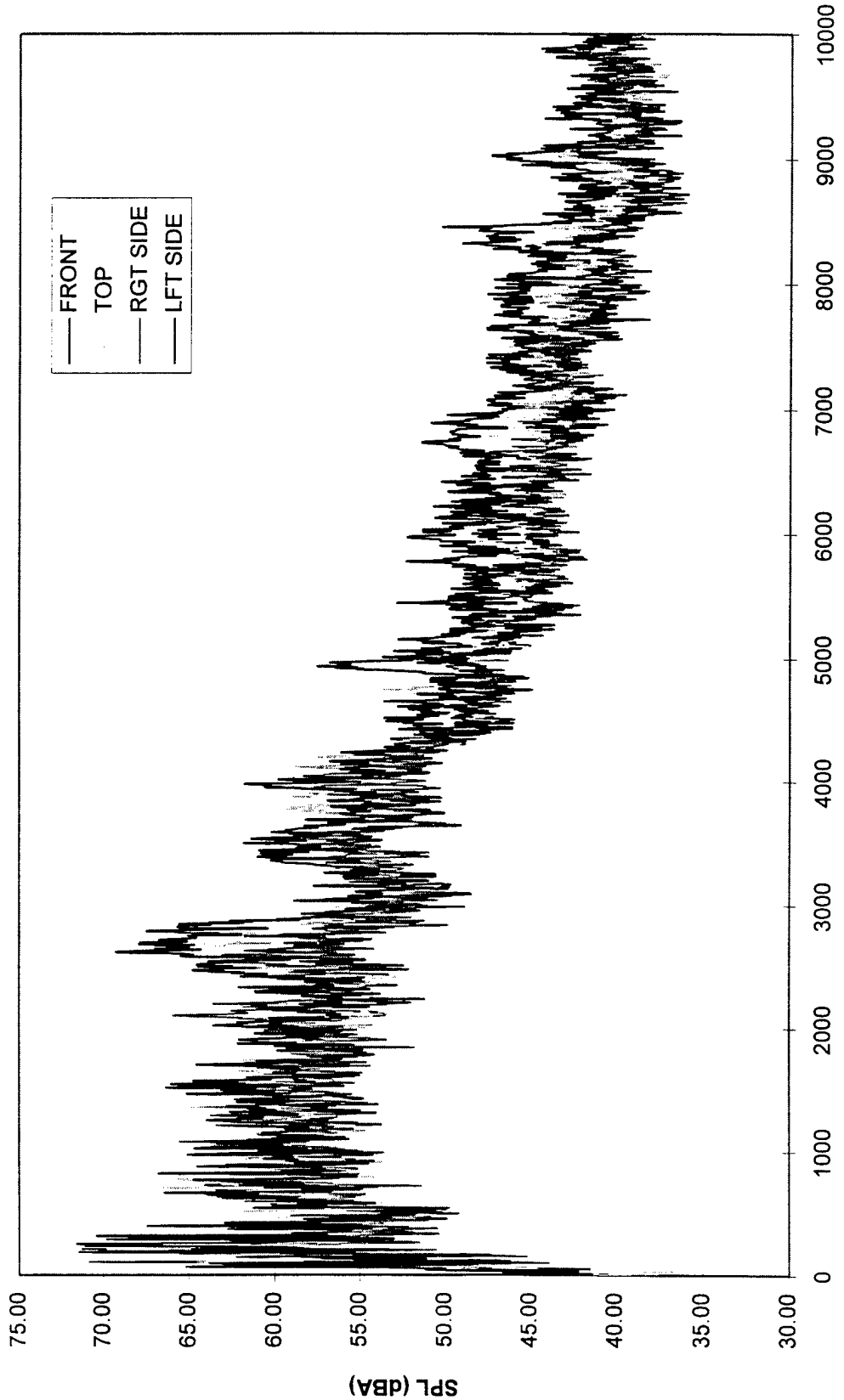

FIGURE 7. SPL MEASUREMENTS AT 1600 RPM

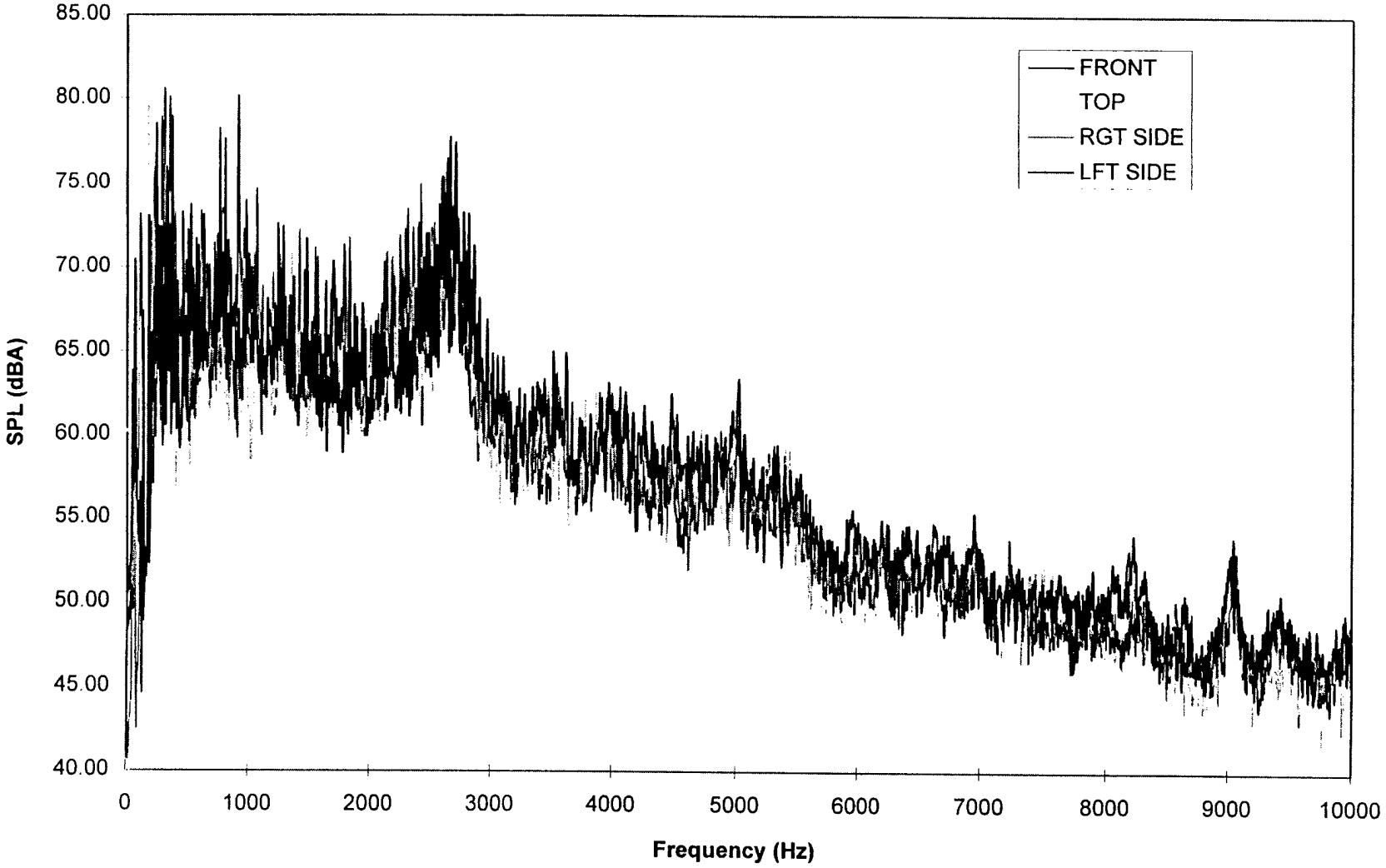

FIGURE 8. SPL MEASUREMENTS AT 2600 RPM

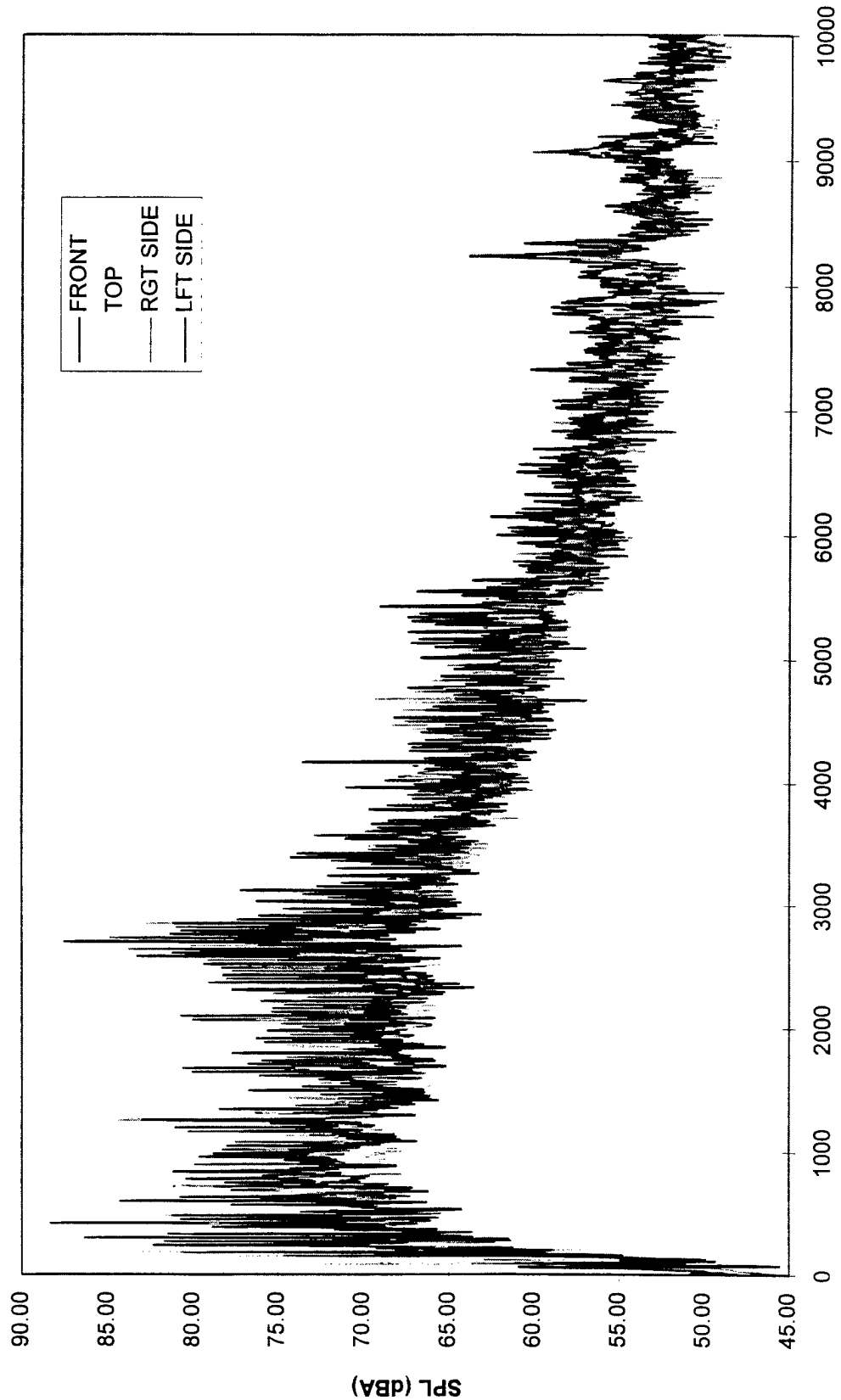

FIGURE 9. SPL MEASUREMENTS AT 3600 RPM

Figures 10 through 12 show the SPL measurements through 3,000 Hz since this frequency range dominates the overall sound emission. Beside the high SPL amplitudes below 500 Hz and near 2,600 Hz, significant peaks occur near 800 Hz at 2600 rpm and near 1,250 Hz at 3600 rpm. Thus, there are a number of potential noise sources that must be addressed to begin reduction of overall noise levels.

The overall SPL levels at each measurement position are listed in Table 1. Again, the test conditions were less than ideal and thus these levels should be used for relative comparison between engines operated in the same environment. Note that the levels at each engine speed are relatively constant at each position. This indicates that the SPL measured is diffuse rather direct and thus dependent on the acoustic environment.

TABLE 1. OVERALL SPL AT EACH MEASUREMENT POSITION*

Measurement Position	Overall SPL (dBA) 1600 rpm	Overall SPL (dBA) 2600 rpm	Overall SPL (dBA) 3600 rpm
Front	86.6	95.0	100.3
Top	87.5	94.5	99.9
Right Side	86.1	94.7	100.2
Left Side	89.1	94.9	100.8
Average	87.3	94.8	100.3
* To be used for relative comparisons only, not for absolute levels			

The conclusions from the SPL survey are:

- Low frequency noise, below 500 Hz, is a significant source of the overall SPL. Noise abatement through sound absorption or transmission loss may be limited in this low frequency range.
- A large increase in noise occurs between 2,500 and 3,000 Hz. This frequency range is consistent for all engine operating speeds which may indicate a structural resonance.
- Since the dominant frequency range is less than 3,150 Hz, a 16 mm spacer and ½-inch microphone combination are adequate for acoustic intensity measurements.

Acoustic Measurements: Sound Intensity Measurements

The sound intensity measurements were performed by mapping a grid over the surface of the engine effectively dividing the engine into grid areas. The intensity measurements were then spatially averaged over each grid area at a distance approximately six inches from the surface. Table 2 lists each grid area and the figure in which each area is shown. The photographs indicated in this table are of a non-operating engine similar to the one used for the acoustic survey. Note that the back of the engine was inaccessible thus only a small area at the back of the top cover was surveyed. Figure 13 is a schematic layout of the acoustic intensity survey grid areas.

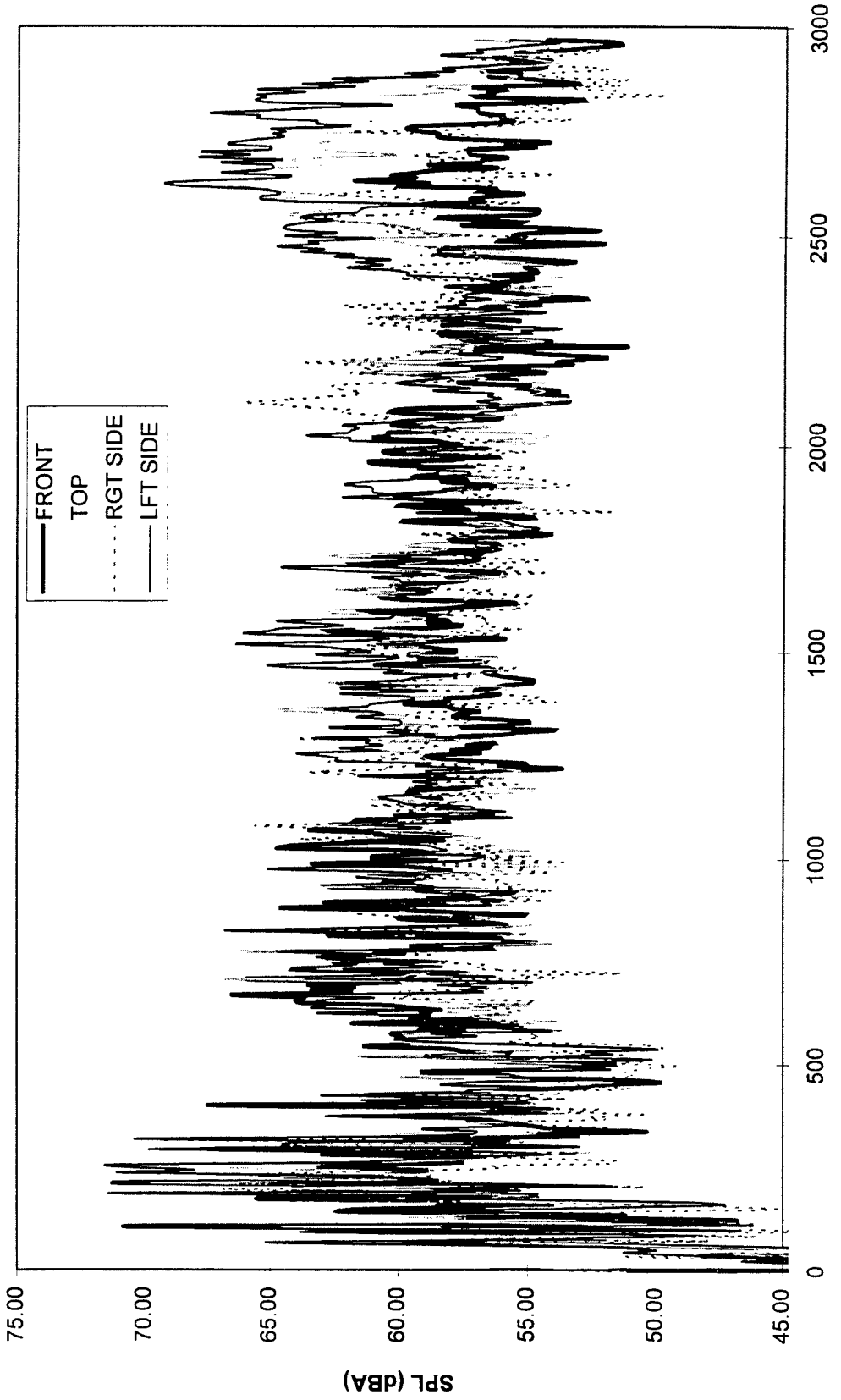

FIGURE 10. SPL MEASUREMENTS AT 1600 RPM (0-3000 Hz)

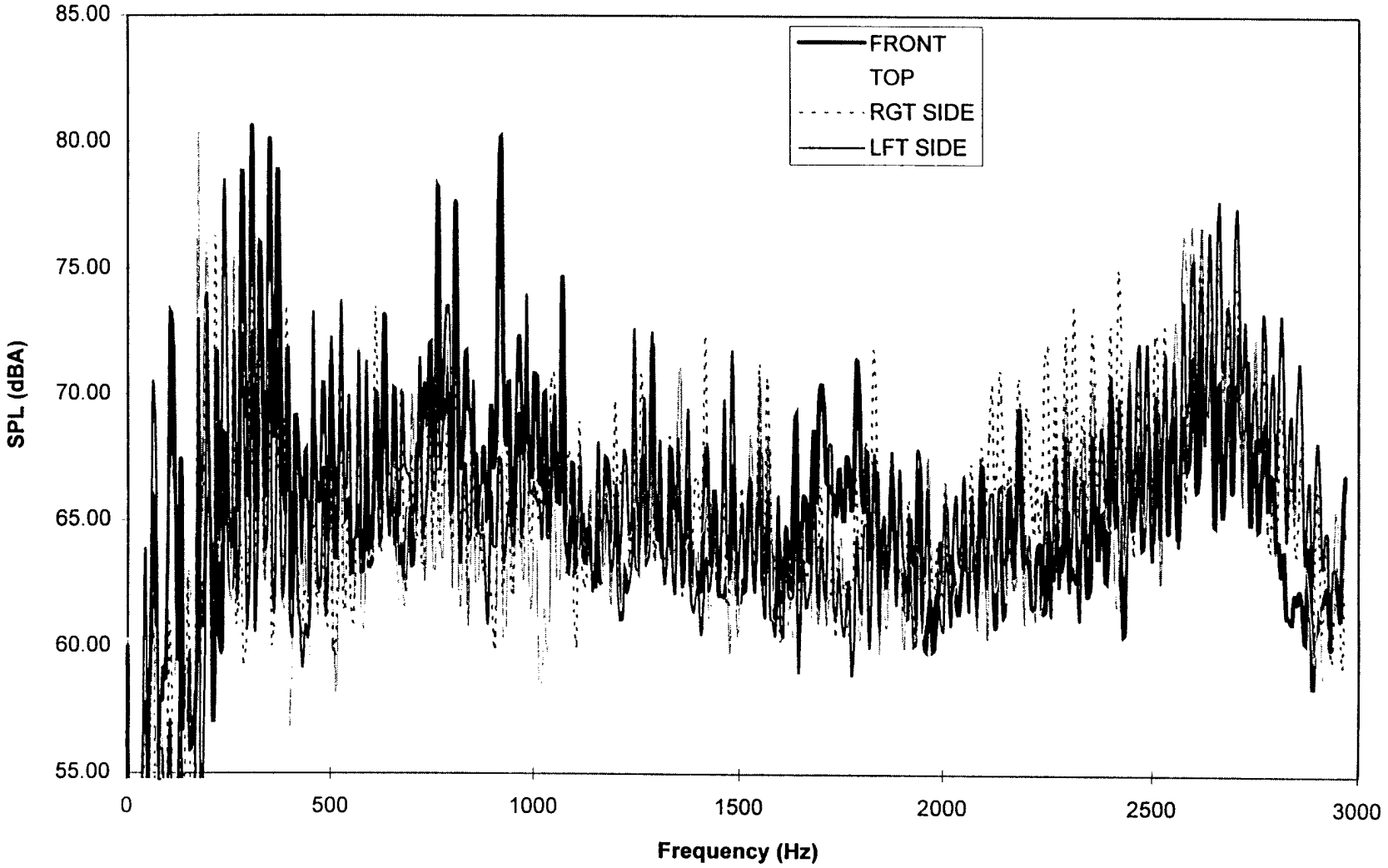

FIGURE 11. SPL MEASUREMENTS AT 2600 RPM (0-3000 Hz)

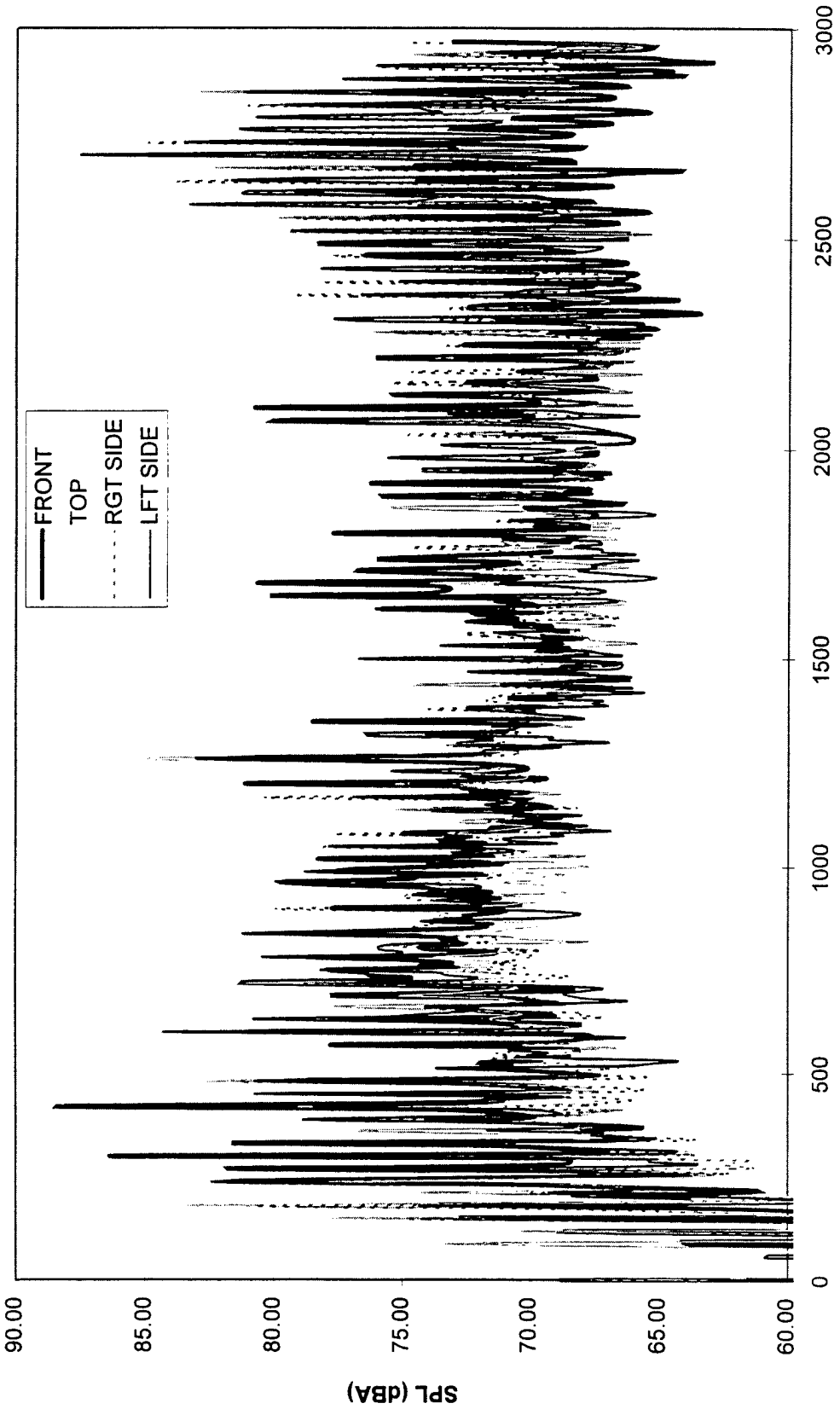

FIGURE 12. SPL MEASUREMENTS AT 3600 RPM (0-3000 Hz)

TABLE 2. ACOUSTIC INTENSITY GRID AREA IDENTIFICATION

Grid No.	Grid Area Identification	Dimensions	Area (in^2)	Figure No.
1	Top Cover Top	9" x 10"	90	14
2	Top Cover Front	9" x 4"	36	14
3	Left Side Top	7" x 10"	70	15
4	Left Side Middle	4" x 10"	40	15
5	Left Side Bottom	7" x 12"	84	15
6	Front Upper Left	6" x 6"	36	14
7	Front Center	12" x 12"	144	14
8	Front Upper Right	6" x 6"	36	14
9	Right Side Top	7" x 10"	70	14
10	Right Side Middle	4" x 10"	40	14
11	Right Side Bottom	7" x 12"	84	14
12	Top Cover Back	9" x 4"	36	16

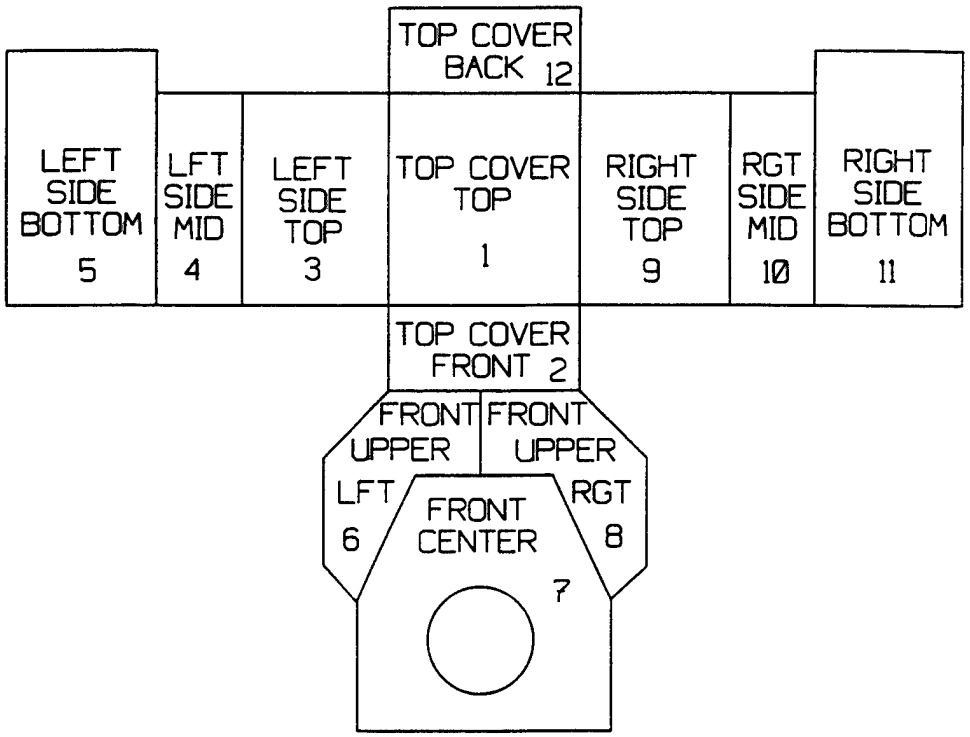

FIGURE 13. ACOUSTIC INTENSITY GRID AREAS, SCHEMATIC LAYOUT

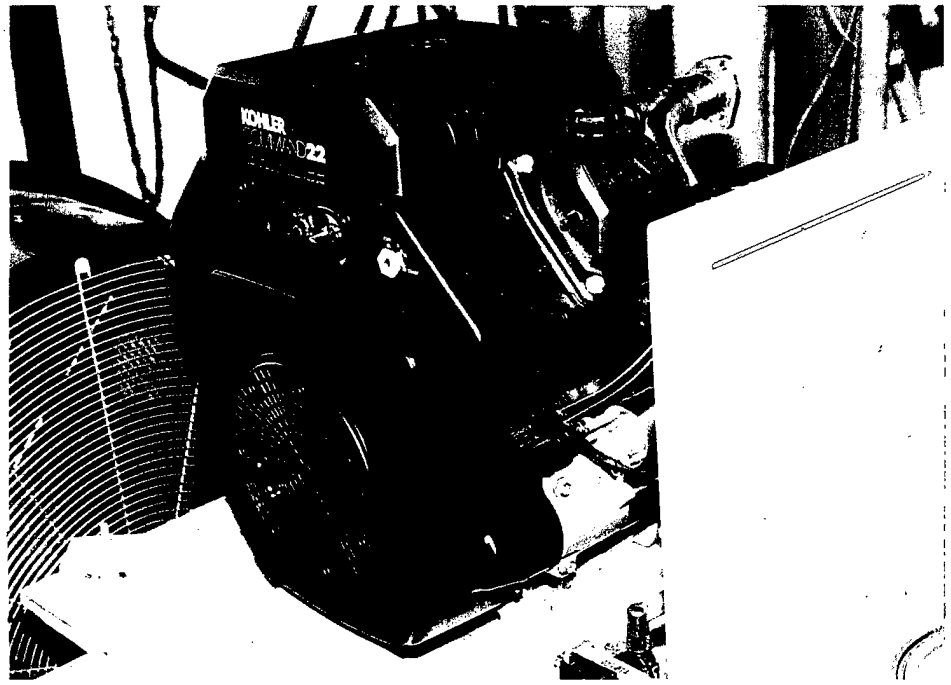

FIGURE 14. ACOUSTIC INTENSITY GRID AREAS, FRONT AND RIGHT SIDE OF ENGINE

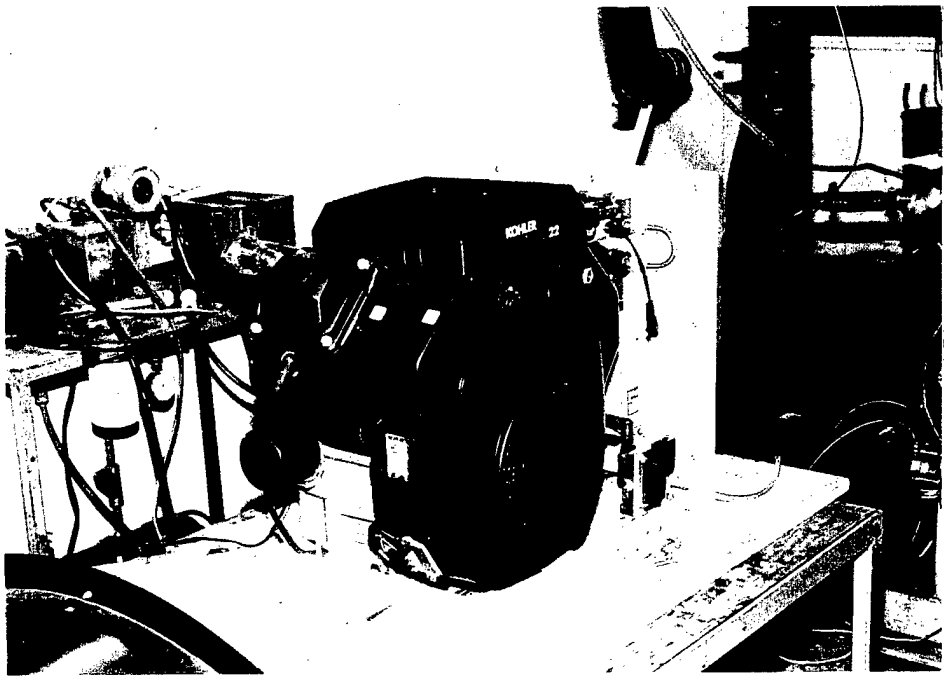

FIGURE 15. ACOUSTIC INTENSITY GRID AREAS, LEFT SIDE OF ENGINE

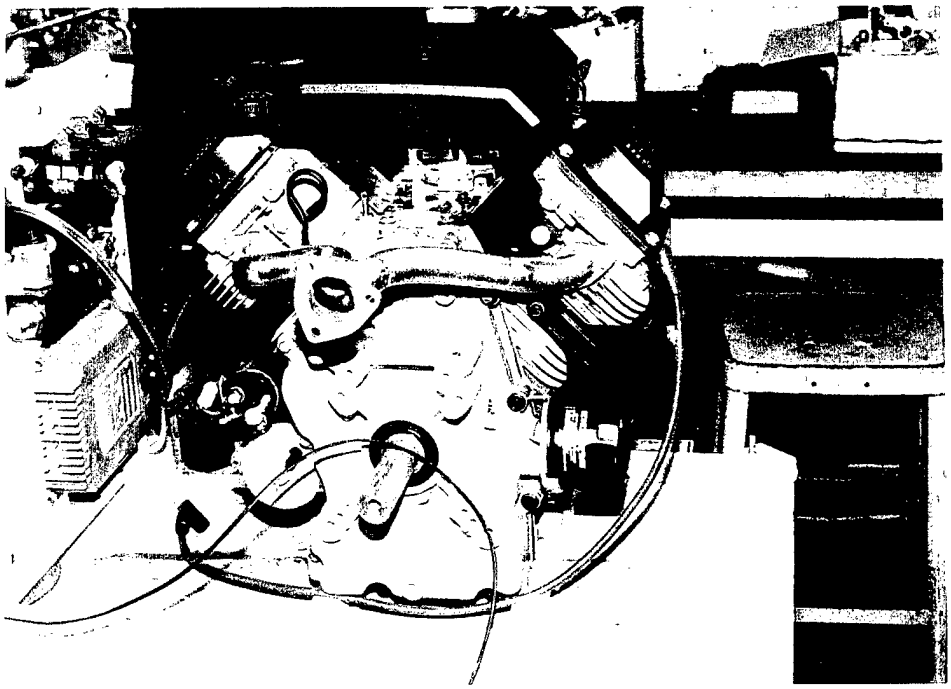

FIGURE 16. ACOUSTIC INTENSITY GRID AREA, BACK OF ENGINE

In addition to the twelve measurements indicated, an intensity survey at 3600 rpm was also conducted on the major components of the engine exhaust system (header, catalytic converter, tail pipe, and muffler). This data is not presented here since these noise sources are not typical of the actual prototype exhaust system. Preliminary results showed that the exhaust system is not a major noise source since the acoustic intensity data showed the noise radiating towards the exhaust components rather than away from them.

The overall sound power radiating from each surface was calculated from the intensity data and is presented in Figures 17 through 19 for each engine rpm. These figures show at a glance where the major noise sources are. Data is not shown where the intensity measurements were negative.

Figures 20 through 22 show the ⅓ octave sound power levels for each grid area at the three engine speeds, respectively. The ⅓ octave band centered at 2,500 Hz is clearly a dominant noise band. Figure 23 through 25 show the sound power levels in the 2,500 Hz band for each grid area. The largest sound power levels lie along the side-to-side axis. This indicates that at this frequency the engine may be rocking side-to-side on the engine support structure. If this were the case, the 2,500 Hz band would not be associated with engine operation but with mounting conditions. A modal survey was beyond the present level of effort.

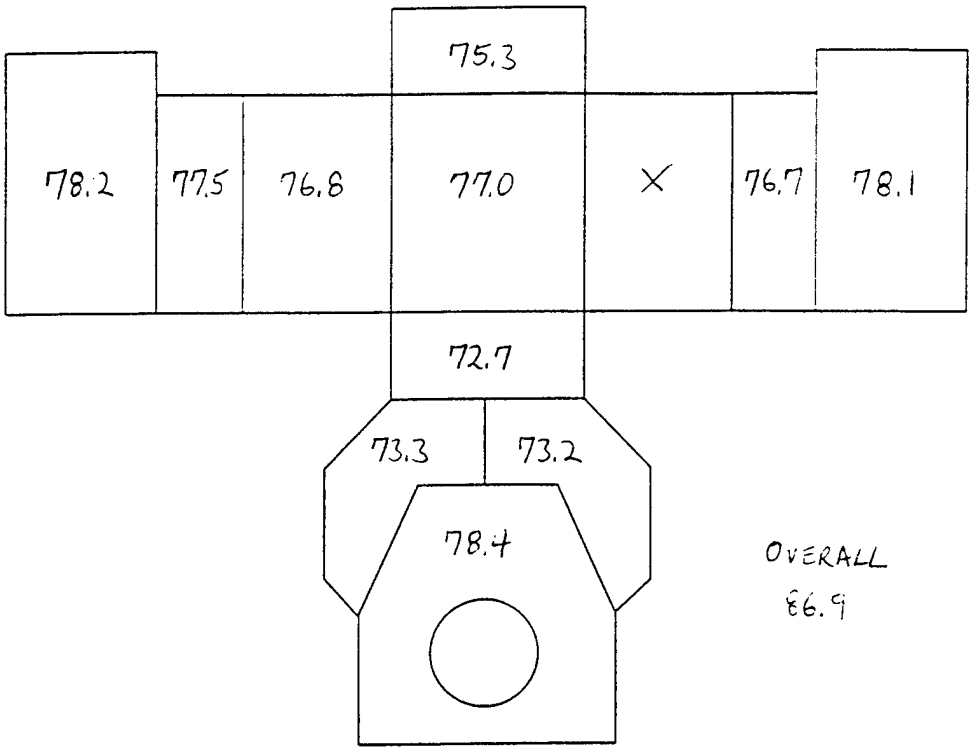

FIGURE 17. OVERALL SOUND POWER LEVEL (dBA), 1600 RPM, 100-3150 Hz

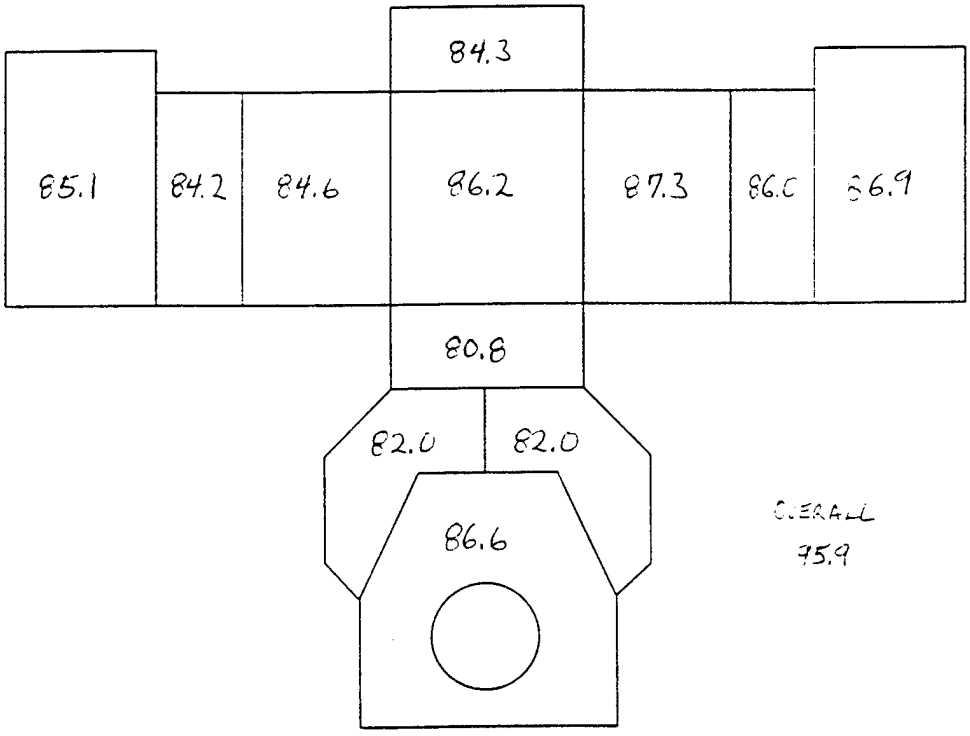

FIGURE 18. OVERALL SOUND POWER LEVEL (dBA), 2600 RPM, 100-3150 Hz

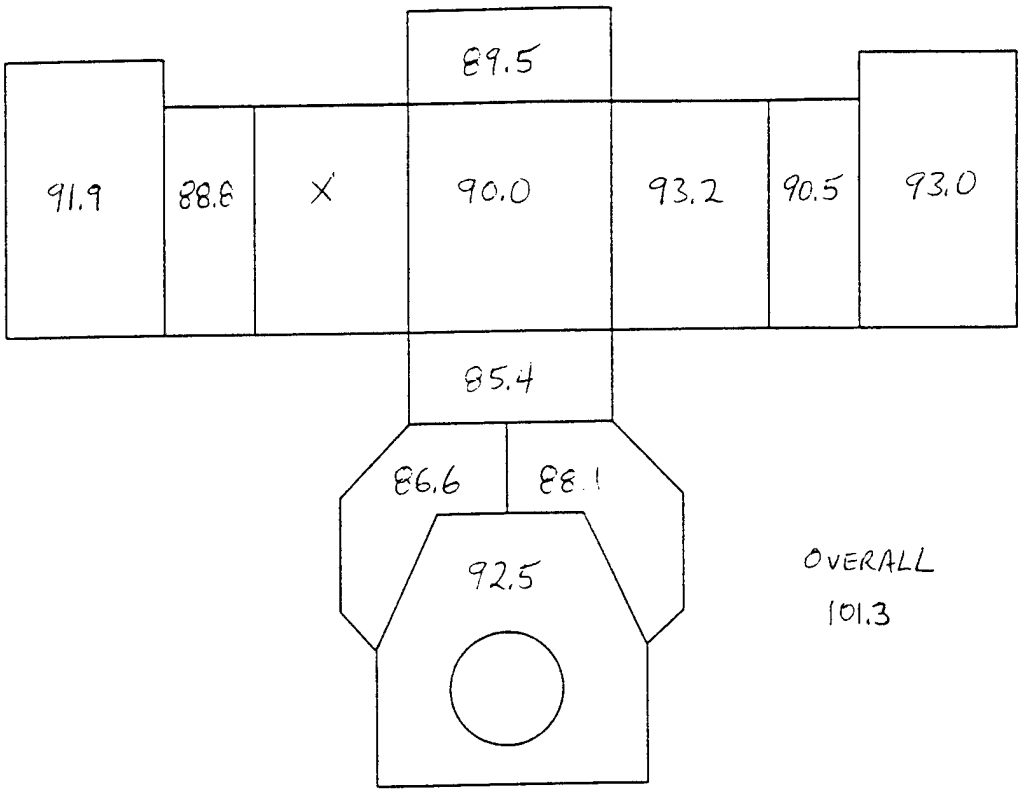

FIGURE 19. OVERALL SOUND POWER (dBA), 3600 RPM, 100-3150 Hz

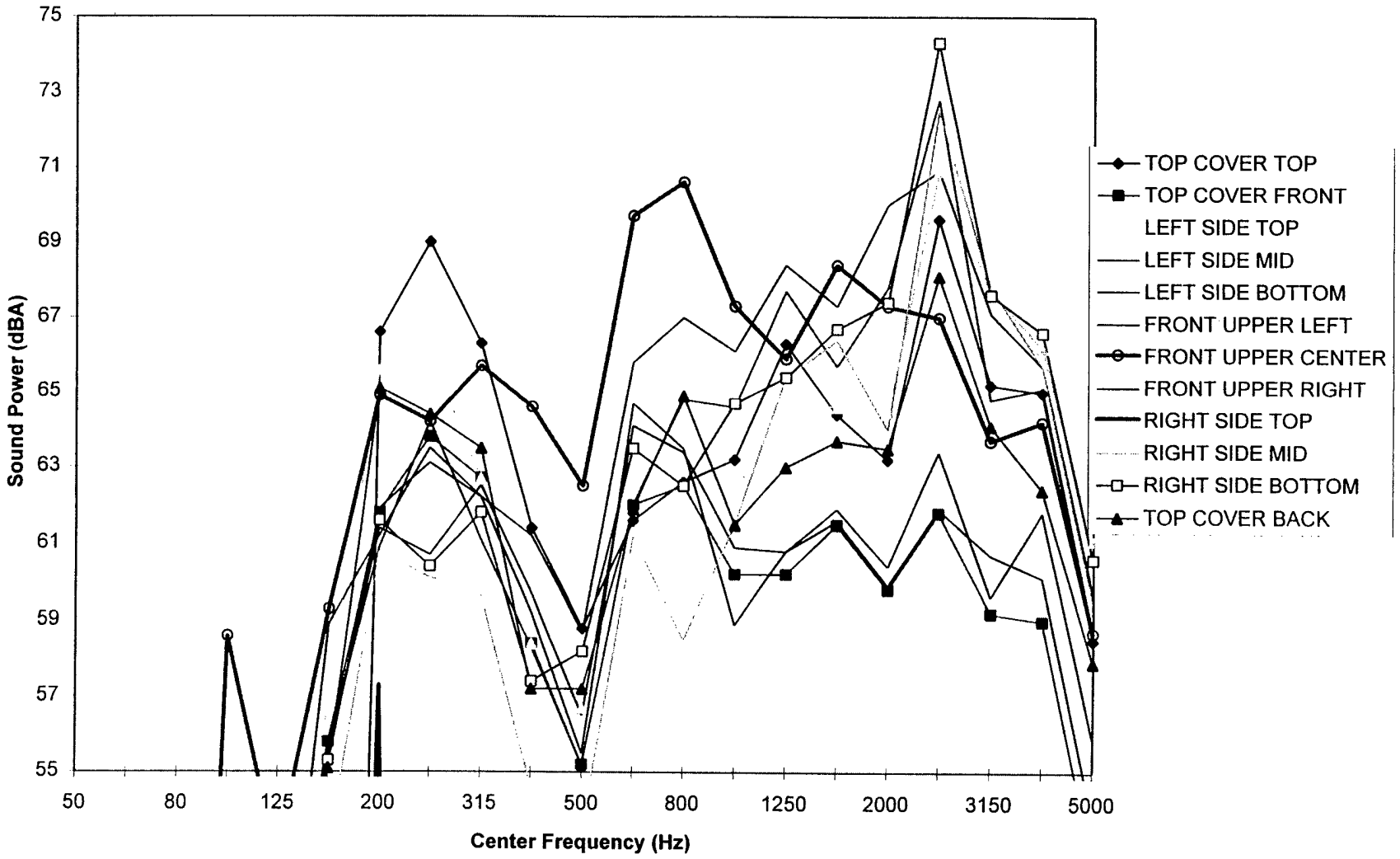

FIGURE 20. THIRD OCTAVE SOUND POWER LEVELS, 1600 RPM

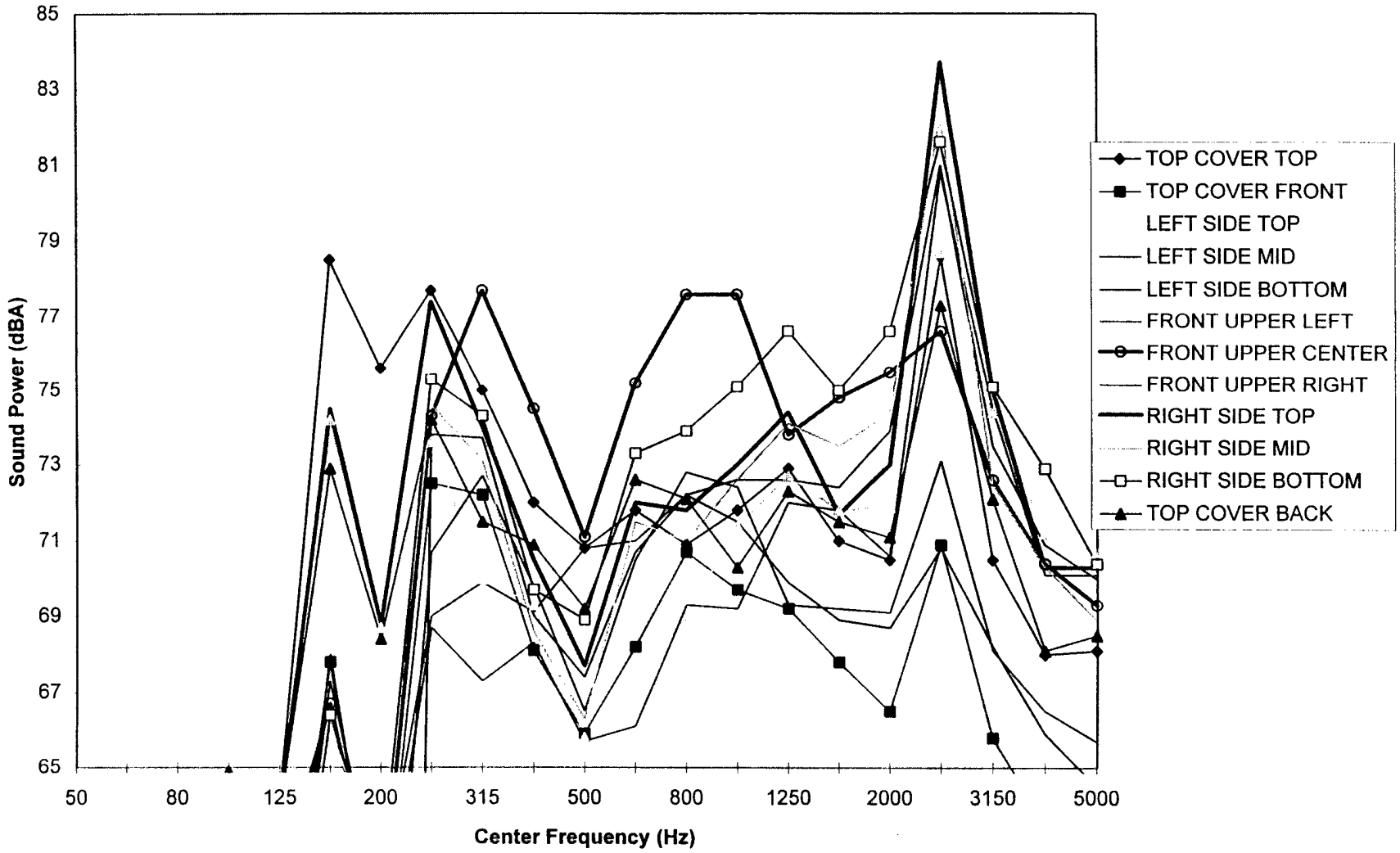

FIGURE 21. THIRD OCTAVE SOUND POWER LEVELS, 2600 RPM

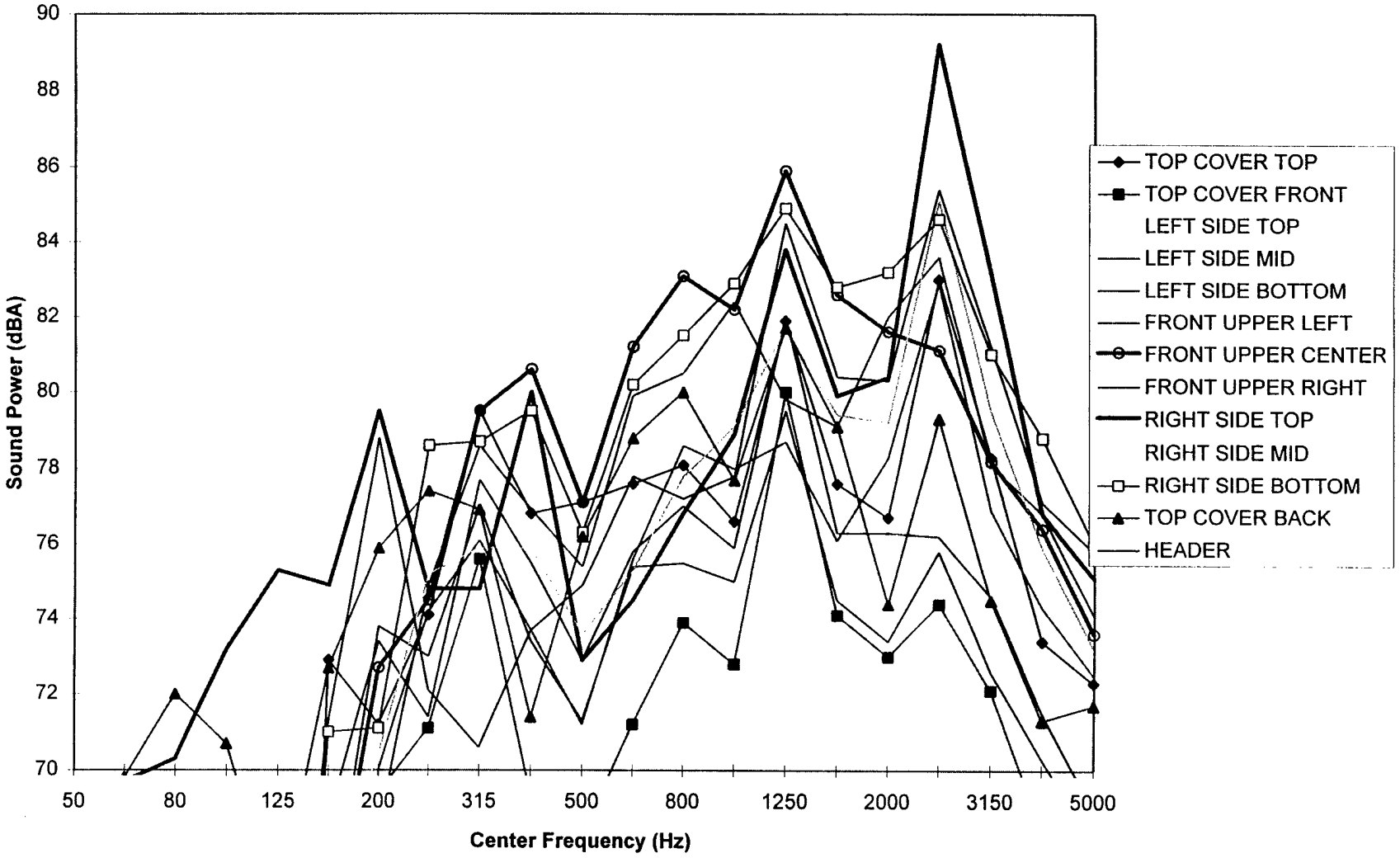

FIGURE 22. THIRD OCTAVE SOUND POWER LEVELS, 3600 RPM

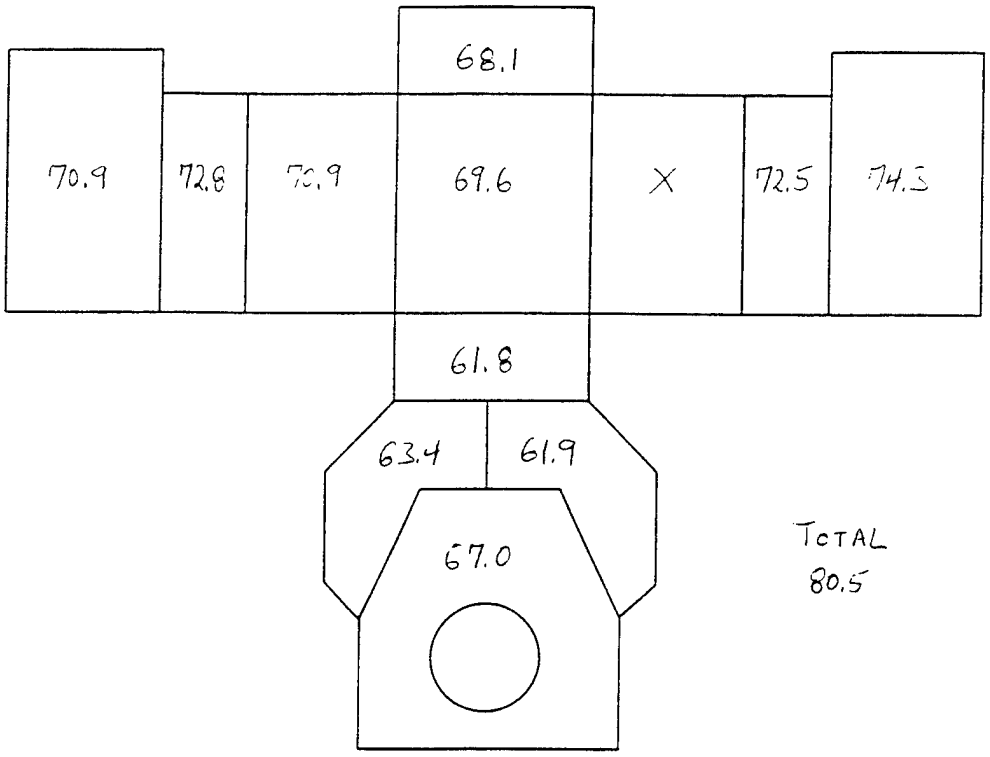

FIGURE 23. ⅓ OCTAVE SOUND POWER LEVEL (dBA), 1600 RPM, 2500 Hz

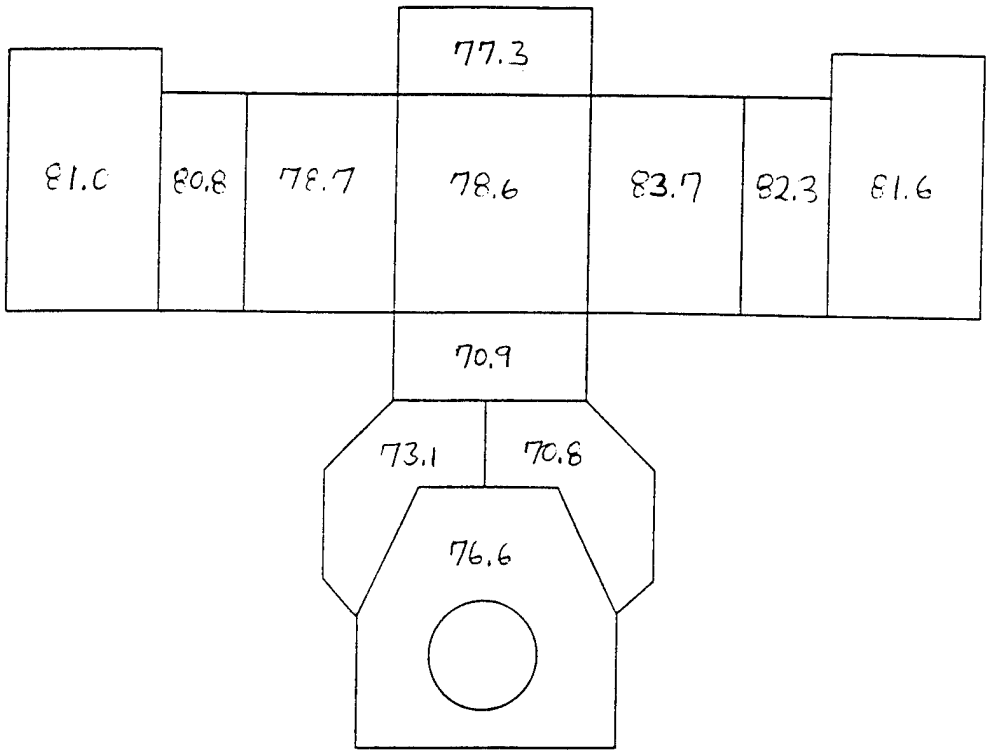

FIGURE 24. ⅓ OCTAVE SOUND POWER LEVEL (dBA), 2600 RPM, 2500 Hz

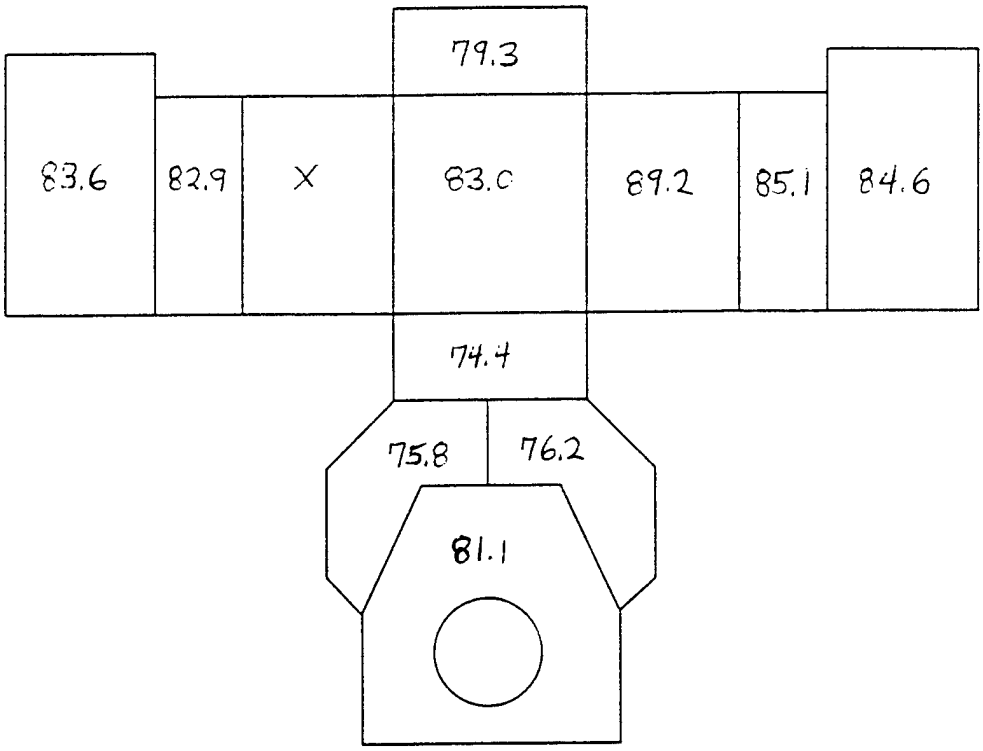

FIGURE 25. ⅓ OCTAVE SOUND POWER LEVEL (dBA), 3600 RPM, 2500 Hz

To concentrate on the lower frequency noise radiation, sound power levels were calculated for the frequency bands from 125 to 1,600 Hz. Figures 26 through 28 show the overall sound power levels radiating from each grid area at each engine speed. Figures 29 through 31 are the corresponding ⅓ octave sound power results. The following are results obtained from this lower frequency survey:

- At a glance, the front upper center grid area is dominant in the 500 to 1000 Hz range. This grid area includes the engine fan which is a likely noise source. As the engine rpm increases, the aerodynamic noise associated with the fan becomes less significant.

- The top cover is a dominant noise source at frequencies below 400 Hz for the lower engine speeds indicating a potential induction noise source. The top, sides, and back of the top cover all radiate significant noise at the 1600 and 2600 rpm engine speeds.

- At the 3600 rpm engine speed, the sound power radiation is dominated by the 1,250 Hz ⅓ octave band. Most of the grid areas have a peak in this frequency range. Narrow band analysis indicates that a single resonance peak is present at 1,260 Hz, the 21st order of the fundamental 3,600 rpm (60 Hz) operating speed. A modal survey may indicate whether this peak is another mounting resonance or an engine structural resonance.

- Other than the front upper center position (where the turbine fan is located) and the 1,260 Hz resonance, significant noise radiators at 3600 rpm are the bottom grid areas of the engine on the left and right sides.

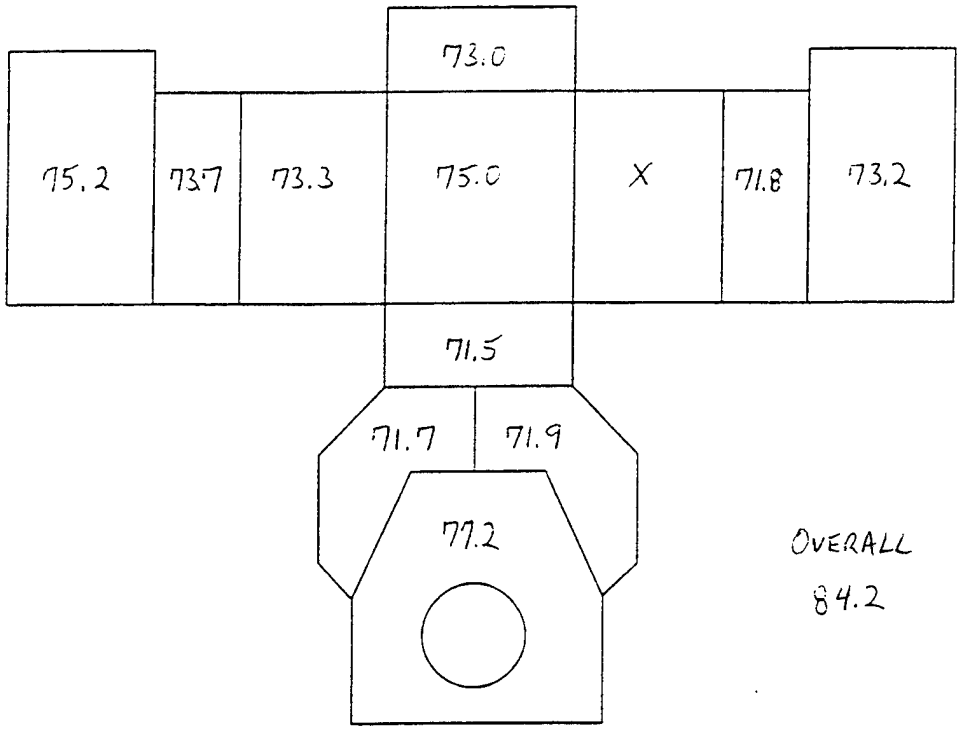

FIGURE 26. OVERALL SOUND POWER LEVEL (dBA), 1600 RPM, 125-1600 Hz

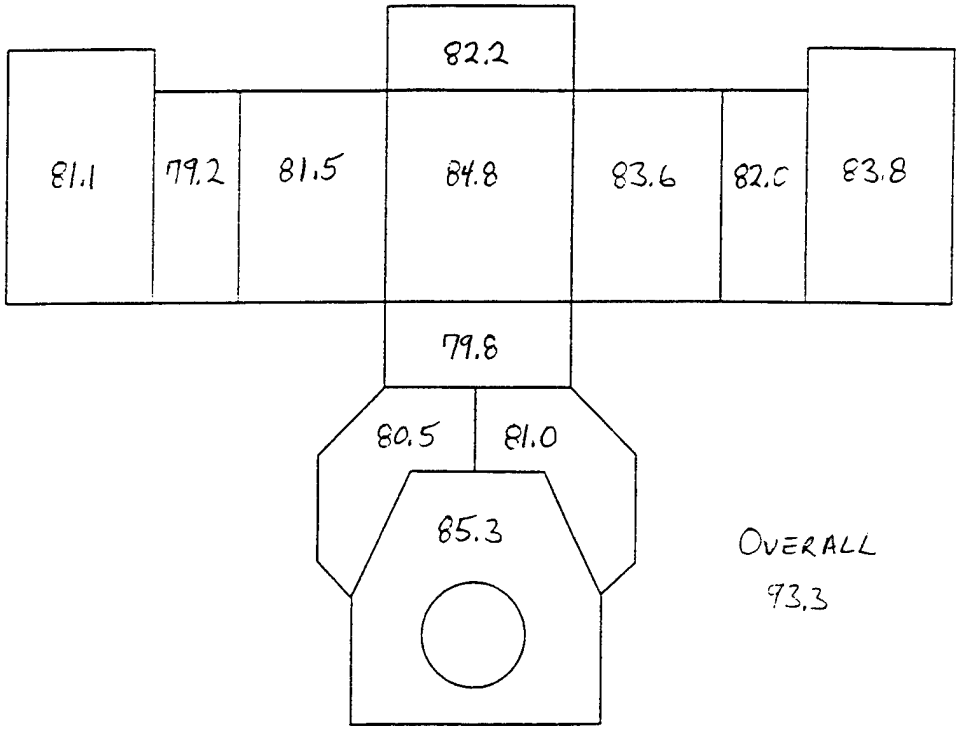

FIGURE 27. OVERALL SOUND POWER LEVEL (dBA), 2600 RPM, 125-1600 Hz

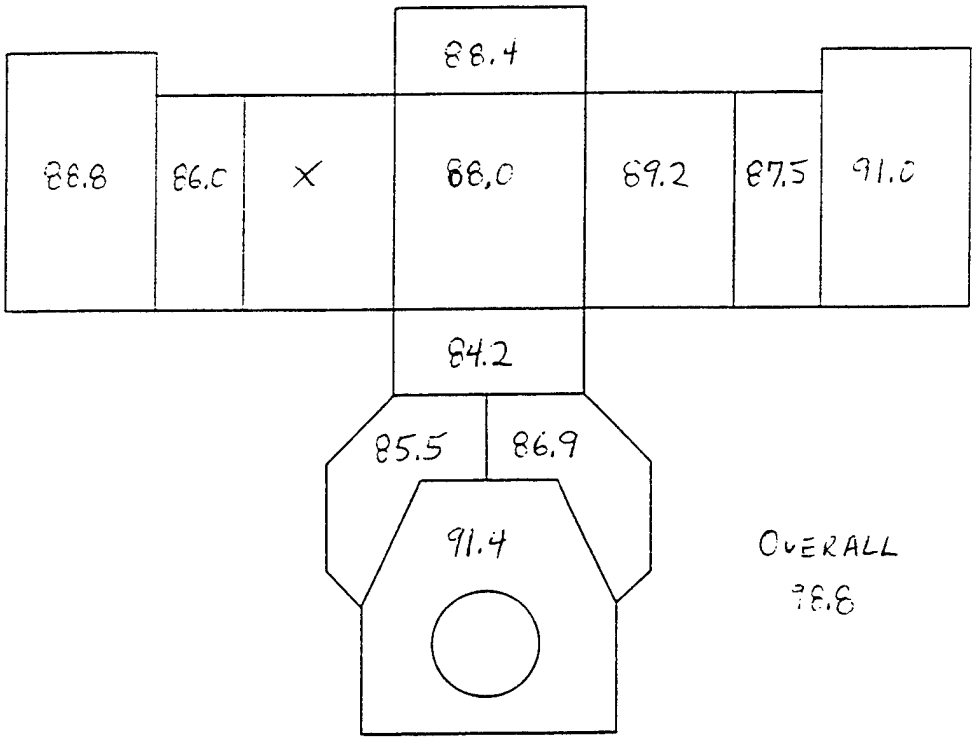

FIGURE 28. OVERALL SOUND POWER LEVEL (dBA), 3600 RPM, 125-1600 Hz

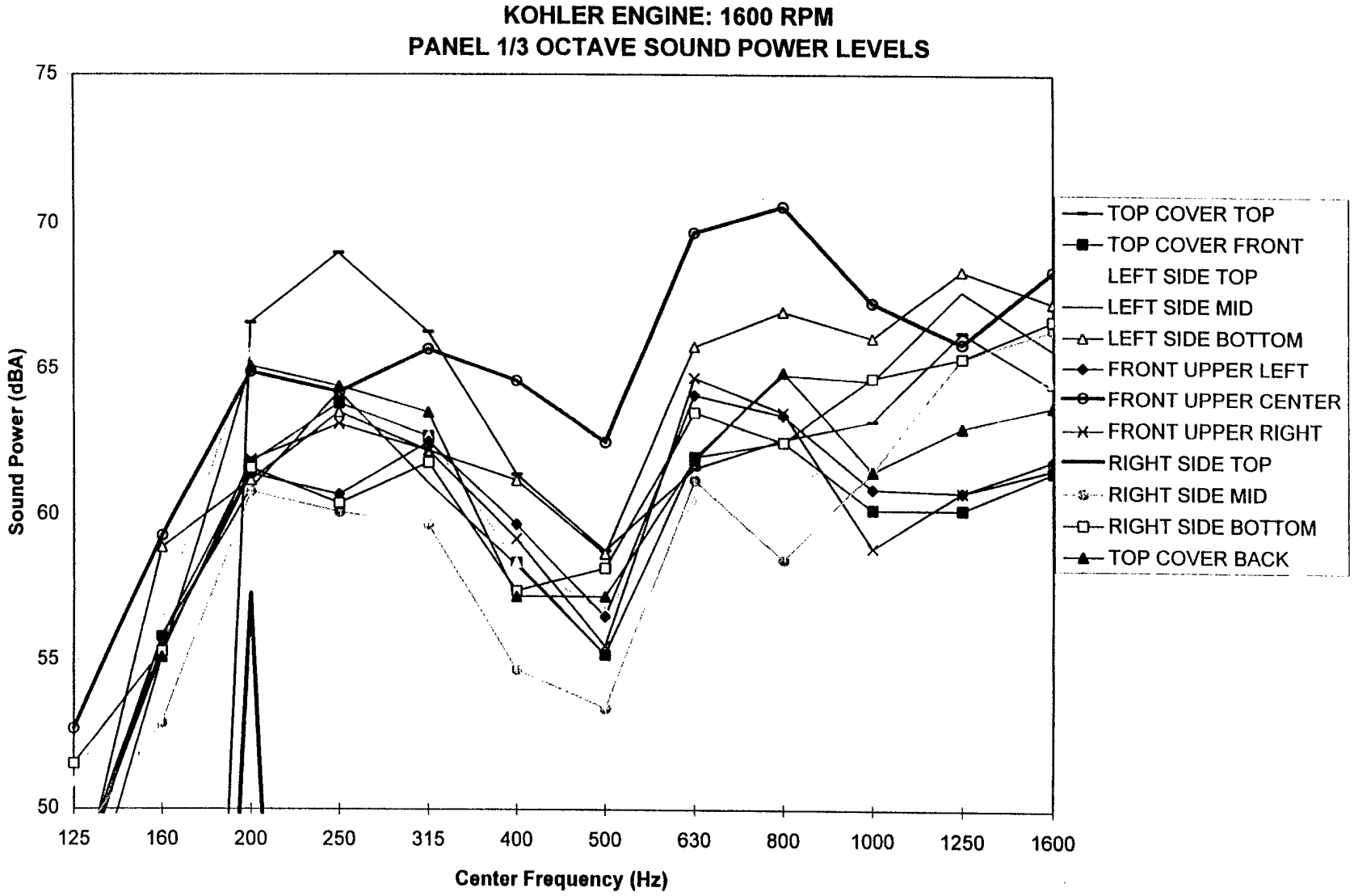

FIGURE 29. THIRD OCTAVE SOUND POWER LEVELS, 1600 RPM

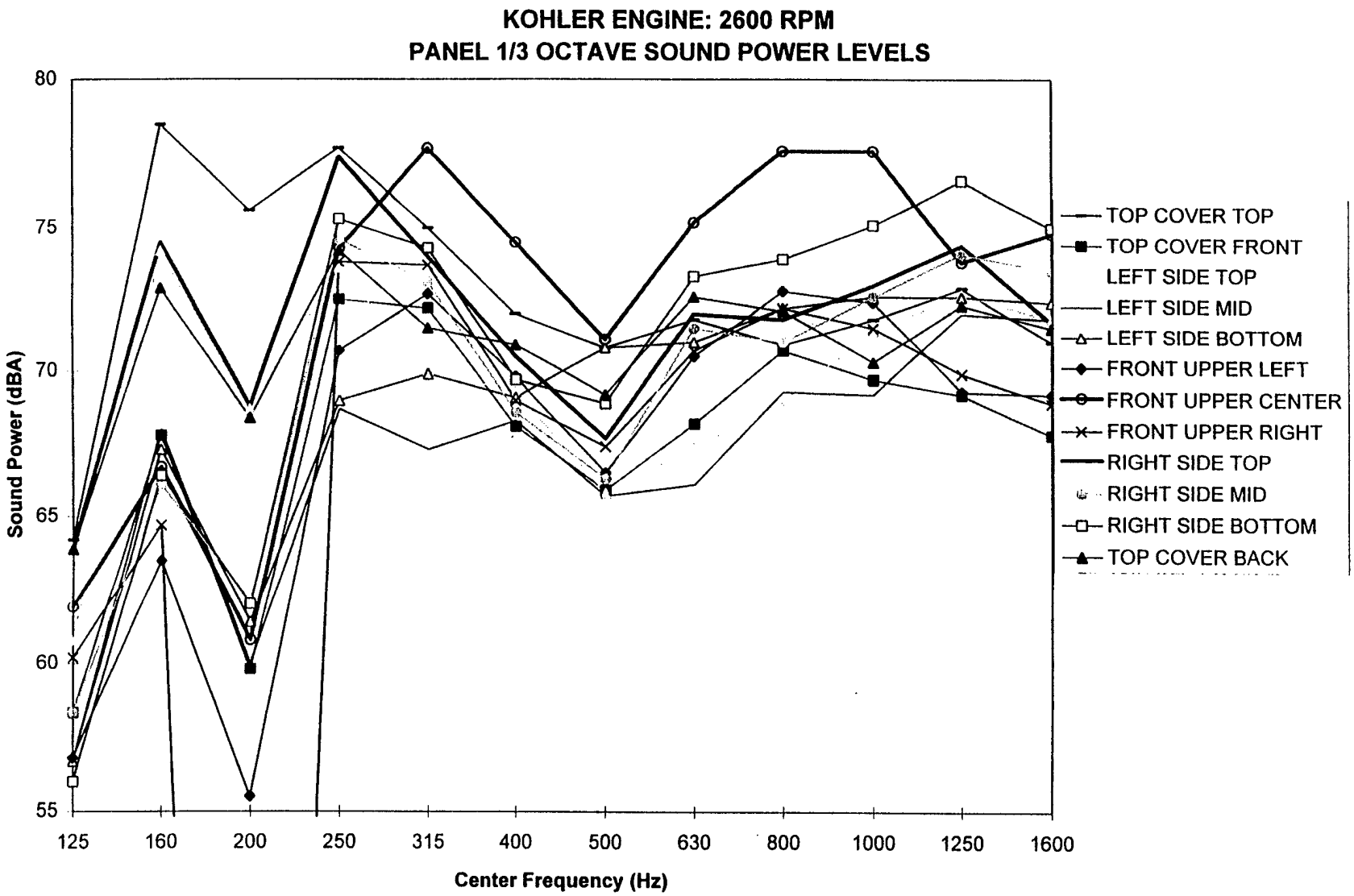

FIGURE 30. THIRD OCTAVE SOUND POWER LEVELS, 2600 RPM

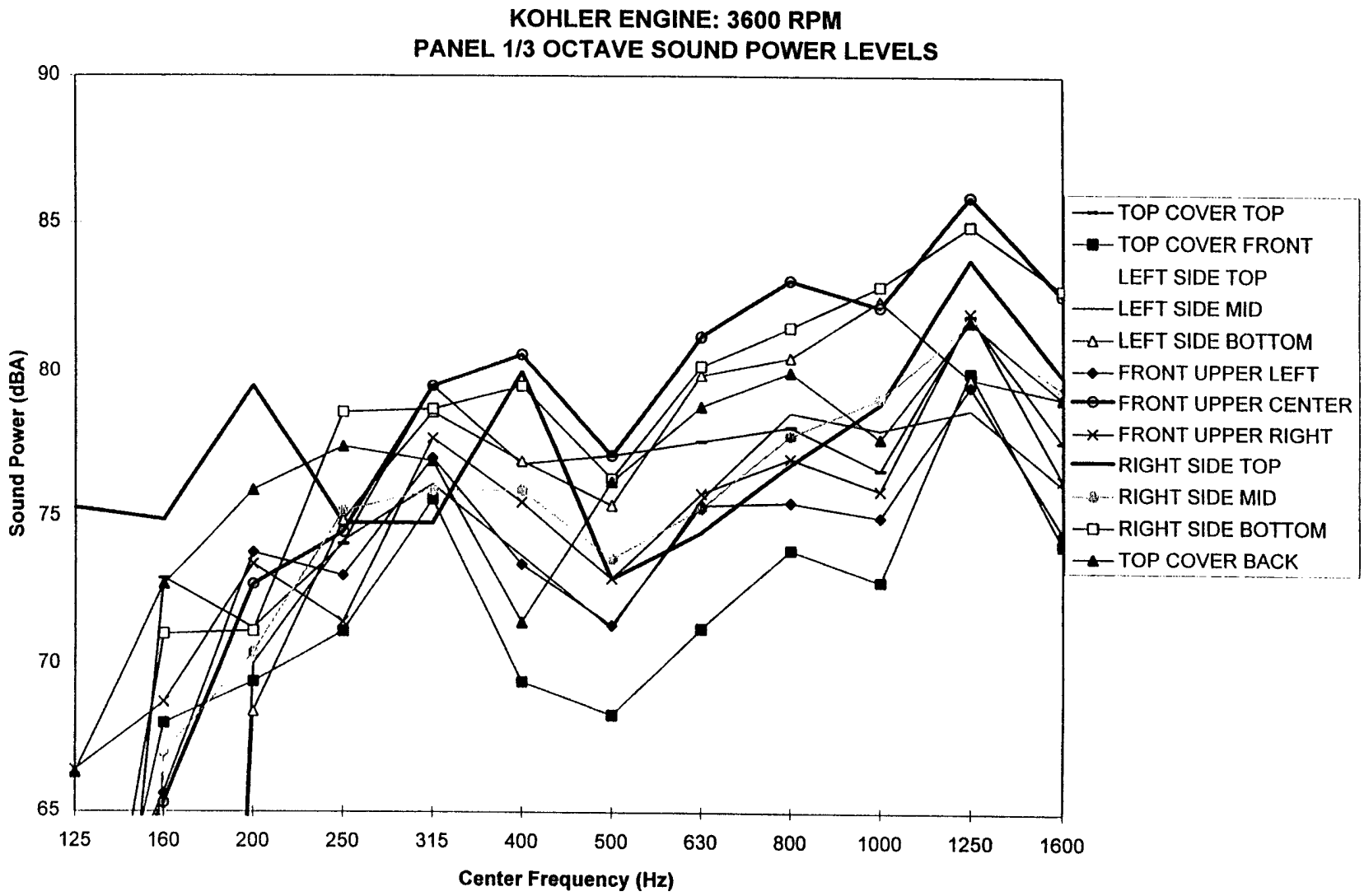

FIGURE 31. THIRD OCTAVE SOUND POWER LEVELS, 3600 RPM

From sound power level measurements, sound pressure levels (SPL) may be predicted. Assuming a spherically radiating body, predicted SPL at 1.0 meters from the engine were calculated. Table 3 lists these predicted SPL results from the sound power measurements and the measured SPL obtained directly in the test cell. The measured SPL are high by about 7 dBA over the predicted levels (for the 100-3150 Hz range).

TABLE 3. SOUND POWER PREDICTED SPL AND MEASURED SPL AT 1 METER

Engine Speed (rpm)	Average SPL Measured in Cell (0-5000 Hz)	Predicted SPL from Sound Power (100-3150 Hz)	Predicted SPL from Sound Power (125-1600 Hz)
1600	87.5 dBA	79.9 dBA	76.2 dBA
2600	94.8 dBA	87.9 dBA	85.3 dBA
3600	100.3 dBA	93.3 dBA	90.8 dBA

Conclusions and Recommendations

From this initial acoustic survey, the following conclusions and recommendations are drawn:

- The high noise levels measured in the higher frequency range may be associated with support structure vibration. A modal survey can determine if support structure resonances were contributing to the noise emission.
- Noise generated in the lower end of the frequency spectrum is of major importance due to expected lower level of absorption and noise transmission loss possible from an insulated enclosure.
- At the lower engine speeds, the top cover noise radiation (possibly generated from induction noise) could be of concern requiring improved induction system noise control.
- The blower cover may require noise control treatment with an additional filter element used in conjunction with the protective screen.
- The engine noise levels obtained at 1.0 meters as predicted from the measured sound power levels are not extremely high. Depending on the acoustic propagation of the engine enclosure, additional noise control development may not be necessary.
- The engine test cell is not an ideal location for acoustic measurements and the engine support structure is not an installed configuration for the engine. Absolute sound levels can only be determined with an end-use supported engine installed in a proper acoustic environment.

Report prepared by:

Douglas J. Fox
Research Engineer
Mechanical & Fluids Engineering Division
Tel: (210) 522-2920; Fax: (210) 522-5122

Dr. James F. Unruh, P.E.
Institute Engineer
Mechanical & Fluids Engineering Division
Tel: (210) 522-2344; Fax: (210) 522-5122

FUELS DISTRIBUTION LIST

Department of Defense

DEFENSE TECH INFO CTR 12
ATTN: DTIC OCC
8725 JOHN J KINGMAN RD
STE 0944
FT BELVOIR VA 22060-6218

ODUSD
ATTN: (L) MRM 1
PETROLEUM STAFF ANALYST
PENTAGON
WASHINGTON DC 20301-8000

ODUSD
ATTN: (ES) CI 1
400 ARMY NAVY DR
STE 206
ARLINGTON VA 22202

HQ USEUCOM
ATTN: ECJU L1J 1
UNIT 30400 BOX 1000
APO AE 09128-4209

US CINCPAC
ATTN: J422 BOX 64020 1
CAMP H M SMITH
HI 96861-4020

JOAP TSC 1
BLDG 780
NAVAL AIR STA
PENSACOLA FL 32508-5300

DIR DLA
ATTN: DLA MMSLP 1
8725 JOHN J KINGMAN RD
STE 2533
FT BELVOIR VA 22060-6221

CDR
DEFENSE FUEL SUPPLY CTR
ATTN: DFSC I (C MARTIN) 1
DFSC IT (R GRAY) 1
DFSC IQ (L OPPENHEIM) 1
8725 JOHN J KINGMAN RD
STE 2941
FT BELVOIR VA 22060-6222

DIR
DEFENSE ADV RSCH PROJ AGENCY
ATTN: ARPA/ASTO 1
3701 N FAIRFAX DR
ARLINGTON VA 22203-1714

Department of the Army

HQDA
ATTN: DALO TSE 1
DALO SM 1
500 PENTAGON
WASHINGTON DC 20310-0500

SARDA
ATTN: SARD TT 1
PENTAGON
WASHINGTON DC 20310-0103

CDR AMC
ATTN: AMCRD S 1
AMCRD E 1
AMCRD IT 1
AMCEN A 1
AMCLG M 1
AMXLS H 1
5001 EISENHOWER AVE
ALEXANDRIA VA 22333-0001

CDR ARMY TACOM
ATTN: AMSTA IM LMM 1
AMSTA IM LMB 1
AMSTA IM LMT 1
AMSTA TR NAC MS 002 1
AMSTA TR R MS 202 1
AMSTA TR D MS 201A 1
AMSTA TR M 1
AMSTA TR R MS 121 (C RAFFA) 1
AMSTA TR R MS 158 (D HERRERA) 1
AMSTA TR R MS 121 (R MUNT) 1
AMCPM ATP MS 271 1
AMSTA TR E MS 203 1
AMSTA TR K 1
AMSTA IM KP 1
AMSTA IM MM 1
AMSTA IM MT 1
AMSTA IM MC 1
AMSTA IM GTL 1
AMSTA CL NG 1
USMC LNO 1
AMCPM LAV 1
AMCPM M113 1
AMCPM CCE 1
WARREN MI 48397-5000

CDR ARMY TECOM
ATTN: AMSTE TA R 1
AMSTE TC D 1
AMSTE EQ 1
APG MD 21005-5006

PROJ MGR PETROL WATER LOG
ATTN: AMCPM PWL 1
4300 GOODFELLOW BLVD
ST LOUIS MO 63120-1798

PROJ MGR MOBILE ELEC PWR
ATTN: AMCPM MEP T 1
AMCPM MEP L 1
7798 CISSNA RD STE 200
SPRINGFIELD VA 22150-3199

CDR
ARMY COLD REGION TEST CTR
ATTN: STECR TM 1
STECR LG 1
APO AP 96508-7850

CDR
ARMY BIOMED RSCH DEV LAB
ATTN: SGRD UBZ A 1
FT DETRICK MD 21702-5010

CDR FORSCOM
ATTN: AFLG TRS 1
FT MCPHERSON GA 30330-6000

CDR TRADOC
ATTN: ATCD SL 5 1
INGALLS RD BLDG 163
FT MONROE VA 23651-5194

CDR ARMY ARMOR CTR
ATTN: ATSB CD ML 1
ATSB TSM T 1
FT KNOX KY 40121-5000

CDR ARMY QM SCHOOL
ATTN: ATSM PWD 1
FT LEE VA 23001-5000

ARMY COMBINED ARMS SPT CMD
ATTN: ATCL CD 1
ATCL MS 1
ATCL MES (C PARENT) 1
FT LEE VA 23801-6000

CDR ARMY FIELD ARTY SCH
ATTN: ATSF CD 1
FT SILL OK 73503

CDR ARMY TRANS SCHOOL
ATTN: ATSP CD MS 1
FT EUSTIS VA 23604-5000

CDR ARMY INF SCHOOL
ATTN: ATSH CD 1
ATSH AT 1
FT BENNING GA 31905-5000

CDR ARMY AVIA CTR
ATTN: ATZQ DOL M 1
ATZQ DI 1
FT RUCKER AL 36362-5115

CDR ARMY ENGR SCHOOL
ATTN: ATSE CD 1
FT LEONARD WOOD
MO 65473-5000

CDR 49TH QM GROUP
ATTN: AFFL GC 1
FT LEE VA 23801-5119

CDR ARMY ORDN CTR
ATTN: ATSL CD CS 1
APG MD 21005

CDR ARMY SAFETY CTR
ATTN: CSSC PMG 1
CSSC SPS 1
FT RUCKER AL 36362-5363

CDR ARMY ABERDEEN TEST CTR
ATTN: STEAC EN 1
STEAC LI 1
STEAC AE 1
STEAC AA 1
APG MD 21005-5059

CDR ARMY YPG
ATTN: STEYP MT TL M 1
YUMA AZ 85365-9130

CDR ARMY CERL
ATTN: CECER EN 1
P O BOX 9005
CHAMPAIGN IL 61826-9005

DIR 1
AMC FAST PROGRAM
10101 GRIDLEY RD STE 104
FT BELVOIR VA 22060-5818

CDR I CORPS AND FT LEWIS
ATTN: AFZH CSS 1
FT LEWIS WA 98433-5000

CDR
BLOUNT ISLAND CMD
ATTN: CODE 922/1 1
5880 CHANNEL VIEW BLVD
JACKSONVILLE FL 32226-3404

CDR
MARINE CORPS LOGISTICS BA
ATTN: CODE 837 1
814 RADFORD BLVD
ALBANY GA 31704-1128

CDR 1
2ND MARINE DIV
PSC BOX 20090
CAMP LEJEUNNE
NC 28542-0090

CDR 1
1ST MARINE DIV
CAMP PENDLETON
CA 92055-5702

CDR 1
FMFPAC G4
BOX 64118
CAMP H M SMITH
HI 96861-4118

Department of the Air Force

HQ USAF/LGSF
ATTN: FUELS POLICY 1
1030 AIR FORCE PENTAGON
WASHINGTON DC 20330-1030

HQ USAF/LGTV
ATTN: VEH EQUIP/FACILITY 1
1030 AIR FORCE PENTAGON
WASHINGTON DC 20330-1030

AIR FORCE WRIGHT LAB
ATTN: WL/POS 1
WL/POSF 1
1790 LOOP RD N
WRIGHT PATTERSON AFB
OH 45433-7103

AIR FORCE MEEP MGMT OFC 1
OL ZC AFMC LSO/LOT PM
201 BISCAYNE DR
BLDG 613 STE 2
ENGLIN AFB FL 32542-5303

SA ALC/SFT 1
1014 BILLY MITCHELL BLVD STE 1
KELLY AFB TX 78241-5603

SA ALC/LDPG
ATTN: D ELLIOTT 1
580 PERRIN BLDG 329
KELLY AFB TX 78241-6439

WR ALC/LVRS 1
225 OCMULGEE CT
ROBINS AFB
GA 31098-1647

Other Federal Agencies

NASA
LEWIS RESEARCH CENTER 1
CLEVELAND OH 44135

RAYMOND P. ANDERSON, PH.D., MANAGER 1
FUELS & ENGINE TESTING
BDM-OKLAHOMA, INC.
220 N. VIRGINIA
BARTLESVILLE OK 74003

DOT
FAA
AWS 110 1
800 INDEPENDENCE AVE SW
WASHINGTON DC 20590